UNIVERSITY OF GENOVA –
ISTITUTO ITALIANO DI TECNOLOGIA

PHD PROGRAM IN BIOENGINEERING AND ROBOTICS
CURRICULUM : BIONANOTECHNOLOGY

Design and processing of star-shaped PLA architectures: a promising tool to tailor conventional linear PLLA performances

Giulia Scoponi

Thesis submitted for the degree of *Doctor of Philosophy* (33° cycle)

February 2021

Dr. Athanassia Athanassiou — Supervisor
Prof. Nicola Tirelli — Co-Supervisor
Prof. Giorgio Cannata — Head of the PhD program

Dibris
Department of Informatics, Bioengineering, Robotics and Systems Engineering

I would like to dedicate this Thesis to my family.

Declaration

I hereby declare that except where specific reference is made to the work of others, the contents of this dissertation are original and have not been submitted in whole or in part for consideration for any other degree or qualification in this, or any other university. This dissertation is my own work and contains nothing which is the outcome of work done in collaboration with others, except as specified in the *Co-Authorship* section. This dissertation contains fewer than 65,000 words including appendices, bibliography, footnotes, tables and equations and has fewer than 150 figures.

Giulia Scoponi

February 2021

Co-Authorship

Chapter 2 includes results which have been published in the form of an original journal article, and *Chapter 3* reports materials which have been recently submitted to a scientific journal for future publication. From the work presented in Chapter 4, a new manuscript is in preparation. The complete citations are provided below:

Chapter 2: **Scoponi, G.**; Guzman-Puyol, S.; Caputo, G.; Ceseracciu, L.; Athanassiou, A.; Heredia-Guerrero, J. A. Highly Biodegradable, ductile all-polylactide blends. *Polymer*. **2020**, *193*,122371.

Chapter 3: **Scoponi, G.**; Francini, N.; Athanassiou, A. Production of green star/linear PLA blends by extrusion and injection molding: tailoring rheological and mechanical performances of conventional PLA. *Macromolecular Materials and Engineering*. **2021** (Accepted, February)

Chapter 4: **Scoponi, G.**; Francini, N.; Donno, R.; Gennari, A.; Paradiso, V.; Capacchione, C.; Tirelli, N. Low-temperature, organocatalytic (DBU) ring-opening polymerization of lactides in NMP. A versatile avenue to well-defined branched macromolecular structure with controlled tacticity, aggregation and degradation behaviour. *In preparation*

The large majority of the experimental work, analysis, and writing of the described chapters has been conducted by the author.
Chapters and manuscripts were co-authored and reviewed by the thesis supervisor Dr. A. Athanassiou. The fourth chapter was also co-authored and reviewed by thesis co-supervisor Prof. N. Tirelli.

For what concerns the experimental work, in Chapter 2 Dr. G. Caputo performed XRD analysis and Dr. S. Guzman-Puyol was responsible for conducting Biochemical Oxygen Demand (BOD) experiments. In Chapter 3, Dr. N. Francini performed GPC measurements.
In Chapter 4, Dr. N. Francini contributed to the preliminary optimization study with monofunctional initiators, as well as to the project conceptualization. The study of polymer tacticity was carried out in collaboration with the Department of Chemistry and Biology (DCB)

of University of Salerno and Dr. V. Paradiso was responsible to conduct homonuclear decoupled ^{1}H-NMR experiments. Dr. A. Gennari performed SLS measurements and AFM characterization was carried out by Dr. R. Donno.

Acknowledgments

First, my special thanks to Dr. Athanassia Athanassiou, for her knowledge and mentorship in my journey as a PhD student in Smart Materials Group. I have appreciated and admired the incredible fairness and availability through which she manages at best the research group. I am also extremely thankful to Dr. Nicola Tirelli for giving me the opportunity to work in Polymers and Biomaterials Group and for his wise guidance into polymer synthesis world.

I would also like to thank Dr. Alejandro Heredia Guerrero for introducing me to PhD/lab life. His friendship, knowledge and availability helped me grow as a researcher.
I also express my immense gratitude to Dr. Nora Francini. Without her assistance, I would have not grown or learned so much in the past two years. Above all, I thank her for the unconditioned friendship, support and optimism.

A special thanks to all my colleagues. It has been a pleasure and a honor to be part of two multidisciplinary and dynamic research groups, SmartMat and PolBiom, collaborating with competent and creative scientists. Particularly, I would like to thank Arek for his kind help and precious scientific advice, and Lara and Giorgio for the great support and availability over these three years.

I am extremely grateful to all my *not-so-genovese* friends; they have been essential for my development (and survival) as a PhD student and have made my time at IIT even more enjoyable. This experience would not have been the same without our laughs and adventures.

Immense gratitude goes to my family, especially to my parents Marco e Carla, for the unwavering love and support. Despite the distance and difficulties, they have never left my side, and for this, I cannot thank them enough. Finally, I would like to thank Simone, my first fan and my greatest strength. Without him, none of this would have been possible.

Abstract

In this *Thesis*, the manipulation of poly(lactide) (PLA) macromolecular architecture, through introduction of controlled star-shaped branching, was exploited to enhance ductility, toughness, degradability and reduce viscosity -for better melt flow during manufacturing- of industrially employed PLA, which is typically a linear semicrystalline PLA. These features are instrumental to the development of flexible and highly biodegradable *all-PLA*-based products with improved processability, without altering the chemical nature of the material, thus making poly(lactide) materials more competitive on the market with respect to petroleum-based commodities.

Firstly, the plasticization performance of short-branched, star-shaped PDLLA as green and compatible additive of conventional linear PLLA was assessed. The miscibility of these two components and the positive effect of increasing branching contents on final mechanical, thermal, and biodegradation properties were evaluated, along with a comparative analysis of the resulting ductile and highly biodegradable star/linear PLA blends with respect to other existing polymer products.

Next, the scalability of the star/linear PLA blends production was investigated, by employing typical large-scale manufacturing techniques for thermoplastic polymers, *i.e.* extrusion -coupled to compression molding- and injection molding. In addition to reduce typical linear PLLA brittleness, progressively higher star-shaped contents were found to gradually decrease the melt viscosity of the final material, while increasing the shear-thinning behaviour, thus facilitating the melt flow during manufacturing and improving overall processability. Moreover, the high compatibility between branched and linear PLA allowed their efficient blending through a single-step injection molding process, avoiding prior mixing by melt extrusion, thus reducing the typically rapid PLA thermo-oxidative degradation, and resulting in materials with enhanced properties.

The possibility to tailor final PLA material properties by varying also the branching degree and tacticity of the selected branched modifier was finally assessed. To this aim, a novel and versatile lactide ROP protocol was developed, giving access to a library of multi-armed poly(lactide) architectures with variable topology (*i.e.* linear, star, comb PLAs with increasing number of arms) and stereoconfiguration (*i.e.* PLLA and PDLLA homopolymers; PLLA-*b*-PDLLA and PDLLA-*b*-PLLA copolymers). The combined effect of these parameters on final PLA materials properties was systematically investigated, in terms of macromolecular conformation,

crystallizability, rheological behaviour and degradability and confirmed the efficient modulation of polymer flexibility (few chain entanglements) and rheology (reduced viscosity), compared to the conventionally used linear semicrystalline PLA. The observed physico-chemical and mechanical properties, as well as the faster hydrolytic degradation kinetics, make the synthesized branched poly(lactide)s extremely interesting for future industrial development of flexible and easily processable PLA-based materials with enhanced biodegradability.

Table of Contents

List of Figures

List of Tables

Chapter 1 .Introduction

1.1 Poly(lactide) - Overview

The growing concerns of this century regarding global warming and plastic pollution has contributed to an increasing demand for bio-based and biodegradable polymers. To this aim, efforts on a global scale are being dedicated to the development of functional polymer products from renewable resources, as more sustainable alternatives to petroleum-based polymeric commodities.[1,2] The European Commission has also recognized the essential role of the so-called "bioplastics" (which includes bio-based and biodegradable polymers) in the bio economy and their potential to accelerate the transition to a circular economy.[3–5] Nevertheless, a yet critical issue for industrial research is the obtainment of biodegradable materials presenting, at the same time, easy processability and good performance at a competitive cost with conventional polymers.[3,6–8] For this reason, despite the exponential growth and rising demand of bioplastics market, these materials still represent less than 1% of the total plastic production (accounting ~320 million tonnes per year).[9]

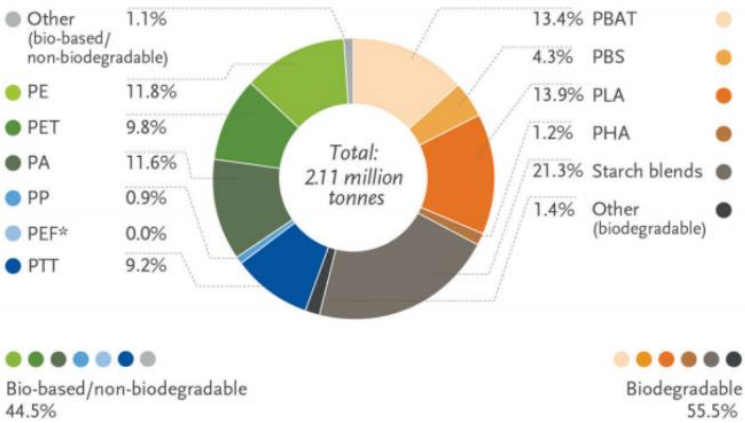

Figure 1.1: Global production of bioplastics in 2019 by material type (*Bioplastic Market Data 2019* report)[9]

In this context, poly(lactide), also called poly(lactic acid) or by its acronym PLA, has been one of the most extensively investigated renewable polymers of the last decades. Indeed, this thermoplastic aliphatic polyester can be obtained from natural sources and exhibits several interesting properties, such as biocompatibility, biodegradability and discrete mechanical performances,[6,10,11] as it will be further discussed in this chapter. As a result, PLA has become one of the most employed renewable polymers among the -yet limited number of- commercially available biodegradable materials in the market, representing 13.9% of the yearly global bioplastics production (2.11 million tonnes for 2019)(Figure 1.1).[9]

The versatility of PLA and the increasing demand for renewable materials has favoured a rapid increase in the production of PLA consumer items.[8,11–13] Initially, most PLA applications were focused on high-value-added biomedical applications such as sutures, stents, and drug delivery systems due to the high initial cost of synthesizing PLA. More recently PLA has gained popularity in packaging, automotive and textile industries.[8,10,14] According to the Food and Drug Administration (FDA), PLA is Generally Recognized As Safe (GRAS).[13,15] Therefore, it has become a sustainable material of choice for numerous single-use object like cutlery, cups and short-life food packaging.[14,16,17] PLA is also widely used in the field of 3D printing for biomedical applications (body/dental implants, tissue engineering scaffolds).[18]

Despite the great progress achieved so far, PLA still exhibits some serious unsolved drawbacks, such as inefficient manufacturing technologies, inferior mechanical properties (brittleness) and overall expensive production, compared to durable polymer commodities.[2] Several strategies have been developed in the attempt to address PLA disadvantages and finally allow its widespread commercialization. Indeed, as for the efficient design of any polymer material, diverse PLA physico-chemical parameters could be modulated in order to enhance certain properties with respect to others, depending on the target application.
In particular, this thesis will focus on the manipulation of PLA macromolecular architecture to tailor PLA rheological, mechanical and biodegradation performances. In fact, introduction of branching represents a promising approach to improve PLA ductility and processability for the production of flexible and highly biodegradable products without altering the chemical nature of the material.

1.2 PLA production

1.2.1 Starting materials and industrial synthesis

Lactic acid (LAc) is the monomer building block of PLA. Due to the presence of chiral centre, this α-hydroxycarboxylic acid exists in two naturally occurring enantiomeric forms: L-LAc and D-LAc (or (S)-LAc and (R)-LAc)(Figure 1.2).[19] The majority of commercial LAc is produced through bacterial fermentation of carbohydrates by homofermentative organisms belonging to the *Lactobacillus* genus, which produce LAc with high selectivity and yields. Depending on the Lactobacillus strain employed the fermentation provides L-LAc, D-LAc or a mixtures of both isomers.[12,15,20]

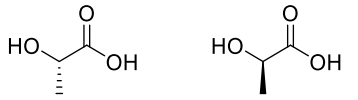

L-lactic acid D-lactic acid

Figure 1.2: Enantiomeric forms of PLA building block lactic acid

The bacteria feed generally consists in starch or other polysaccharides, which are easily available from corn, sugar beet, sugar cane, potatoes and other biomasses.[21–23] In recent years, the implementation of pre-treatment purification methods allowed the replacement of pure sugars and starch-based crops with cheap biomasses and agricultural residues as direct raw sources for lactic fermentation process.[12,24] Corbion®, one the major PLA producers, developed an innovative fermentation technology allowing the use of second-generation agricultural feedstocks (*e.g.* sugar bagasse, corn stover, wood manufacturing wastes).[16] NatureWorks® LLC plant (Nebraska, USA), with a PLA production capacity of 150000 tonnes-per-year, operates with agricultural lignocellulosic residues supplied by certified farms located within 5 miles from the facility.[25]

Once produced and purified, LAc needs to be efficiently converted into high-molecular weight (high-MW) PLA, in order to ensure better performances, durability and higher commercial values in diverse applications (*e.g.* agriculture, packaging, fibre industry).[16] Despite polycondensation was the first employed PLA synthetic route, it is rarely applied nowadays, as this method mainly yields PLAs with relatively low molar masses and high dispersities.[16,23] The major current industrial processes are based on ring-opening polymerization (ROP) via lactide formation (Scheme 1.1).[12,26]

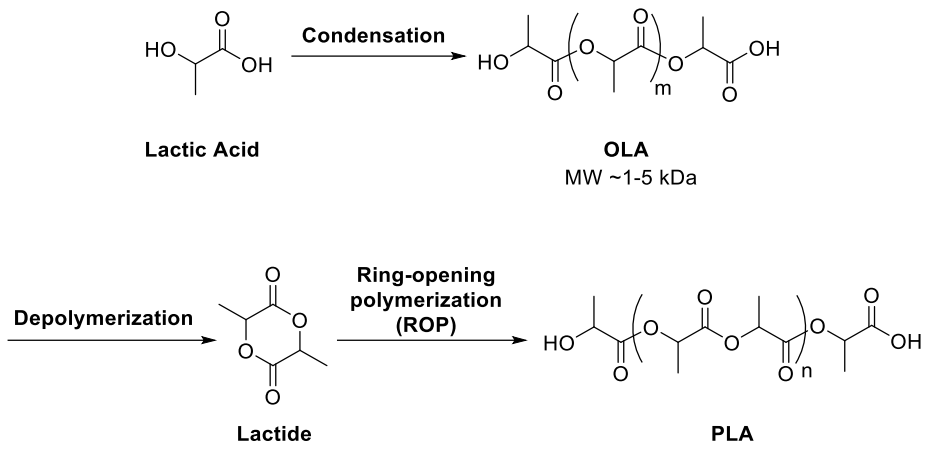

Scheme 1.1: Conventional synthesis of high-MW PLA via ring-opening polymerization of lactide.

Lactide (LA) is cyclic dimer of lactic acid and allows the production of high-MW PLA through a multiple-step method.[27] Firstly, polycondensation of LAc is performed, yielding oligomeric lactic acid (OLA, MW~1-5 kDa).[28] Lactide is produced by subsequent catalytic depolymerization of OLA, which is performed in vacuum at high temperatures to facilitate dimer distillation and separation.[29,30] ROP of lactide provides controlled kinetics and high-MW and can be performed in melt or solution, through ionic (cationic or anionic) mechanism, via enzymatic catalysis or via metal-catalysed coordination-insertion, depending on the initiator utilized, as it will be further explained in *Chapter 4*.[12,16] Given the optical activity of lactic acid, the corresponding cyclic ester LA can be found in different stereoconfigurations: L-lactide (L-LA), D-lactide (D-LA), the symmetric *meso*-lactide (meso-LA), as well as D,L-lactide (*rac*-LA or DL-LA), which consists of the racemic mixture of D-LA and L-LA (Figure 1.3). Depending on the composition of the monomer isomer in the feed (in the absence of a stereoselective catalyst), it is possible to adjust the tacticity of PLA, from isotactic poly(L-lactide) (PLLA) and poly(D-lactide) (PDLA), to syndiotactic and atactic poly(D,L-lactide) (PDLLA), which in turn affect the final properties of the polymer (see *Section 1.4.1*).[27] It is worth to mention that the term poly(lactide) is frequently used alternatively to poly(lactic acid) in the literature, referring to the polymer obtained respectively through ROP (lactide monomer) or polycondensation (lactic acid monomer).[15]

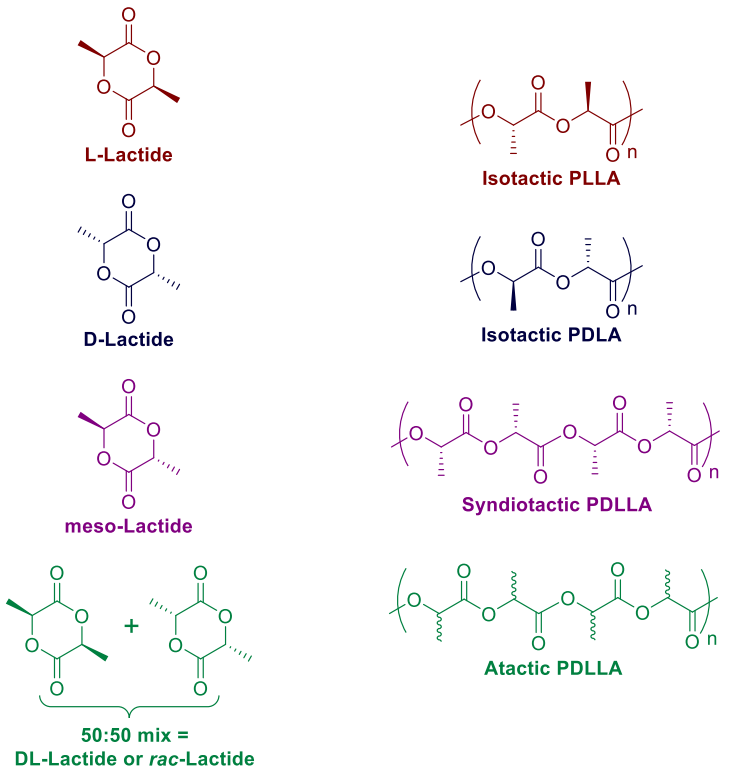

Figure 1.3: Stereoisomers of LA and corresponding PLA tacticities. In the case proper stereoselective polymerization is performed, DL-LA could potentially yield isotactic, syndiotactic or also heterotactic PLA.

1.2.2 Processing technologies

PLA can be processed through well-established manufacturing techniques for petroleum-based thermoplastics to produce diverse items, *e.g.* films, fibres, sheets, containers or other molded parts.[16,31] However, depending on the applied processing method and desired application, the process needs to be adjusted to cope with inherent characteristics of natural and/or biodegradable polymers, such as low thermal stability and shear resistance and moisture sensitivity.[16,32,33] Melt processing is the main approach for conversion of the PLA resin into its end products: the material is heated above its melting temperature to shape the molten polymer into the desired shape and finally is cooled to stabilize the final dimensions. The major manufacturing techniques used for PLA processing are presented below.

Extrusion is the most important technique for continuous melt processing of PLA, and in general thermoplastics. The extruder system is equipped with a heated (single or double) rotating screw for melting the polymeric material (Figure 1.4A) and it constitutes, with minimal modifications, the main apparatus of several polymer manufacturing machines (*e.g.* injection molding processes, fibre spinning). Extrusion generally represents the first processing step in the conversion of polymer resins into finite products, especially when additivation, blending or

compounding with other components is required. Indeed, it provides higher shear heating and residence times with respect to other common processing methods, resulting in better mixing also for poorly miscible components.[31] The solid material conveys into the screw through a hopper. Given the combined electrical heating and friction towards the screw, the polymer is gradually compressed and melted, while transported by the rotating screw through the different heating and metering sections of the extruder.[34] Finally, the molten material exits though the die section and rapidly solidifies by fast (water or air) cooling.[10] The PLA extruded filament can be directly drawn and shaped into the desired item (*i.e.* sheet and film casting extrusion, blown film extrusion, fibre spinning, foaming).[35] More frequently, the additivated or compounded PLA product from the first extrusion cycle is sold, in the form of sheets or pellets, for subsequent re-molding through new processing cycles into the final products (*i.e.* thermoforming, compression molding, even new extrusion or injection cycles).[23,31,36,37] Most of the extrusion machines for fossil-based polymers have a high screw L/D ratios (flight length of the screw to its external diameter)[32] ensuring higher torques and residence times for more homogenous mixing, compared to other processing techniques. However, such conditions determine significant material degradation in the case of poorly thermally and shear resistant bio-based polyesters like PLA. In the attempt to alleviate this problem, PLA may be processed through the relatively low-shear rate screws for processing poly(ethylene terephthalate) (PET) by carefully controlling the heating profile, despite the consequent low production rates.[31,36,38]

When the extruder is directly integrated with a molding system, the processing technique is referred to as injection molding (Figure 1.4B). Such method is widely used to process thermoplastics like PLA for production of items with complex shape or which require high dimensional precision (*e.g.* containers, cutlery, cups, gears or automotive components).[39] Through a reciprocating screw extruder, the polymer melt is directly injected into the mold cavity, where the material is cooled to a fixed shape and then ejected by opening the mold platen.[31,35] PLA with lower viscosities (easier melt flow) are preferred for injection molding, as high shear rates are required to ensure proper filling of the mold.[35,40] Additionally, a controlled mold cooling profile is essential to avoid typical PLA shrinkage phenomena and a fast cooling rate is generally applied to ensure amorphous and transparent products.[31,39]

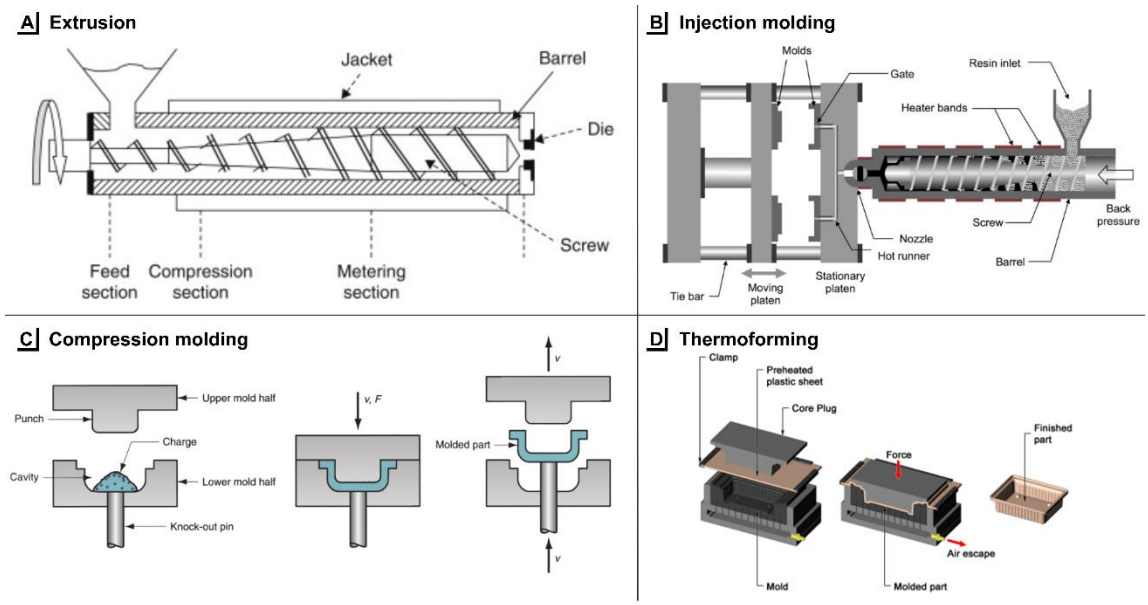

Figure 1.4: Representation of some of the main melt processing techniques of PLA: **A,** Extrusion.[34] **B,** Injection molding.[31] **C,** Compression molding.[35] **D,** Thermoforming.[41]

Blended and/or additivated polymeric materials are generally prepared by extrusion (better mixing) before shaping the final product by injection molding, as less prolonged mixing is performed through the latter method (shorter compression section), especially if poorly compatible components are used.[39] Stretch-blow molding machines are used for production of PLA product such as bottles and tanks, as this injection molding process allows additional biaxial orientation of the polymer when filling the mold. However, PLA poor elongation performances upon strain (process is applied at $T_g<T<T_m$) and melt elasticity restrict its use in this field.[31,35]

Compression molding and thermoforming (Figure 1.4A and B) are the most direct and easy solvent-free methods for forming simple shaped PLA products. In compression molding, the polymer material (in powder or pellet form) is placed into a heated mold cavity. The mold plug member is then used to seal the system upon application of a certain torque pressure and the material is directly melted in the mold by means of heating and pressure to obtain the desired shape. The mold is then cooled below the polymer glass transition temperature to allow solidification and ejection of the molded product. This method is generally employed for polymer sheeting or for production of items with simple design and shape.[35,42,43] Although it does not allow high-throughput production, as processing techniques based on injection molding and extrusion, this melt-processing method is widely used for plastic materials molding simulations on small scales and polymer testing.

Similarly to compression molding, in thermoforming process a pre-formed plastic sheet is heated and then pressed into a final shape by vacuum/air or mechanical pressure, by using a plunger and heated mold. This method is widely used for packaging, such as clamshell containers and food trays.[23] However, both compression molding and thermoforming are static processing configurations. Dynamic processing techniques, such as extrusion, might be preferred for first compounding and blending of PLA, as the screw motion allows more homogenous plasticization and melting of the polymer as well as lower pressures.

1.3 PLA Properties: Potentials and Drawbacks

1.3.1 Mechanical performances, barrier properties and processability

Conventional commercially available PLA is a linear semicrystalline polymer produced by a mixture of the different lactide isomers, with the L-isomer constituting the main or unique fraction. The reported D-isomer content is generally lower than 12% to allow crystallization.[30,44] PLA shows numerous interesting properties compared to petroleum based commodities, such as high elastic modulus, competitive mechanical strength values, as well as discrete optical and barrier properties (Table 1.1).[17,37,45–47] Particularly, it most closely resembles poly(ethylene terephthalate) (PET) and poly(styrene)(PS) and thus holds great potential in substituting these materials for several applications in the near future (*e.g.* cutlery, bottles, rigid or flexible containers). Nevertheless, PLA still exhibits some significant drawbacks, such inherent brittleness (further affected by the typically high crystallinity of commercial PLA materials, see *Section 1.4.1*), with a mean elongation at break of 5%, and poor stress resistance, especially compared to PET.

Conventional semicrystalline PLA is indeed rigid and brittle at room temperature due to its glass transition temperature (Tg) of ~55 °C.[48] This results, in crazing fracture behaviour and the poor toughness, which limit its use in applications requiring plastic deformation at higher stress levels (*e.g.* flexible packaging, biomedical devices, single-use cutlery).[37,49] Fort this reason, despite PLA will probably fulfil soon the industry requirements for most of the rigid articles, it needs to be plasticized to be used as soft films, flexible packaging or beverage containers,[14,50] as it still exhibits -in the form of neat polymer- film tearing or cracking when subjected to stresses during manufacturing or use.[3,13,31]

As several other bio-based polymers, PLA possesses a relatively polar polymeric chain and shows susceptibility to moisture. Nevertheless, it presents discrete barrier properties compared to other commercially available polymers, with lower or comparable gas permeability than

several petro-based materials such as PS, PP (polypropylene) and PE (polyethylene), yet still being uncompetitive with respect to PET performances.[17,49] In terms of water vapour barrier properties, PLA shows lower vapour transmission rates (WVTR) than PS or other bio-based polymers, such as PCL (poly(ε-caprolactone)) or PBS(poly(butylene succinate)),[49,51] and comparable values with respect to PET, although PP and PE are still preferable for moisture protection. Such features restrict PLA applicability to short shelf-life packaging.[16,17]

Table 1.1: Typical mechanical,[17,37,45–47,52] thermal[30,37,45,47] and barrier properties[17,37,45] of PLA with respect to PET and PS, the most similar petroleum-based commodities.

	PLA[a]	PS	PET
MECHANICAL PROPERTIES			
Tensile yield strength (MPa)	41-66	34-46	47-100
Tensile elongation at break (%)	1.5-8	1-3.5	60-165
Tensile modulus (GPa)	3.5-4.2	3-4	2.2-4.3
Notched Izod impact (J/m)	13-22	16-26	79-100
BARRIER PROPERTIES			
Oxygen permeability, $P(O_2)$ ($x10^{20}$ m^3 m/m^2 s Pa)[b]	130-300	2000	10-60
Water vapour transmission rate, WVTR (g mm/ m^2 day)[c]	1.8-6	1-10	0.5-2
THERMAL PROPERTIES			
Glass transition temperature (°C)	50-60	70-115	73-80
Melting Temperature (°C)	130-175	-	245-250
Processing Temperature (°C)	200-210	230	255

[a]Average data for commercial amorphous and crystalline PLA materials with diverse D-LA content and stereoregularity; [b]measured at 23 °C, 50% relative humidity (RH); [c]measured at 23 °C, 85% RH

Thermal behaviour is another important aspect: PLA possesses low heat resistance with respect to the petroleum-based counterpart, which determines serious problems during its processing.[53] PLA presents melting temperature (Tm) of approximately 155 °C and generally requires processing temperatures 40-50 °C above its Tm to ensure complete melting of the crystalline phase.[15,48] However, when temperature approaches 200 °C, PLA undergoes chain scission and inter- or intramolecular transesterification reactions, resulting in rapid loss of

molecular weight and material deterioration.[15,54] As a result, commercially available semicrystalline PLA reports a very narrow processing window.[23]

Despite PLA can be processed through major processing techniques employed for petroleum based polymers, its low thermal resistance at the required processing conditions results in poor melt strength.[55] This represents a critical issue for its manufacturing, especially for flexible products requiring stretching or orientation (e.g. cast film extrusion, stretch blow molding) or high shear rates (e.g. injection molding).[55] Moreover, PLA shear viscosity strongly varies (decreases) with temperature. Therefore, the impossibility to further increase operative temperatures generally results in significant resistance to flow during processing of semicrystalline PLLA when plasticizing and/or fluidizing agents are not employed.[56] This generally forces to keep lower shear rates to avoid further degradation, thus resulting in reduced production throughput.[54] Alternatively, PLA can be modified through structure manipulation (architecture, stereochemistry) or by bulk modification (*e.g.* additivation) in order to enhance the processability (lower viscosity) or decrease processing temperatures, thus reducing material degradation (more detailed description in *Section 1.5*).

1.3.2 Biodegradability

PLA biodegradability is another important aspect to consider when designing PLA-based materials.

Indeed polyesters degradation process is the result of the interplay between chemical hydrolysis and the diffusion of water and oligomers[57] and largely depends on the molecular weight, crystallinity, macromolecular architecture, sample geometry, and surrounding environment (*i.e.* temperature, moisture, pH, presence of micro-organisms *etc.*).[58]

Biodegradation mechanism of PLA involves two main steps.[30] The first step consists in a non-enzymatic process: when immersed in aqueous medium (seawater biodegradation) or in contact with moisture (soil burial biodegradation), the polymer is firstly subjected to random chain scission though chemical hydrolysis, gradually reducing the molecular weight due to ester groups cleavage (Figure 1.5).[13,33] As the molecular weight decreases, enzymatic digestion begins (second step), converting the produced oligomers in CO_2, water and biomass. Numerous studies showed that microorganisms are able to degrade PLA only after oligomers with molecular weight lower than 10 kDa,[33,59] although high-MW crystalline PLA is typically employed to ensure competitive performances with fossil-based plastics, conventional PLA is known to present very low (bio)degradation, especially in marine environment.[60]

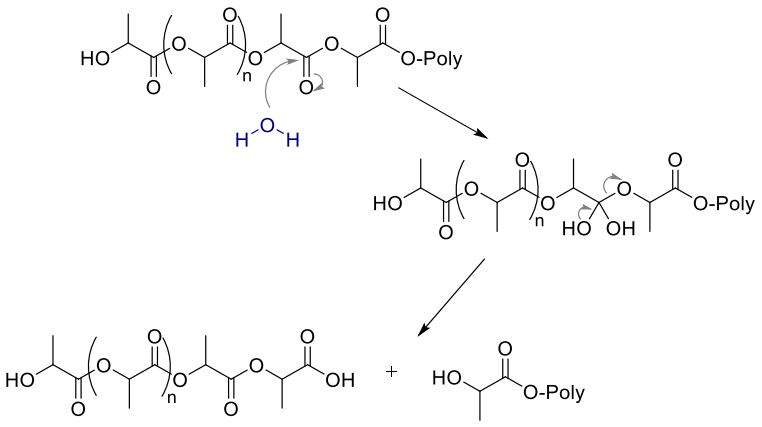

Figure 1.5: Mechanism of PLA hydrolysis (adapted from Farah *et al*[13]). A higher number of chain ends or hydrophilic functionalities, as for low-MW and/or branched PLAs, could favor water diffusion into the material bulk, with resulting enhanced susceptibility to chemical hydrolysis, as well as enzymatic attack.

Indeed, it has been shown that commercially available PLA can easily degrade if treated in industrial composters at 50–60 °C for 90 days; conversely, its biodegradation in land littering or seawater is rather slow[7] PLA degrading microorganisms occur significantly less in the environment compared to other bio-based polyester.[61–63] As an example, Urayama *et al.* reported weight losses of approximately 20% in soil for 20 months. On the other hand, amorphous PDLLA reported 75% weight loss upon identical conditions.[64] Therefore, it is clear that the molecular weight and the structural properties (*i.e.* stereoconfiguration, molecular mobility) of the designed PLA play an important role to ensure optimal biodegradation rates.

The above-described macroscopic properties of PLA are strongly dependant on several microscopic chemico-physical parameters of this rising polymer, *i.e.* stereochemistry, molecular weight, macromolecular architecture. Moreover, also the applied processing methods and conditions can drastically affect PLA final properties.

The research process for the improvement of any polymer material implies a trade-off between these different factors depending on the desired final properties, as no common solving strategy exist for all possible PLA applications.

Therefore, a deep understanding of the influence of each of these parameters (*i.e.* stereoconfiguration, macromolecular architecture, molecular weight, processing method) on PLA final thermal, mechanical and rheological behaviour is essential for efficiently overcoming the still unsolved drawbacks of this material for its exploitation in various application fields, as it will be discussed in the next section. Indeed, it is of outmost importance to find the optimal

balance between these properties to improve PLA performances for the desired application while preserving, if not enhancing, its biodegradability.

1.4 Structure-Process-Properties relation in PLA

1.4.1 Effect of stereoconfiguration and crystallinity

As previously introduced, the ratio of the lactide isomers determines PLA chain stereochemistry (polymer tacticity). Modulation of the polymer stereoconfiguration leads to dramatic changes in PLA macroscopic properties, as it affects crystallinity, hence, the final thermal, mechanical, permeability and (bio)degradation performances. Indeed, isotactic PLLA and PDLA are semicrystalline polymers, due to the enantiomeric purity of the starting monomers and the stereoregularity of the polymer chain. Atactic PDLLA is instead an equimolar random copolymer of L- and D-lactide. Therefore, it is fully amorphous, as it lacks structure stereoregularity. [65] Indeed, a completely pure PLLA has a melting point of around 175 °C, which can be reduced to as low as 130 °C with increasing stereo-irregularity,[13,65] until complete suppression of the crystallization ability when D-lactide content exceeds 15%.[44] Similarly, the crystallinity (and crystallization rate) of isotactic PLA could be easily tailored also after polymerization, by blending with different ratios of atactic PDLLA.[66] Conversely, physical blending of PDLA and PLLA may provide higher-order supramolecular assembly through stereocomplex formation, with consequent high crystallinity. The resulting material exhibits high crystallinity and higher Tm (~230 °C), despite the important increase in product cost.[67,68] Although high crystallinity might be necessary for certain applications requiring high mechanical strength, stiffness and barrier properties (long shelf-life food packaging, articles for automotive), the lower crystallinity and/or melting point benefit by allowing decrease of melt-processing temperatures, hence decreasing degradation. The reduction or absence of a crystalline compact phase (increase in free volume), as in the case of neat PDLLA, may determine a certain decrease in Young's modulus, yet along with a great improvement in polymer ductility,[69] higher permeability values[70] and material transparency. Such properties are desired for numerous products, *e.g.* flexible packaging, breathable fabrics, wound dressing, and could thus be exploited for broadening PLA scope of applications. Most importantly, polymer crystallinity has dramatic effects on degradability of PLA, since the chains in crystalline regions of PLA are more resistant to hydrolysis, compared to those in amorphous regions.[71,72] Therefore, diffusion and chain cleavage proceed preferentially in the amorphous regions, resulting in higher degradation rates.[57]

1.4.2 Effect of molecular weight

The molecular weight has a significant impact on the properties of polymers such as degradation, mechanical strength and solubility.[13] PLA chains with lower molecular weights possess higher molecular mobility and higher density of hydrophilic terminal groups per unit mass compared to high-MW PLA, making them more susceptible to microorganism degradations. Therefore, low-MW PLAs should be preferred when high biodegradation rates are needed, either for end-of-life disposal requirements or for in vivo biomedical applications (*e.g.* wound dressing, tissue engineering or body implants). However, high-MW PLAs are generally preferred from the industry.[73,74] Indeed, the use of high-MW polymers is known to provide higher mechanical strength and sufficient thermal stability to withstand the high temperatures and stresses of melt-processing without significant loss in performances.[69,73] In general, the overall molecular weight of the polymer material is always proportionally related to the mechanical strength and thermal resistance of the final product, thus any consistent reduction in molecular weight during manufacturing needs to be avoided. Therefore, when designing a valuable bioplastic product, it is essential to find the proper balance between sufficient mechanical performances (hence high molecular weight) and biodegradability (influenced by hydrophilicity, chain mobility and molecular weight) according to the desired application.[10,30]

1.4.3 Effect of Processing

The applied processing conditions are strictly related to the rheological and thermal properties of the PLA. Indeed, as PLA rapidly undergoes polymer chain scission and transesterification when heated above 200 °C, the processing temperature must be greater than Tm to form a homogeneous melt and allow proper flow of the polymer, but low enough to minimize thermal degradation. However, both Tg and Tm of PLA can drastically vary depending on degree of crystallinity, molecular weight, polymer architecture, presence of plasticizers and thermal history of the polymer.[13] Similarly, the in-mold cooling phase strongly depends on the Tg, and in turn on chain mobility and crystallization rate. Processing conditions can also affect final PLA morphological properties. As an example, the high resistance to flow of semicrystalline PLA at the safe extrusion processing temperatures may lead to extrudate defects, such as "stick-spurt" effect (alternating smooth and rough regions as the material exits the die) or sharkskin-melt fracture,[17,75,76] even increasing material deterioration. Also the degree of crystallinity of the polymeric product could be influenced by the processing conditions. For example quenching the polymer from the melt at a high cooling rate results in a highly amorphous polymer, while

a slow rate of cooling allows lamellae formation. Strain-induced crystallization or orientation can also be achieved through processing (*e.g.* stretch blow molding)[55]. Therefore, all these parameters can be exploited in order to improve PLA performances for the intended application.

Nevertheless, it is well known that bio-based polyesters, like PLA, undergo drastic degradation at every processing step they are subjected to prior getting to the market (*i.e.* from batch compounding of the raw material to the molding of the final commercial item), determining drastic loss in mechanical and optical performances.[13,37] Stress and strain at break, Young's modulus and hardness of PLA have been found to rapidly decrease at each thermo-mechanical cycle, with increasingly significant effect after each processing cycle.[38,77] PLA may also exhibit resistance to flow and colour change through injection molding process due to the elevated shear rates.[16,78] Such dramatic effect is ascribed to the several degradation phenomena (random chain scission, intramolecular transesterification, oxidative degradation) caused by the thermo-mechanical stresses applied during processing, yielding significant drop in molecular weight and broadening of the molecular weight distributions (effecting in turns the mechanical properties).[37,79] The extent of such degradation can be evidenced and quantified through molecular weight measurements by means of GPC (gel permeation chromatography) analysis. The evolution of number average (Mn) and weight average (Mw) molecular weight as a function of the processing cycle number is represented in Figure 1.6 for a commercial semicrystalline PLLA.[13,38]

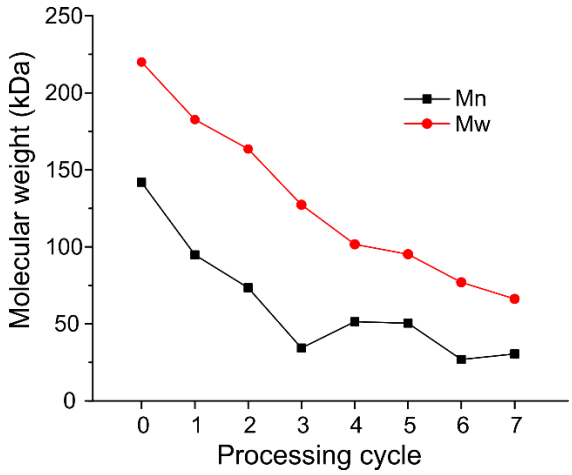

Figure 1.6: Variation of Mn and Mw values of a semicrystalline PLLA with the number of injection cycles, as measured by GPC analysis.

1.4.4 Effect of macromolecular architecture

Compared to linear polymers of equal MW, branched macromolecules present reduced capability of entanglements, which is proportional to the branching degree (number of branches). This feature leads to higher coil mobility (suppression of crystallinity) and lower viscosity. Moreover, branched structures are also more susceptible to hydrolytic degradation compared to their linear counterpart, because of the higher number of terminal functionalities and the more amorphous structure (compared to linear analogues of equal overall molecular weight).[80,81] Given these interesting properties, branched polymers have been widely used in the years to enhance thermoplastics flexibility and processability.[82,83] The use of well-defined branched architectures can indeed be exploited to reduce PLA brittleness and improve the melt flow during processing, reducing material deterioration and ductility.[84,85] Introduction of branching may be performed in several ways, such as blending different PLA architectures, creation of randomly branched frameworks from pre-made linear PLA by using multifunctional radical agents, leading also to different final properties. Indeed, the kind of branching, the branch chain-length and preparation method employed can dramatically affect the performances of the resulting PLA. More detailed discussion regarding the manipulation of PLA chain architecture and its effect on macroscopic PLA properties is provided in *Section 1.6*.

1.5 Major strategies to improve conventional PLA properties

In spite of its availability and the progress achieved on its properties and production, PLA still has a number of drawbacks that limit its application in some fields. For example, even though the toughness of PLA is greater than that of PS, it is still lower than those of PET and PC (poly(carbonate)); this might limit the applicability of PLA as a structural material. Thermal degradation and resistance to flow during processing is another crucial aspect, which is still affecting PLA manufacturing and consequent performances. In addition, biomedical applications of PLA are usually restricted by its slow biodegradation rate and hydrophobicity. The main challenge with renewable polymeric materials like PLA is indeed to achieve products with relatively high durability and structural strength to be competitive on the plastics market, while also preserving their essential biodegradability. Therefore, in the last ten years numerous methodologies for PLA modification have been developed to meet the specific applications. Such strategies involve either bulk modification of PLA, like additivation, blending, compounding and application of different processing methods, or alteration of PLA chemistry, *i.e.* copolymerization, manipulation of polymer stereochemistry and architecture. This section

summarizes the major up-to-date bulk and chemical modification strategies developed for improving PLA performances.

1.5.1 Bulk modifications

1.5.1.1 Plasticizers

Bulk modification of PLA through blending is probably the most extensively used and cost-effective method to improve PLA properties. In this context, plasticizers are widely used to improve processability (improve melt flow) and ductility of polymers.[13] In the case of semicrystalline polymers like PLA, an efficient plasticizer should reduce the Tg, improving its ductility, while also depressing the Tm and overall crystallizability of the material to allow lower processing temperatures and faster biodegradation. Traditionally, the most used plasticizers for PLA have been its monomers lactide and lactic acid (in diverse enantiomeric forms).[38,86–89] In the years, also other non-toxic small molecules, such as glycerol, epoxidized vegetable oils, citrate esters and oligo-PEGs (MW < 5kDa) have been extensively used.[10,90–93] Despite the generally great increase in flexibility (due to large Tg decrease),[90,94] such compounds tend to migrate to the material surface, due to the extremely low molar masses and poor interfacial adhesion with the matrix, determining stiffening of the PLA product over time.[13,95] These feature still represents a critical issue, especially due to the very restrictive legislative requirements for food-contact or biomedical applications.[13]

1.5.1.2 PLA blends

A practical very common approach is to blend PLA with other polymers.[10] The optimal blending component is selected in order to tailor ductility and/or toughness of PLA. Several renewable and/or fossil-based polymers have been blended with PLA, providing plasticization, toughening effect or enhancement of crystallinity, depending on the intended application. Major effects for different PLA blends, in terms of toughness and stiffness of the final material, are displayed in the Ashby plot in Figure 1.7.[2] Among the yet limited commercially available renewable materials, thermoplastic starch (TPS)[96][27] and polyesters like PCL,[97] PBS[98] and poly(butylene adipate-co-terephtalate) (PBAT),[99] have attracted great attention for the production of binary PLA blends.[2,20,27,100] Despite the great potential in terms of achievable ductility and toughness, the development of such blended materials still presents serious difficulties, often resulting in slow changes or dramatic drops in in mechanical performances compared to neat PLA.[2] This is caused by the low miscibility between these polymers (also at low proportions) and requires the use of efficient compatibilizers (such as grafted or

functionalized copolymers to decrease the interfacial tension between the components), as well as further addition of plasticizers.[100] After incorporation of compatibilizers and additives an increase of >100% was observed for PLA/PCL blends, although accompanied by reduction in biodegradation rates.[101] Compatiblized (80/20) PLA/PBS blends reported decrease in both Tg and Tm, along with a discrete increase in elongation at break (60%).[102] In the case of PLA/TPS blends, addition of up to 30% of compatibilizer increased crystallinity and slightly improved elongation.[27,103] Despite the progress achieved so far, most of the compatibilizers used for PLA blends have been developed only on small scales and require further optimization for optimal blend miscibility and performances, thus limiting the exploitation of such renewable PLA-products on industrial scale.[14]

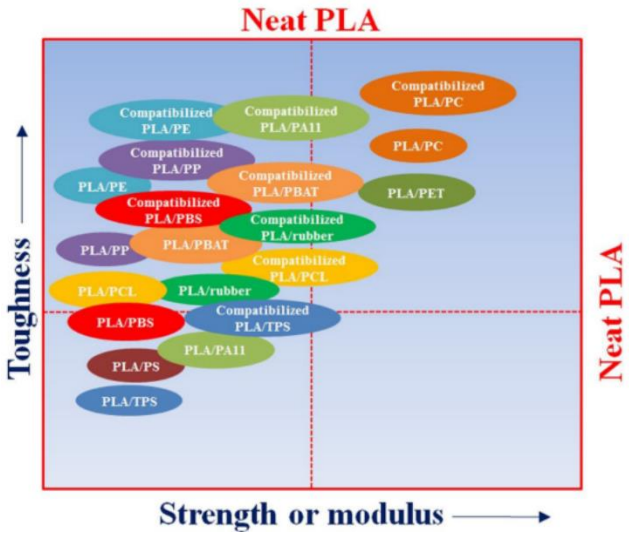

Figure 1.7: Toughness vs strength and modulus of PLA polymer blends compared with those of neat PLA

Among PLA blends with non-biodegradable polymers, the development of PLA-rubber through dynamic vulcanization with diverse elastomers,[2] such as thermoplastic poly(urethane) (TPU)[104,105] or natural rubber (NR),[106,107] has been extensively studied, reporting dramatic improvements of impact strength and toughness with respect to neat PLA. In the attempt of improving polymer ductility and heat resistance, as well as decreasing the production cost, also diverse blends with fossil-based commodities, such as PP,[108,109] PE[110][111] and PS[112], and have been investigated.[2,10,20] Also in this case the low affinity of the diverse polymer structure required further compatibilization studies in order to avoid phase separation, especially in the case of the apolar polyolefinic chains.[14,111] However, the bio-based content is nowadays a driving force in the development of durable polymeric materials and the main goal in bioplastics

development is to –at least partially- substitute petroleum-based commodities in the near future. Therefore, the use of fossil-based polymers to create improved PLA products should be avoided.

1.5.1.3 PLA composites

PLA composites cover a wide research field and have been extensively studied in the recent years.

Indeed, enhancing matrix crystallization through compounding with nucleating agents has been reported to be an effective strategy toward creating heat resistant and highly crystalline PLA materials,[19,26] as in the case of the widely exploited nanoclays[113,114], talc,[115,116] graphene[117,118] and lignocellulosic fillers.[119,120] The faster crystallization kinetic and higher thermal resistance can improve PLA performances for processes requiring significant strain hardening behaviour (*e.g.* stretch blow molding)[121] or for short shelf-life packaging application (higher barrier properties).[26,115,122] However, this approach is not desired to improve flexibility of PLA products and can drastically decrease PLA transparency and biodegradability. Moreover, numerous PLA fillers are inorganic compounds, which cannot degrade or reduce PLA biodegradability.[122] According to the stringent requirements of European standard, minimal use of even 5% of filler may prevent the product to be certified as compostable (and thus also biodegradable).[122]

1.5.2 Chemical modifications

1.5.2.1 Copolymerization

PLA and its copolymers are very interesting in biomedical field as they exhibit exceptional qualities than that of their respective individual polymers. Lactide could be co-polymerized with a large number of monomers, leading to the formation of new copolymers with varied properties. For example, the monomers like ε-caprolactone (CL), trimethylene carbonate (TMC), ethylene glycol (EG), glycolide (GA), valerolactone (VL), are widely used for copolymerization, as reviewed by Puthumana *et al.*[123]

Through selection of proper co-monomers, degree of polymerization and monomers ratios, copolymerization gives the possibility to easily tailor degradation rate, mechanical and thermal properties of PLA, with lower issues of miscibility with respect to direct blending[13,20]. For example, poly(lactide-co-glycolide) (PLGA) exhibits lower crystallinities and Tm values than PLA and PGA alone,[29] as well as faster degradation kinetics compared to neat PLA.[8] In poly(ε-caprolactone-co-lactide), enhanced flexibility can be achieved by increasing CL contents,[124] despite a certain loss in toughness and slower biodegradation.[125][29]

Despite copolymerization approach provides excellent results on small scales and high-value products for pharmaceutical and biomedical applications (*e.g.* drug-delivery, bioimaging, tissue engineering), the production cost of such materials still restricts their exploitation on industrial scale with respect to the corresponding homopolymers.[123]

Noteworthy, PLA products obtained by using different ratio and distribution of L-LA, D-LA and D,L-LA units can be referred to as (stereo-)copolymers, differentiating from isotactic PLA homopolymers, composed by identical LA isomers repeating units. As previously mentioned, by varying the L/D isomer content and arrangement, it is possible to tailor stereoregularity, hence crystallinity, of PLA. The production of block or statistical copolymers of LA isomers it is thus a promising approach to tailor crystallization behaviour of final PLA, hence its thermal and mechanical properties.

1.5.2.2 Branching

By altering the macromolecular architecture, it is possible to impart diverse rheological and mechanical properties to the material. Introduction of branching has been widely exploited to improve processability and flexibility of polyolefins[82,83] and is recently attracting attention as a promising strategy to enhance bio-based polyesters performances.[85,126–129] When conventional linear PLA is built into a branched structure, chain entanglements are dramatically reduced, leading to lower viscosity and capability of chain arrangement into lamellae for crystallization, for equal molecular weights. Moreover, branched PLA is expected to increase (bio)degradation rate, due to the higher number of hydrophilic chain ends per mass unit readily available for ester hydrolysis, as well as the typically lower molecular weight per branch (compared to linear analogues with similar overall MW), which should facilitate microorganisms digestion.[88] Therefore, this strategy is of particular interest as it gives the possibility of tailoring PLA physical properties without changing the chemical nature of the material. Indeed, branched PLA could be processed alone or exploited as efficient plasticizer and/or flow modifier for PLA (as a polymer blend) for alternative biodegradable PLA materials (*e.g.* flexible packaging, breathable fabrics, cutlery and cups). Although branching may be achieved through direct radical-mediated reactive extrusion of linear PLA, this approach results in randomly branched (or even cross-linked) materials, which may lead to opposite properties than the ones expected for a branched structure (*i.e.* higher crystallinity and viscosities, lower biodegradability).[84,126,130,131] Therefore, when designing the final branched PLA product, important factor such as the branch chain-length (as the branch could be able to entangle once exceeded a certain MW), depending on the intended application.

1.6 Branched polymers: tailoring conventional PLA properties

In the last decade, branched poly(lactide)s have attracted great attention from both a scientific and a commercial point of view, as a promising approach to overcome conventional PLA disadvantages on industrial production.[132] Despite initially branched polyesters application was mainly restricted to the biomedical field (*e.g.* drug-delivery, tissue engineering, bioimaging, thermoplastic hydrogels),[80,133–135] recently a number of ways to develop diverse branched polyester architectures have been reported because of their interesting and easily tuneable thermal, rheological, mechanical and degradation properties with respect to their linear analogues.[81,126,127,130,132,136] Indeed, the well-defined branched PLA structure provides decrease of viscosity and crystallinity, thus reducing of typical PLA brittleness and improving processability without loss in mechanical performances.[81,137] As a matter of fact, branching strategy has been widely exploited to improve thermoplastic polymers performances. This approach gave rise to successful and well-known products such as LLDPE (linear low density PE) and LDPE (low density PE), which present polyethylene frameworks bearing different branching chain-length and concentration.[82,138–140] Therefore, branching PLA represents a valuable tool to finally enable high-performance and versatile PLA materials. To this aim, fundamental understanding of branched architectures and their influence on polymer properties could provide functional tailoring of poly(lactide) properties depending on the desired application.

1.6.1 Types of branched polymers

As previously mentioned, topology manipulation provides an alternative mean to modulate the material properties of polymers. Other than the linear polymeric structure (no branching), several types of branched architectures exist, showing either similarities or peculiar characteristics, depending on the number/kind of branch points and their arrangement in the macromolecular backbone. Branched macromolecules are divided in the following major groups (Figure 1.8):[141,142]

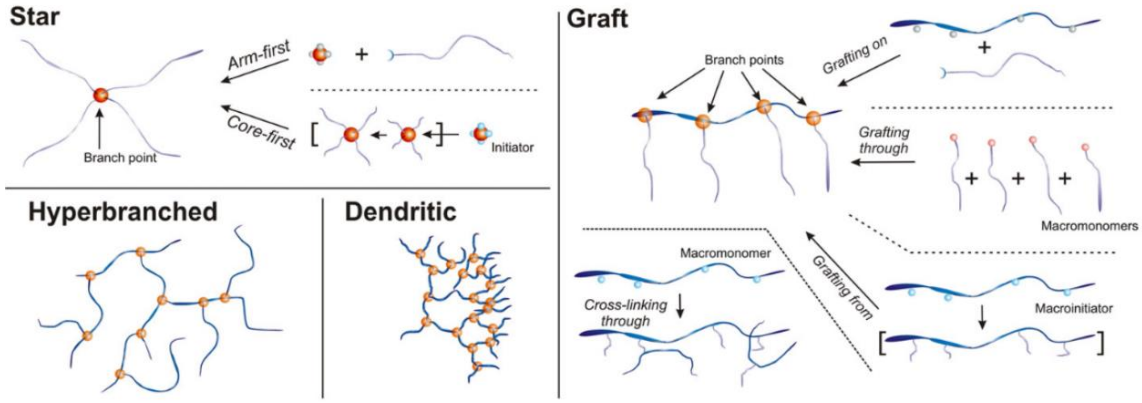

Figure 1.8: Summary of the major branched macromolecular architectures[142]

I) Star polymers: macromolecular architectures which present a single central branch point, defined as the "core", from which diverse linear chains originate, defined as "arms".[142] The core can be either a small compound or a macromolecule. The arms have typically equal chain length and can be formed by homo- or copolymers (statistical or block), as well as differ from each other in chemical nature of the backbone (miktoarm stars). The most used synthetic method, *called core-first*, employs a pre-synthesised multifunctional initiator (core) to form star polymers by divergently growing linear polymer chains (arms).[133] The independent synthesis of the arm (*arm-first*, convergent approach) is less frequent, as the steric hindrance between close polymeric chains typically prevents quantitative functionalization of the core. Indeed, a well-defined star-shaped structure should present arms of identical chain length and equal functionalization of all core molecules (same number of arms).

II) Graft polymers: macromolecules composed of side polymeric chain(s) (characterized of any configuration or conformation feature) connected to a main chain with different chemical composition. In one case the side chains can be pre-formed and directly coupled onto the main chain (*grafting on*) or used as macromonomers to form the main chain (co-)polymerization (*grafting through*). Alternatively, the side chains can act as macroinitiator, thus directly polymerizing the side chains from pendent groups present on the main chain (*grafting from*). Comb polymers are frequently used types of graft polymers where linear polymeric side chains (>1) depart from (regularly or irregularly spaced) branch points presents on the main chain.[142]

III-IV) Dendritic and hyperbanched polymers: macromolecules bearing a nested structure of branching points. This structure forms a regular and cascade-like architecture in the case of dendrimers, while is randomly organized for hyperbranched polymers, which have statistically identical number of sub chains in any direction (yet they can have different length). They can be prepared similarly to star-polymers.[132,142]

1.6.2 Rheological properties and effect of branch length

In the same environment (temperature and solvent), a branched polymer presents a higher segment density and lower hydrodynamic volume compared to a linear polymer with comparable molecular weight.[143] This can be always demonstrated by comparing branched and linear polymers of same Mw through triple detection GPC analysis, where the former yield lower intrinsic viscosity (lower hydrodynamic volumes) than their linear counterparts, due to the contracted structure.[144–148] The value of [η] is measured directly by the viscosity detector, given the Mark Howink (MH) relationship:[149,150]

$$[\eta] = K M_w^a$$

where *K* and *a* are the Mark-Howink constants. An example of intrinsic viscosity reduction with increasing branching (star polymers with increasing number of arms) is reported in the log-log plot of [η] vs Mw in Figure 1.9.[151]

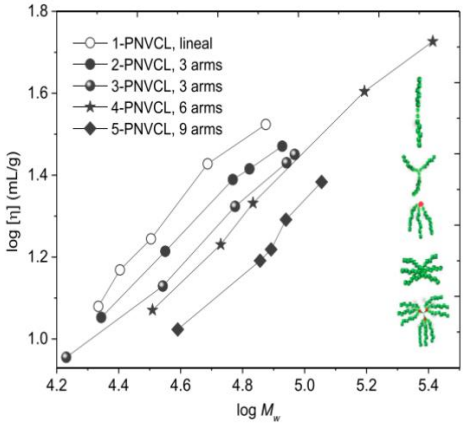

Figure 1.9: Log-log plot of intrinsic viscosity vs weight average molecular weight for linear and star-shaped poly(N-vynilcaprolactam)s (PNVCL).[151]

Noteworthy, the MH exponent *a* (typically assuming values <2) is characteristic for the solvent quality and polymer flexibility. The value *a* =0.5 indicates a *theta* solvent.[152] For the same solvent and conditions, a high value, such as *a* =0.9, indicates a good solvent and a stiff polymer chain (e.g. perfect rod geometry). Given the reduction in intrinsic viscosity for branched polymers, *a* systematically decreases toward values lower than 0.5 is observed for increasing contraction, hence increasing branching, as the macromolecule approaches a globular structure (*e.g.* star and

comb polymers).[17,153] However, the extent of *a* variation with the branching strongly depends on the chemical nature of the polymer backbone.[154,155]

Other useful parameters related to macromolecular conformation and topology are the hydrodynamic radius (R_H) and is the root-mean-square radius of gyration, R_g (or simply radius of gyration). R_g^2 is defined as the average distance of the points of the polymer chain from the centre of mass of the chain. Roughly, the chain occupies a sphere of radius R_g[152]. Therefore, both R_g and R_H parameters give information regarding the polymer size, which tends to decrease with the branching degree. The radius of gyration is typically calculated from multiangle light scattering measurements (MALS), while the hydrodynamic radius is determined by dynamic light scattering (DLS) or viscosimetric measurements (as R_H can be approximated to the viscosimetric radius Rη).[156,157] Both analysis may be coupled to GPC columns, thus allowing parallel evaluation of molecular weight. By dividing the R_g^2 of branched polymer to the corresponding value of a linear analogue with equal Mw, it is possible to calculate the contraction factor *g* (also known as index of branching): [149]

$$g = \frac{Rg^2_{branched}}{Rg^2_{linear}}$$

This parameter expresses indeed the degree of branching. For a linear chain, *g* is equal to 1.0 and decreases toward 0 along with increasing branching degree[143]. Alternatively, for a given branched structure, the ratio of its radius of gyration to the hydrodynamic radius results in the shape factor (ρ), as shown in the following equation:[157,158]

$$\rho = \frac{R_g}{R_H}$$

As a reference, the characteristic ρ value for a globular macromolecule is ~0.8. However, when chain conformation deviates from globular to non-spherical or elongated structures (*e.g.* linear polymers in *theta* conditions), then ρ tends to increase toward values higher than 1.5, as R_g becomes larger than R_H.[149,157,158] Unfortunately, MALS measurements of radius of gyration are generally non reliable for low-MW chains polyesters (R_g<10nm, generally for Mw≈10 kDa) due to the absence of detectable anisotropic scattering,[143,159] thus analyses of [η] and *a* constant values are more frequent for characterization of polymer topology in solution.

Even though branched polymers present much lower capability of forming chain entanglements than the linear ones, it is important to mention that the branch length plays an important role in defining the viscoelastic properties of the final branched polymer. Indeed when exceeding a certain critical branch size (entanglement molecular weight, *Me*), the branches start to entangle and may eventually reach higher viscosities than corresponding linear polymers, due to resulting lock of longitudinal motion.[143]

In this context, melt rheological properties of linear and branched PLA were firstly studied by Dorgan and co-workers.[160,161] From shear rheometry measurements at 200 °C, it was calculated that linear PLA (98:2 *L*/*D* enantiomeric ratio), has *Me* of approximately 9 kDa, while for the corresponding branched PLA the estimated molecular weight for branch entanglements ($Me_{,branch}$) was estimated to be 35 kDa. Additionally, as expected the observed branched viscosity was always lower the linear architectures, especially at high shear rates and for lower molecular weights materials. Indeed, it has been demonstrated that the viscosity of branched polymers increase faster with molecular weights than the linear ones.[152,157,160] The branched architectures are also known to exhibit more significant shear thinning, which provides easier melt flow during processing and represents a useful feature for numerous manufacturing processes (*e.g.* cast extrusion, stretch blow molding, foaming).[85,131]

However, several recent works lack specific information regarding the effective molecular weight and the type of branching structures employed, as the branching is often introduced by direct reactive extrusion, through functional groups or free-radical agents (*e.g.* epoxy, peroxides, diisocyanates).[85,126,130,132] With such processing methods, branching is introduced in a random and poorly controlled fashion through *arm-first* approach (*i.e.* existing linear PLA chains are connected to form a branched framework by means of coupling reagents). This results in long chain-length and highly entangled branches, along with a broad distribution of branch densities and, if the branching agent content is too high, partially cross-linked networks. These branching methods thus make difficult to separate the effect of branching distribution and molecular weight, as branching through reactive extrusion may also increase the molecular weight.[135] Indeed, the resulting polymeric structures often present high degree of entanglements, yielding increased viscosities, lower degradation rates and, if stereoregularity is achieved, higher crystallinity values than the corresponding linear PLA.[130,132,162–164]

Unlike randomly branched polymers, the direct use of well-defined branched architectures, such as star or comb PLAs, allows higher degree of control over the molecular structure,[143] as well as the most significant change with respect to linear PLA,[85] thank to their highly controlled architectures.[81,132] For this reason, the discussion will be focused on the properties of these

valuable macromolecular architectures of PLA, also considering reasonably short branch chain-lengths.

1.7 Star-shaped PLA

1.7.1 Functional features and potential applications

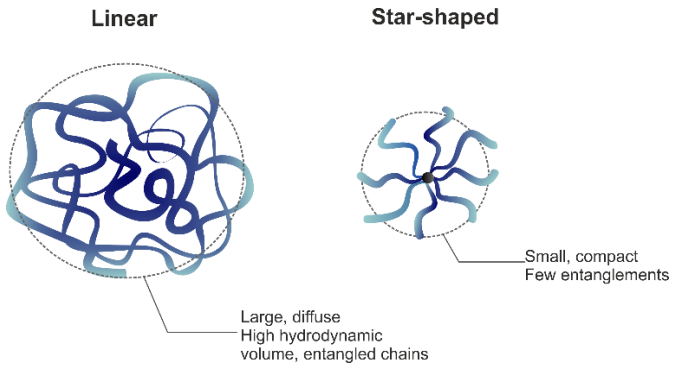

Figure 1.10: Graphical representation of linear vs star macromolecular conformations (with comparable MW)

The rising interest of bioplastics producers towards star PLA macromolecular frameworks is due to their controlled, easy-tailorable and functional features to improve common linear PLA disadvantages. As mentioned, the introduction of branch points is an interesting strategy to reduce both viscosity and crystallinity of a polymer and, as a result, also enhance ductility and processability without drastic material degradation.[81,132,143] The presence of a single branch point per macromolecule, as the well-defined star-shaped structures, can be already sufficient to drastically reduce entanglements, while providing optimal control on final PLA properties with respect to randomly branched structures.

Such features are particularly interesting for the production of green plasticizers (increasing ductility and toughness) and/or fluidizers (decreasing polymer viscosity) of conventional linear PLA, without the need of compatibilizers or altering the chemical nature of the material, due to the identical chemical backbone.[81,165]

In this context, it is of outmost importance to tailor the balance between topology (location and number of branches) and also tacticity (as stereoregularity affects crystallizability) to rationally affect the processing performance of a polymer using branched additives.[132,166]

1.7.2 Thermal properties and combined effect of stereochemistry

Given the low entanglements, branched polyesters exhibit lower melting point and glass transition temperature.[81,133,145,167,168] The presence of the branch points in fact reduces the capability of both inter- and intramolecular chain folding, with consequent suppression of crystallinity and lower crystallization temperatures (Tc).[81,129,168–171] However, also the thermal decomposition temperatures of star PLA was shown to be slightly lower than that of linear PLA (*i.e.* 287 °C vs 307 °C for star-shaped and linear PLLAs with Mw ≈ 70 kDa)[172].

In general, by increasing the number of arms, the branching effect becomes more significant, with further decrease in Tm, crystallization rate and crystallinity, although small changes in glass transition are generally detected with varying branching.[81,173] However, increasing number average molecular weights per arm (Mn_{arm}) reasonably results in higher glass transition and melting temperatures, independently of the branching (as typical effect of increasing molecular weight on polymer thermal properties).[129,174]

As for linear PLA, the arms stereospecificity in polymer stars also plays an important role. For example, atactic PLA (PDLLA) stars exhibits the lowest Tg, compared to isotactic star-shaped PDLA and PLLA.[80,81] Similarly, Tm can be tuned either by increasing the stereoerrors into the frameworks or by incorporation of increasing atactic star PDLLA contents in a given PLA-based polymeric blend[166]. Therefore, star-shaped atactic PDLLA can be used to obtain lower Tg values and suppress crystallinity, due to the combined effects of increasing macromolecular disorder and lack of stereoregularity.

1.7.3 Mechanical properties

Branched PLA can be either blended with other polymer architectures or processed alone in order to enhanced mechanical performances compared to conventional linear PLA-based materials.[80,81,132,133] As a consequence of the reduction in Tg and crystallinity, star-shaped PLA presents a more ductile mechanical behaviour.[133] The introduction of star-shaped PLA architecture typically determine significant improvements in elongation at break, as well as higher yield elongation and toughness values. However, this is often accompanied by a certain loss in stiffness and strength, which is a common consequence to mechanical ductilization.[168,175] As an example, Karidi *et al.* compared the tensile stress-strain curves of diverse low-MW star PLLAs with the corresponding linear PLLA, revealing that the presence of even 4 arms (star-shaped) can already significantly change the elongation at break and the elastic modulus with respect to the linear structure (+ 680% and -20%, respectively).[176] In another work, a star-PLLA obtained from a trifunctional polyether polyol core was successfully blended with a

semicrystalline linear PLA, reporting increased flexibility and heat resistance without affecting the compostability, due to plasticizing effect of the branched architecture.[177]

1.7.4 Degradability

As previously discussed, branching greatly affects the crystalline content of PLA. Therefore, much research has focused on tailoring PLA (bio)degradation kinetic through chain architecture manipulation.[143,178] Since degradation preferentially occurs in the amorphous regions of semicrystalline PLLA, an increase in the number of branches enhances both enzymatic and hydrolytic degradation of the material.[179,180] In general, poly(lactide)s with graft or star architectures are mostly amorphous and have more flexible structures than their linear analogues, thus showing faster hydrolysis.[179,181] Indeed, also in the case of a star-shaped PDLLA, the observed biodegradation rate was higher than the linear PDLLA of similar molecular weight (Mw≈30 kDa).[182] Moreover, the higher density of hydrophilic terminal groups of star-shaped PLLA (xylitol core) has shown to dramatically improve hydrolisability compared to linear PLLA, with faster erosion profiles (weight loss vs time) along with increasing branching degree.[183] Interestingly, the enzymatic degradation rate was often found to be dependent on the average molecular weight of the polymer arm, rather than the overall molecular weight of the PLA.[128,169,179]

It is important to mention that also barrier properties could be affected by the presence of branching, due to their increased hydrophilicity and flexibility. However, the use of star-shaped PLA is expected to determine less significant changes than in the case of hydroxylated low-MW plasticizers such as oligo-PEGs, at least in terms of gas permeability, due to the increased density of these frameworks.

1.7.5 Future perspectives

Given their high versatility and functional properties with respect to common linear PLA drawbacks, star-shaped poly(lactide)s may be efficiently exploited as highly-compatible plasticizers and flow modifiers of conventional PLA.[81] This bulk modification strategy holds great potential for industrial applications, as it would provide high-performance and tailor-made PLA materials with lower costs than the challenging implementation of PLA co-polymers and compatibilizers for large-scale production.

The rising demand in branched polymers for PLA modification has stimulated extensive research (from both an academic and industrial point of view) for the development of versatile

and scalable methods to produce well-defined, easy-tailorable branched poly(lactide)s structures.[133,163,184]

Nevertheless, the complex design and often troublesome synthetic methods available for star-shaped (as well as other branched architectures) polyesters production compared to their linear analogues, have limited their vast exploitation for industrial purposes.[133,169] Despite the advances in living polymerization protocols have improved the accessibility to star-shaped polymers, the existing methods still provide several difficulties in the obtainment of controlled architectures with high MWs and narrow MW distributions,[133,142] which would ensure suitable performances as functional additives of conventional PLA on industrial scale.[185]

This is a crucial issue and thus need to be addressed in order to promote extensive exploitation of star-shaped PLA, as it will be thoroughly discussed in *Chapter 4*.

1.8 Thesis objectives and organization

The main aim of this work is to improve the mechanical, rheological and (bio)degradation performances of conventional PLA (linear semicrystalline PLLA). This is a hot area of research, which is instrumental to make poly(lactide) materials more competitive on the market, and, in principle, to allow them to replace oil-derived commodities. It was planned to achieve this aim by employing and, when needed, producing polyesters with tailor-made macromolecular architecture and optimizing their processing. Specifically, this *Thesis* focused on poly(lactide) structures with a controlled degree of branching as the means to improve conventional poly(lactide) performance for the efficient production of flexible and highly biodegradable PLA products with enhanced processability.

Randomly branched polymers, with broad distributions of MW, branch chain-length and dispersities, have been employed as modifiers of the flow properties of thermoplastics. However, the presence of a single branching point per macromolecule, as in the much better defined star-shaped polymers, may be already sufficient to drastically reduce entanglements, with consequent impact on linear PLLA typical brittleness, troublesome processing and slow biodegradation.

Indeed, the introduction of branching is an interesting strategy to modulate (decrease) both viscosity and crystallinity of conventional PLA and, as a result, enhance its ductility, biodegradability and melt flow. Given these interesting properties, star-shaped PLAs holds great potential as green and highly compatible modifiers of conventional linear PLLA.

As previously discussed, several parameters need to be taken into account when designing a new PLA-based system, according to the desired application. Therefore, this study followed specific research phases in order to assess the potential of branched poly(lactide)s structures in terms of material performance, processability, relevance in the polymer market and customizability for diverse purposes.

Chapter 2

Preliminary assessment of the potential of short-branched star PLA as efficient plasticizer of conventional PLA was firstly required. To this aim, the effect of a star-shaped PDLLA on rheological, thermal, mechanical and biodegradation properties of a linear PLLA was evaluated, through melt-blending of the two components. Commercially available polymeric compounds and direct melt-fabrication methods (compression molding) were employed in this first research phase to maximize material availability and assess the feasibility of this strategy to improve

conventional PLA properties. Performances of the resulting star PDLLA/linear PLLA (SL PLA) blends were compared to the major commercially available petroleum-based and bio-based polymers. Most importantly, the effect of increasing star PDLLA contents on biodegradability of these *all-PLA*-based products in seawater was analysed, as essential assessment of star-shaped PLA relevance in the development of functional PLA-based materials.

Chapter 3

In the second phase of this work, the scalability of star PDLLA/linear PLLA blends production, as well as the effect of processing on final material properties, were assessed. PLA products based on diverse mixtures of a star-shaped PDLLA and semicrystalline linear PLLA were developed through industrially relevant manufacturing techniques, *i.e.* extrusion coupled to compression molding and injection molding. The tunability of rheological and mechanical performances of conventional PLA through branched PLA incorporation was investigated by complete characterization of the materials after each processing cycle.

Chapter 4

Given the promising results achieved, the research moved to a phase of properties-by-design, employing a library of multi-armed poly(lactide)s with varying architecture (linear, star, comb) and tacticity (PDLLA, PLLA, PLLA-*block*-PLLA) for a systematic investigation of these variables on the rheological, thermal and mechanical performances. As a necessary step to this aim, a gap in the existing literature was tackled, which is the development of a versatile and controlled synthetic method for the production of branched poly(lactide)s with relatively high-MW and narrow molecular weight dispersity, in addition to a well-defined multi-armed architecture. Therefore, the first optimization phase of a novel lactide ring-opening polymerization (ROP) protocol is described in the first part of this chapter, followed by critical material characterization of the diverse branched structures produced, according on their topology and stereoconfiguration.

For each research phase of this work, careful selection for the diverse chemico-physical parameters, *i.e.* topology, stereoconfiguration, molecular weight, of the branched structure was performed. Indeed, it is essential to rationally tailor the balance between these structural factors in order to maximize the effect of the branched PLA architecture on conventional PLA performances, according to the desired properties: higher ductility and toughness, enhanced processability and biodegradability.

Chapter 2 .Evaluation of star PDLLA effect on conventional PLA properties

2.1 Introduction

As discussed in *Chapter 1*, commercially available poly(lactide) (which is a semicrystalline linear PLLA) knowingly present excessive brittleness and poor toughness. Such disadvantages still limit its application for flexible and transparent single-use products (*e.g.* packaging films and containers, cups and bottles, bags, cutlery) as well as its processability.[10] Bulk modification of PLA through blending represents the most direct and cost-effective approach to improve such properties. However, it may imply some complications caused by the poor interfacial adhesion of the blending components with PLA. Indeed, common strategies such as blending PLA with plasticizers (*e.g.* lactic acid or oligo-PEG)[90,186] or rubbery polymers (Tg < RT)[14,187] often lead to additive migration or phase separation phenomena, which result in weak mechanical performances and thus poor applicability of the material.

Alternatively, blending branched and linear PLA architectures represents an interesting strategy to tailor conventional PLA properties without changing the chemical nature of the materialhe use of a branched PLA modifier would ensure high miscibility without need of compatibilizers (due to the identical chemical backbone), and enhance material flexibility.[143,188] Particularly, the incorporation of a well-defined star-shaped PLA structure could be even more effective in improving ductility and stress resistance of the material, as well as its processability, given the low likelihood of entanglements, highly compact structure and reduced viscosity of such PLA architecture.[85,132]

Moreover, branching introduction would potentially accelerate the well-known slow biodegradation (both in soil and marine environment) of commercially available PLA.[60,189] Indeed, biodegradability is an essential yet still challenging property to achieve for currently crystalline high-MW PLA consumer products.[64] It is thus essential to develop PLA-based

materials with sufficient strength and durability while also being biodegradable. In this context, branching inherently multiplies number of peripheral hydrophilic functionalities available for hydrolysis and enzymatic digestion, with interesting impact also on the overall material hydrophilicity and water permeability.[179,180]

Despite the use of a high-MW PLA component may be required to impart sufficient structural strength and durability to the final material, the incorporation of a star-shaped PLA with relatively low molecular weight (hence bearing short-chain branching) and random stereoconfiguration (PDLLA) could enhance the plasticizing effect and decrease melting and crystallization points for better processability.[129,190] Therefore, the functional features of star-shaped PDLLA could provide miscible and flexible *all-PLA*-based materials with improved biodegradability.

Although in some cases branched PLLA/linear PLLA blends have been investigated for improvement of mechanical and thermal properties of conventional PLA,[85,188,191–193] the information regarding performances resulting from branching of PDLLA are still very limited, especially considering properties different from the mechanical ones.[178,179,194] Moreover, such methodologies rarely consider scalable or solvent-free fabrication methods.[192,193]

2.1.1 Abstract

Diverse star PDLLA/linear PLLA blends were developed, in order to evaluate the miscibility of star PDLLA and linear PLLA components and study the effect produced by increasing star-shaped structure concentration on final material performances. To this aim, the polymeric components were blended through a direct and simple melt-processing method, *i.e.* compression molding (Figure 2.1). Optical, thermal, mechanical, morphological and hydrodynamic properties of the final star PDLLA/linear PLLA blends (SL PLA blends, Figure 2.1) were characterized and compared to other commercially available petroleum-based and renewable polymers, thus evaluating the relevance and versatility of the novel polymeric systems. Since performance improvement is hardly useful without, at least, maintaining the original PLA biomass content, biodegradability of the produced SL PLA blends in seawater was investigated.

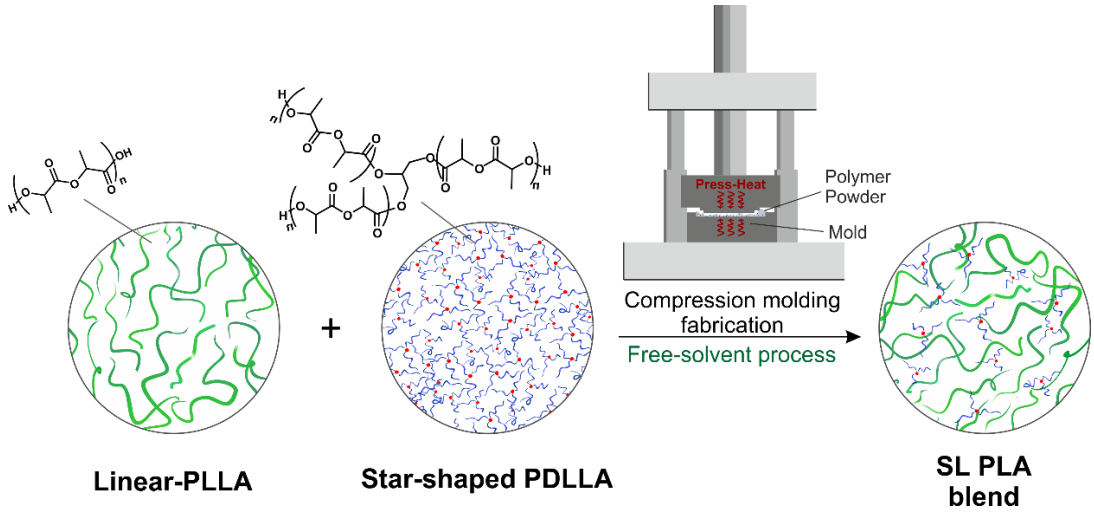

Figure 2.1: Schematic macromolecular representation of linear PLLA and star PDLLA melt blending process through compression molding.

2.2 Materials and Methods

2.2.1 Materials

3-Armed star-shaped poly(D,L-lactide)-glycerol (atactic star PDLLA) powder, a product of PolySciTech®(USA), was supplied by Microtech Srl (IT). High L-content linear poly(lactide) (D isomer content of ~4.25%, 4043D Ingeo® polymer), hereafter denoted as linear PLLA, is a multipurpose grade PLA and was purchased from NatureWorks LLC (USA) in the form of pellets. Molecular weight of the components was assessed by GPC analysis: A Mw of 8.5 kDa MW distribution (Đ) of 1.2 was measured for star PDLLA; linear PLLA reported Mw equal to 142 kDa and 1.3 Đ value. Linear PLLA was grinded into a powder of 3 mm particle size prior to use by means a Pilotina MC-IKA dry mill (IKA-Werke GmbH, DE), to ensure better blend homogenization during the fabrication process. Both starting materials were dried at 50 °C under reduced pressure for 8 hours prior to use in order to remove any adsorbed water moisture (< 250 ppm).

2.2.2 Fabrication of SL PLA blends

Six blends with different star PDLLA contents (sample labeling and composition is reported in Table 2.1) were fabricated by applying identical compression molding method: the appropriate amounts of linear PLLA and star PDLLA were mechanically mixed at room temperature and the mixture was subsequently melted in a square mold (~100μm thickness) by means of a bench CH Carver Press (Carver, Inc. (US)). First, each sample was heated above melting temperature

(170 °C) for 10 minutes with no pressure, thus allowing the polymeric materials to gradually melt and diffuse into the other component phase. Under the same temperature conditions, a 200 Pa pressure was then applied for 10 minutes to shape the final material into a homogeneous film. Finally, keeping the same pressure, the mold was rapidly cooled down to room temperature (RT) to stabilize product dimensions by means of a hydraulic cooling system, thus reducing possibility of crystallization. For all star PDLLA/ linear PLLA compositions, free-standing films were obtained. SL-0 film (100% w/w of linear PLLA) was also prepared as reference. SL-100 (100% star PDLLA) was subjected to identical conditions but a proper free-standing film could not be obtained given its Tg<RT.

Table 2.1: Labels of the fabricated samples and corresponding content in star PDLLA and linear PLLA.

Sample label	Star PDLLA content (% w/w)	Linear PLLA content (% w/w)
SL-0	0	100
SL-5	5	95
SL-10	10	90
SL-20	20	80
SL-50	50	50
SL-100	100	0

2.2.3 Morphological characterization

Surface micromorphologies of the SL PLA films were investigated by scanning electron microscopy (SEM), using a JEOL JSM-6490LA microscope working in high vacuum mode, with an acceleration voltage of 10 kV. The samples were previously mounted on metal stubs and, then, coated with a 10 nm gold layer by using a high-resolution sputter coater Cressington 208HR.

X-ray diffraction (XRD) measurements were performed on a PANalytical Empyrean X-ray diffractometer using a Cu Kα anode (λ = 1.5406 Å) operating at 45 kV and 40 mA. The diffraction patterns were collected in the range 2-70° 2θ with a 0.04° step size.

2.2.4 Mechanical characterization

Mechanical properties of the SL-PLA films were measured by uniaxial tensile tests. A dual column Instron 3365 universal testing machine equipped with a 500 N load cell was employed for the analysis. The tensile measurements were conducted according to ASTM D882 Standard Test Methods for Tensile Properties of Thin Plastic Sheeting.[195] All stress-strain curves were recorded at 25 °C. Ddumbbell shaped samples were stretched at a rate of 10 mm/min until failure. Ten measurements were conducted for each sample and averaged to obtain a mean value. The values of Young's modulus, tensile stress at maximum load, elongation at break, and toughness (area below the stress-strain curve, by definition the amount of energy per unit volume that a material can absorb before rupturing) were calculated from the stress-strain curves.

2.2.5 Thermal characterization

Differential scanning calorimetry (DSC) thermograms were acquired by a Diamond DSC (Perkin Elmer) though a single heating scan from -20 to 200 °C under a dry nitrogen flow (50 mL/min) at 10 °C/min heating rate. For this analysis, small pieces (~5 mg) were cut from the films and loaded in hermetic aluminum pans before running the DSC experiment. The melting (Tm) and cold crystallization (Tcc) temperatures were measured as maximum of the corresponding phase transition peaks. Glass transition (Tg) temperature was calculated by inflection method. Cold crystallization and melting enthalpies (respectively labeled as ΔH_{cc} and ΔH_m) were determined by integration of the corresponding DSC thermograms transition peaks and subsequent normalization to the relative star PDLLA fraction (being this component incapable of crystallization). Crystallinity (Xc) was finally calculated as follows:

$$X_c = \frac{\Delta H_m - \Delta H_{cc}}{\Delta H_m^{\,0}} \cdot 100$$

Where $\Delta H_m^{\,0}$ is the enthalpy of fusion of 100% crystalline PLLA (poly(L-lactide), 93 J/g).[196]

The thermal degradation behaviour of SL PLA films was investigated by thermogravimetric analysis (TGA) using a Q500 analyzer from TA Instruments. The measurements were carried out under an inert N_2 atmosphere on 3 mg samples in an aluminum pan at a heating rate of 10 °C/min from 0 to 800 °C. The weight loss (TG curve) was recorded as a function of temperature.

2.2.6 Water vapour transmission rate (WVTR) characterization

The WVTR of the samples was determined at 25 °C and under 100% relative humidity gradient (ΔRH%) according to the ASTM E96 standard method.[197] In this test, permeation cells with a 7 mm inside diameter and a 10 mm inner depth were used, filled with 400 μL of deionized water (which generates 100% RH inside the permeation cell).[198] The samples were cut into circles and mounted on the top of the permeation cells. The permeation chambers were then placed in 0% RH desiccator with anhydrous silica gel as a desiccant agent. The water transferred through the film was determined by the weight change of the permeation cells every hour during a period of 8 h using an analytical balance (0.0001 g accuracy). WVTR measurements were replicated three times for each film. The weight loss was plotted as a function of time and the slope of each curve was calculated by linear fitting. Then, the WVTR, normalized to the sample thickness, was determined as indicated below:[199]

$$\mathrm{WVTR}\left(\frac{\mathrm{g{\cdot}mm}}{\mathrm{m^2{\cdot}day}}\right) = \frac{\mathrm{Slope}\cdot\mathrm{Film\ thickness}}{\mathrm{Area\ of\ the\ film}}$$

2.2.7 Wettability and water uptake characterization

In order to characterize the surface wettability of the samples, water contact angles (W-CA) were measured with the sessile drop method at room temperature at ten different locations on each surface using a contact angle goniometer (DataPhysics OCAH 200). 5 μL droplets of milli-Q water were deposited on the surfaces and slide view images of the drops were captured. W-CAs were automatically calculated by fitting the captured drop shape. To evaluate W-CAs at equilibrium, the values were measured 2 min after drop deposition.

Water uptake measurements were carried out as follows: all samples were dried prior to use by conditioning in a desiccator until no change in sample weight was measured. The dry samples were then weighed (~30 mg) on an analytical balance (0.0001 g accuracy) and placed in different chambers at respectively 0 and 100% RH conditions. After conditioning in different humidity chambers until equilibrium conditions, each film was weighed and the amount of adsorbed water was calculated as the difference with the initial dry weight.

2.2.8 Biodegradation test

Biodegradability was evaluated on selected samples through a standard biochemical oxygen demand (BOD) test by measuring of the oxygen amount consumed during a biodegradation

reaction in seawater. For each sample, three measurements were collected and the results were averaged to obtain a mean value. Carefully weighed samples (~200 mg) were finely minced and immersed in 432 mL bottles containing seawater collected from Genoa (Italy) shoreline area. Oxygen consumed during the biodegradation process was recorded at different time intervals by using sealed OxyTop caps on each bottle, which can assess the oxygen levels. BOD from blank bottles filled with only seawater was also measured for reference.

2.3 Results and discussion

2.3.1 Material surface and structural morphology

Free-standing star PDLLA/linear PLLA (SL PLA) films were obtained through the compression molding process, hence avoiding the use of harmful solvents generally required for high-MW PLLA solubilisation.[200] The applied melt processing method allows good homogenization while also preventing linear PLLA crystallization, providing clear and flexible films. All SL PLA samples were obtained as transparent films (Figure 2.2A), due to the rapid cooling process, and showed increasing flexibility along with increasing star polymer content.

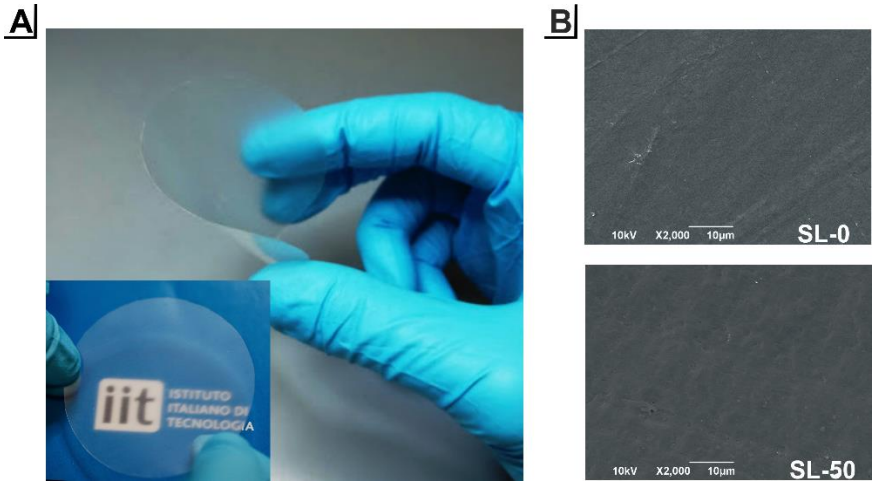

Figure 2.2: **A,** Representative photographs (SL-20) of the fabricated transparent and flexible star PDLLA/linear PLLA films. **B,** SEM top-view images of SL-0 and SL-50 samples. Scale bars: 10 µm.

Indeed, the incorporation of the star-shaped atactic structure into the high-MW linear PLLA matrix could favor the formation of a more ductile and tough material, without significant loss in structural strength and heat resistance. SEM surface analysis showed also homogenous and smooth surfaces of the SL PLA samples, independently of star PDLLA content (Figure 2.2B).

In order to evaluate possible differences in polymer crystallinity upon incorporation of the branched architecture, XRD diffractograms of the SL PLA films were acquired and compared to the pristine (pre-processing) linear PLLA (Figure 2.3). Pristine linear PLLA showed typical XRD pattern of a semi-crystalline α'-polymorph poly(L-lactide)[201] and crystalline planes were assigned as follows: (103) at ~12.3°, (104) at ~14.7°, (200) at ~16.6°, (203) at ~18.9°, (211) at ~22.2°, (213) at ~24.8°, (303) at ~27.1°, (310) at ~28.9°, (217) at ~31.0°, (126) at ~35.1°, (127) at ~37.8°, (416) at ~41.2°, and (135) at ~48.1°.[202] Characteristic peaks of crystalline PLLA were not observed for the SL PLA films, reporting in all cases a broad halo centered at ~19-20°, as the rapid cooling applied during the compression molding process did not allow ordering of the polymer chains. However, increasing integrals and intensities were clearly visible along with decreasing branching content, reasonably revealing certain contribution of overlapped crystals diffractions relative to PLLA crystalline domains. Therefore, SL-0 and blends containing low branched PLA content seem to exhibit a certain capability of chain association, with consequent increasingly amorphous character for increasing star PDLLA concentrations, due to the higher flexibility of the polymer coil.

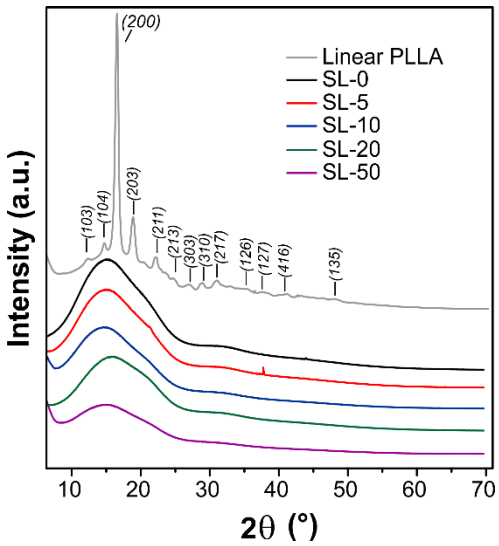

Figure 2.3: XRD patterns of SL-0, SL-5, SL-10, SL-20 and SL-50 films as a comparison to semicrystalline linear PLLA (pristine pellet). The assignment of the main diffraction planes for PLA is included.

2.3.2 Blend miscibility and thermal properties

In order to ascertain miscibility of the PLA architectures and evaluate the effect of star-shaped PDLLA on final thermal properties, the fabricated SL PLA films were characterized by DSC analysis (Figure 2.4). As shown in the reported thermograms, all samples present only one glass

transition, confirming the high miscibility of the two PLA architectures at the different components ratios (up to 50% w/w star PDLLA efficiently incorporated). Moreover, it should be mentioned that no change in mechanical, thermal or optical properties of the blends over time was detected. This demonstrated that no migration or phase separation of the polymeric components occur under normal usage conditions, due to the high compatibility of the two PLA architectures.

DSC curves showed certain enthalpic recovery in the glass transition region for all SL PLA films, as expected given the fast cooling rate during the fabrication process. Interestingly, gradual reduction of the glass transition temperature (Tg) was achieved through star PDLLA incorporation. Tg decreased from 59 °C for SL-0 up to 48 and 41 °C for SL-20 and SL50, respectively (Table 2.2). Such thermal behaviour clearly revealed the plasticizing effect of star-shaped PDLLA into the linear PLLA matrix.

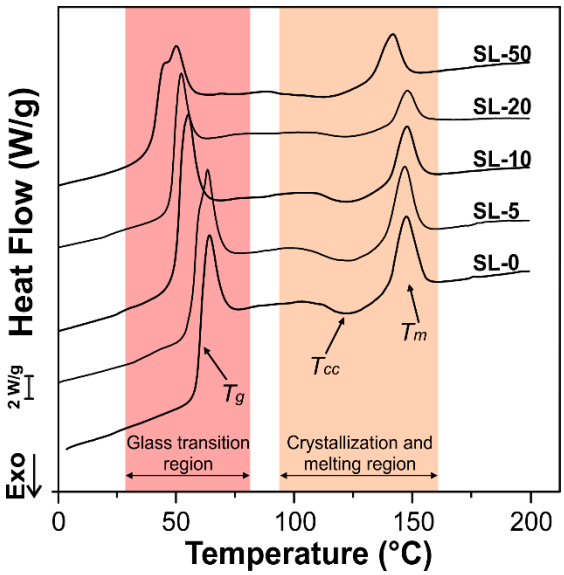

Figure 2.4: Differential scanning calorimetry traces of SL PLA films

Moreover, it should be noted that melting temperature (Tm) values remained substantially steady for all blends, with a maximum reduction of 3 °C in the case of SL-50 (Table 2.2) with respect to neat linear PLLA sample (SL-0). Crystallization was instead significantly affected by star-shaped PDLLA inclusion. Samples SL-5, SL-10, SL-20 and SL-50 showed progressively broader cold crystallizations exotherms and temperatures, due to crystals diversity and imperfection. The presence of PDLLA in fact inherently decreases the overall amount of crystallizable chains. Furthermore, here the increasing contents of the highly mobile and amorphous star-shaped structure hampered the growth of large PLLA crystalline domains and disturb crystallization of the linear PLLA chains. As a result, the capability of crystallization of

linear PLLA was reduced when higher amounts of star-shaped PDLLA were present, especially for contents higher than 10% w/w star PDLLA (Figure 2.4). A clear decreasing trend in crystallinity (Table 2.2) was observed, with values shifting from a 6.2% crystallinity for SL-0 to a minimum of 3.2% for SL-50. Such thermal behaviour confirmed indeed the evidences obtained from XRD analysis, thus demonstrating the contribution of star-shaped structure to the amorphous character of final SL PLA blends.

Table 2.2: Thermal properties of the fabricated star PDLLA/linear PLLA blends calculated from DSC thermograms, with respect to the pure linear PLLA (SL-0)

Sample	Tg, °C	Tcc, °C	Tm, °C	ΔH_{cc}, J/g [a]	ΔH_m, J/g [a]	Xc, % [a,b]
SL-0	59	125	148	28.6	34.4	6.2
SL-5	57	123	148	27.7	32.5	5.2
SL-10	50	123	148	23.4	26.8	3.6
SL-20	48	121	147	20.7	23.5	3.0
SL-50	41	115	145	21.3	24.3	3.2

Measured Tg for pure star PDLLA sample subjected to identical processing conditions (SL-100), was 15 °C. [a]Normalized values with respect to the corresponding star PDLLA fraction. [b]ΔH_m^0 =93 J/g for pure crystalline PLLA.[203]

2.3.3 Mechanical performances

The influence of the star-shaped PDLLA on the mechanical properties of the SL PLA blends was determined by tensile tests and resulting typical stress-strain curves are reported in Figure 2.5A. The graph clearly shows that mechanical behaviour progressively changed from rigid to ductile from SL-0 to SL-50.

As visible from Figure 2.5B, star-shaped PDLLA incorporation determined a linear decrease of the Young's modulus from 2.8 GPa for SL-0 to 2.0 GPa for SL-50 (*i.e.* a decrease of ~29%). Ultimate tensile strength was reduced from 45 MPa for SL-0 to 32 MPa for SL-10, then, the drop was attenuated to 25 MPa for SL-50 (*i.e.* a total decrease of ~44%). Despite this reasonable loss in material elastic response, the fabricated SL PLA blends reported a dramatic enhancement in tensile elongation at break, which was increased from 2.5% for SL-0 and SL-5 to 27.5% for

SL-20 and SL-50 (*i.e.*, an increase of 1100%). Moreover, toughness was also improved from 0.9 MJ/m^3 for SL-0 and SL-5 to 8.75 MJ/m^3 for SL-50 (*i.e.*, an increase of ~972%).

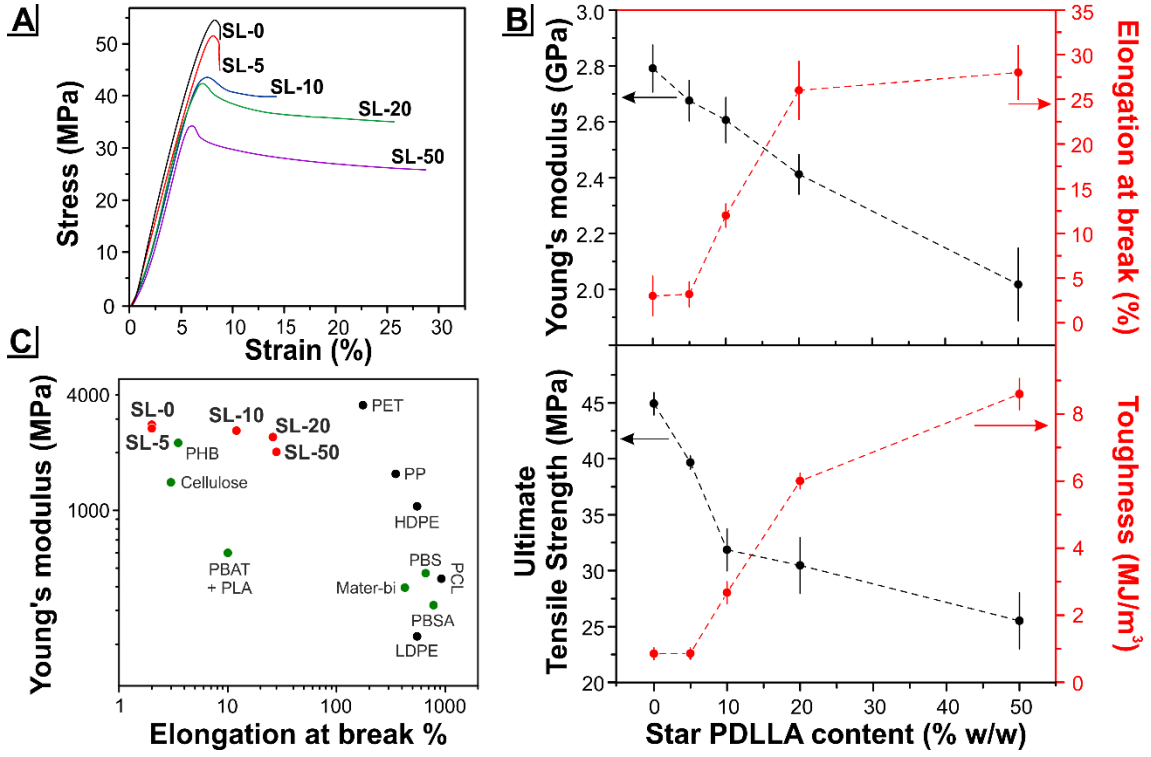

Figure 2.5: **A,** typical tensile stress-strain curves of the SL-PLA blends. **B,** variation of Young's modulus, elongation at break, ultimate tensile strength, and toughness as a function of star PDLLA content. **C,** Ashby plot of elongation at break versus Young's modulus data for various bio-based polymers (green) and petroleum-based commercial plastics (black) as a comparison to the SL PLA films (red) fabricated in this work.

Such results are very interesting if compared to commonly available employed small molecules used as plasticizers (*e.g.* lactic acid, citrate esters, oligomeric PEG) as they typically generate a more significant loss in original structural strength and stiffness, which is collateral to plasticization.[90,94,204] For a better evaluation of the mechanical properties of the produced SL PLA blends with respect to the plastic market demand, they were compared with other bio-based and petroleum-based polymers: PHB, cellulose, PBS, poly(butylene succinate adipate) (PBSA), Mater-bi® (a commercial composite trade name composed of corn starch and PCL), a PBAT/PLA blend, PET, PP, HDPE, LDPE and PCL.[6,17,47,205–207] Mechanical performances of these diverse polymers are displayed as an Ashby plot of elongation at break versus Young's modulus, Figure 2.5C. It is visible that SL-0 and SL-5 are more rigid than high-performance PHB, while SL-10, SL-20, and SL-50 samples cover the gap between high-performance and bio-

based polymers, such as PHB and cellulose, and the fossil-based PET and PP commodities, as they presents anyway discrete tensile modulus values.

These results denote the complementarity, in terms of mechanical properties, of these flexible SL PLA blends with commonly employed and commercially available polymers. Therefore, the introduction of star-shaped PDLLA allows the production of more flexible and resistant PLA product, which could be suitable for diverse applications, ranging from flexible packaging to agricultural mulching films.

2.3.4 Thermal degradation behaviour

The thermal stability of the SL samples was evaluated by TGA, Figure 2.6. In all cases, a single thermal decomposition step was observed, with a weight loss of 100%. Such behaviour of PLA thermal degradation can be associated with random main-chain scission, depolymerization, oxidation, and intra- and intermolecular ester exchange reactions.[208–210] Degradation temperature of the SL PLA films was found to be strongly dependent on the star PDLLA content (Figure 6B). Indeed SL-0 and SL-100 samples showed initial decomposition temperature (here defined as the temperature at which 1% of the mass is lost) was reduced from ~337 ºC for SL-0 to ~176 ºC for SL-100. A certain decrease in thermal stability was expected given the lower MW and branched structure of star component and such results are in accordance with previous findings for other low-MW additives.[211,212] Although SL-5, SL-10 and SL-20 blends reported a gradual decrease in degradation points, a further significant drop was observed for SL-50 (256 °C), suggesting that a lower star PDLLA content should be preferred if high operating or processing temperatures are required.

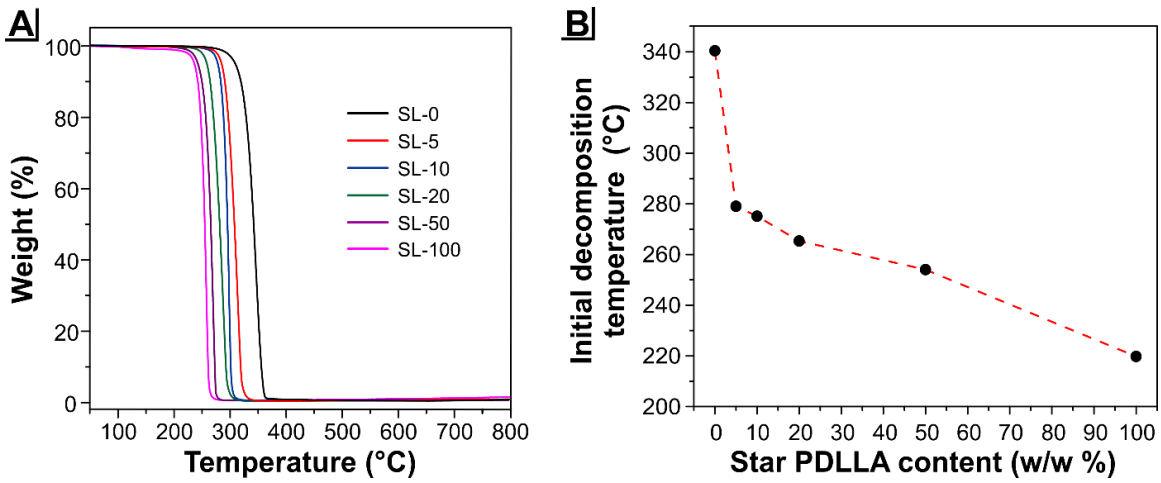

Figure 2.6: **A,** TGA thermal degradation traces of SL PLA samples, SL-100 is also shown for comparison. **B,** initial thermal decomposition temperatures as a function of star-shaped PDLLA content.

2.3.5 Water vapour barrier properties, wettability and water uptake

The incorporation of a star-shaped PLA with relatively low molecular weight in the conventional linear PLLA matrix can dramatically affect the hydrophilicity of the final material, as well as its permeability to water and moisture sensitivity. Indeed, the branched component presents a more mobile structure and higher number of terminal functional group available for polar interactions. However, conversely from the diffuse linear polymeric chains, star PDLLA possess a compact and dense core and this characteristic may reduce wettability and moisture sensitivity of the final blend.

In order to investigate such properties, water vapor transmission rate (WVTR) of the SL PLA blends was firstly characterized (Figure 2.7A). The measured WVTR values were: ~13.6 g mm m^{-2} day^{-1} for SL-0, ~17.4 mm m^{-2} day^{-1} for SL-5, ~25.9 mm m^{-2} day^{-1} for SL-10, ~296.6 mm m^{-2} day^{-1} for SL-20, and ~720.4 mm m^{-2} day^{-1} for SL-50. Such results allow to divide SL PLA blends into two groups, as SL-5 and SL-10 present low water vapor transmission rates, whereas for SL-20 and SL-50 films the WVTR was enhanced with respect to linear PLLA values. This can be related to the fact that diffusion of water molecules is facilitated in presence of the star-shaped component, due to the higher mobility of its macromolecular structure (negligible capability of chain entanglements) and the increased number of hydroxyl groups in comparison to the linear PLLA. Such polymeric framework may thus increase the possible water diffusion pathways, if the amount of star PDLLA is sufficiently high. Consequently, the final material could be employed for very different applications by simply varying star PDLLA content. WVTR values of SL PLA blends were compared with those reported in the literature for both high-water

barrier and breathable bio-based polymers used in food packaging (semicrystalline linear PLLA, poly(3-hydroxybutyrate-co-3-hydroxyvalerate) (PHBV), PCL and PBS) and biomedical scaffolds and textiles (cellulose acetate (CA), chitosan, and cellulose), respectively.[17,51,213,214] SL-5 and SL-10 were placed among the polymers used for food packaging, while SL-20 and SL-50 were compared to other breathable polymeric materials. Crystalline linear PLLA clearly reported a relatively lower WVTR than SL-0 (~10 mm m^{-2} day^{-1}).

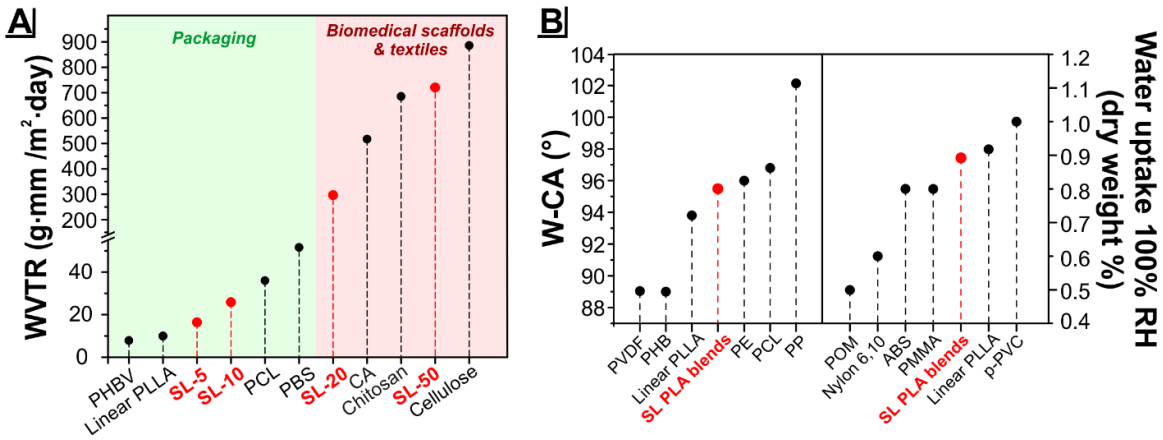

Figure 2.7: **A,** WVTR results for SL-10, SL-20 and SL-50 (red). Other commercial bioplastics and biopolymers (black) are reported for comparison purposes. Green area: typical WVTR data for packaging materials. Red area: suitable materials for biomedical systems and textiles. **B**, mean values of wettability and water adsorption (100% RH) data for SL PLA blends are shown in comparison to various conventional plastics presenting similar typical values.

The averaged W-CA and water uptake of SL PLA blends were measured in order to investigate the hydrophilicity and moisture sensitiveness of the produced blends, with respect to crystalline PLLA and other commercially available polymers (Figure 2.7B). Interestingly, all SL PLA films showed similar values of W-CA (95 ± 3°) and water uptake (0.9 ± 0.2 %), indicating that linear PLLA matrix controlled the interaction with water. Most probably, the branched macromolecules are mostly localized in the polymeric coil core (immersed in the material bulk), thus not affecting the original polymer-water interaction behaviour.

The W-CA were typical of hydrophobic materials (Figure 2.7, left). When compared to those of crystalline linear PLLA and other conventional hydrophobic polymers (*i.e.* polyvinylidene difluoride (PVDF), PHB, PE, PCL, and PP),[6,215] SL PLA samples reported average W-CA properties, with lower values than fossil-based polyolefins (widely used for their hydrophobic and apolar character), but better than PHB and PVDF (commercialized for water-resistant textiles). On the other hand, water uptake for all blend films was very low (<1%), also compared

to other hygroscopic polymers (*e.g.* nylon 6,10, polyoxymethylene (POM) acrylonitrile butadiene styrene (ABS), poly(methyl methacrylate) (PMMA), plasticized polyvinyl chloride (p-PVC)),[215] with an intermediate behaviour between PMMA and p-PVC, Figure 2.7 right. Interestingly, both W-CA and water-uptake parameters were close to commercial crystalline linear PLLA values, showing that star PDLLA did not caused deterioration of such properties.

2.3.6 Biodegradability in seawater

In principle only PLA modification methods which could increase (or at least preserve) original PLA biodegradability should be applied, independently of the improvement in polymer performances. Therefore, once ascertained the enhancement of conventional PLA performances through incorporation of star-shaped PDLLA, the biodegradation of the SL PLA blends was tested in seawater, as PLA generally reports the lowest biodegradability in marine environment.[63] The experiment was performed by measuring the biochemical oxygen demand (BOD) resulting by samples incubation in this active environment for a 30-days period. Figure 2.8A shows the oxygen consumption for all the SL PLA samples and a control of unprocessed linear PLLA (12% Xc). Interestingly, final BOD values increased along with star PDLLA content from ~2 mg O_2/L for SL-0 to ~13.9 mg O_2/L for SL-100. Star PDLLA-containing blends showed intermediate and progressively higher oxygen consumptions with branching content. Moreover, final BOD of linear PLLA was ~0 mg O_2/L, indicating a negligible biodegradation in 30 days. This result is in accordance with an insignificant degradation of poly(lactide) in seawater at room temperature previously described in the literature.[216] Noteworthy, star PDLLA reported enhanced biodegradation kinetics: the biodegradation process begun almost immediately for SL-100. Approximately 6 days were necessary for the SL PLA blends, with slower biodegradation rates (lower slopes) for decreasing star PDLLA content. Conversely, semicrystalline linear PLLA was not subjected to any biodegradation in the testing period. The higher biodegradation rates of SL-0 (processed 100% linear PLLA sample) with respect to the unprocessed linear PLLA sample were ascribed to the different crystallinity (detected by XRD), as they present identical chemical structure and molecular weight.[72,217] These results suggested that star PDLLA easily and rapidly breaks down in lactic acid oligomers compared to linear PLLA, due to the lower MW and higher hydrophilicity. Despite no enzymatic activity was detected after 15 days for all SL PLA samples, the enhanced coil flexibility and crystallinity reduction promoted by the branched structure induced higher biodegradation kinetics.

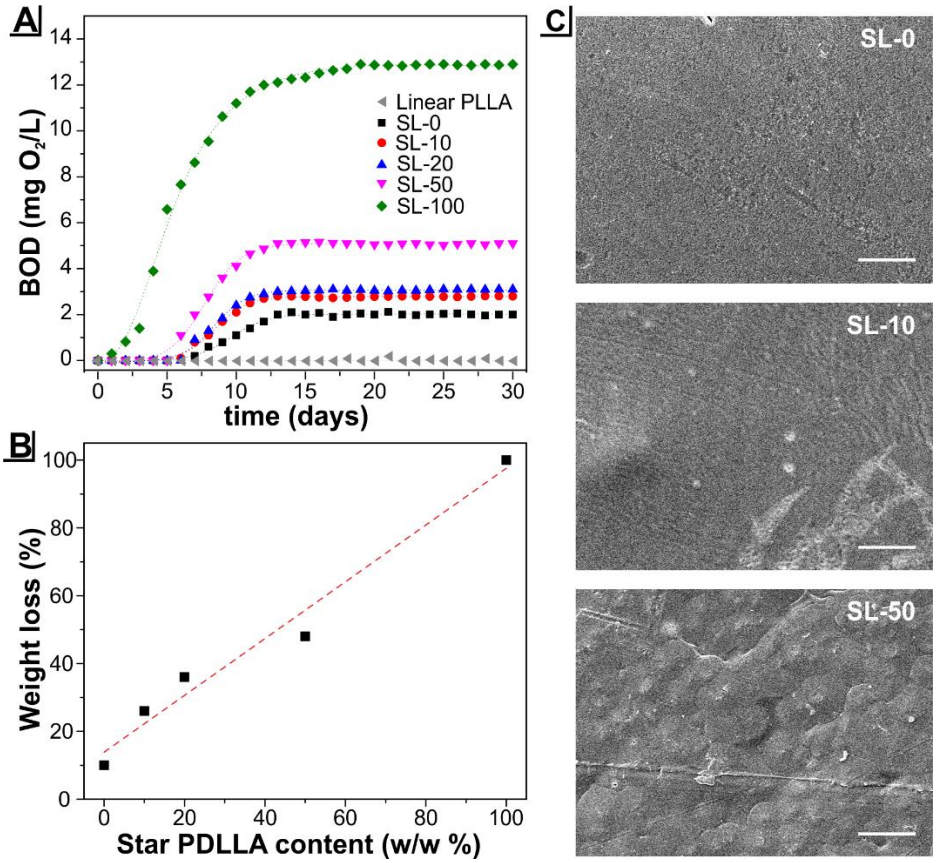

Figure 2.8: **A,** BOD curves of the SL PLA samples and pristine linear PLLA. **B,** weight loss of the fabricated samples caused by biodegradation after 30 days. **C,** SEM top-view images of SL-0, SL-10 and SL-50, respectively, after BOD experiment (30 days). Scale bar: 10 μm.

After biodegradation tests, remaining pieces were collected from the seawater solution to determine the weight loss, Figure 2.8B, and characterize surface morphology by SEM analysis, Figure 2.8C.

As expected, the weight loss was increased with the star PDLLA content ranging from ~10% for SL-0 to ~99% for SL-100 while the weight loss of the pristine linear PLLA was close to zero, in agreement with BOD results. SEM images showed a smooth surface with no apparent variation for SL-0, some defects and rough spots on SL-10 surface; SL-50 showed even rippled and cracked surface, generated by a more accelerated and intense biodegradation process.

These results are very promising if compared to other biodegradable polyester films, which have been subjected to biodegradation in marine environment under similar conditions in previous works: P(3HB) (Poly(3-hydroxybutyrate), 130 kDa, 70% Xc) reported a mass loss of ~25% after 3 weeks immersion in sea water;[218] the co-polymer P(3HB-co-11%HV) (Poly(3-hydroxybutyrate-co-11%hydroxyvalerate), 132 kDa, 69% Xc) has been shown to reduce is

weight of ~15% after 20 days upon biodegradation in marine environment;[219] also PCL (Poly(ε-caprolactone), 80 kDa, 52% Xc) showed a mass loss of ~21% after 4 week biodegradation in marine water.[220]

Therefore, the incorporation of the branched structure progressively increased water diffusion and available chain ends for hydrolysis, thus facilitating both the hydrolysis and enzymatic degradation processes. As a result, star containing blends present enhanced biodegradability with respect to linear PLLA sample.

2.4 Conclusions

In this Chapter, the production and tunable properties of diverse green blends, based on a star shaped PDLLA and a linear semicrystalline PLLA (conventional PLLA), were discussed. The direct and simple melt-manufacturing process of compression molding was used for the efficient fabrication of these *all-PLA*-based blends, obtaining transparent and flexible free-standing films.

This first research phase was indeed essential to understand the potential of star-shaped PLA as green and compatible modifier of conventional PLA, in terms of material performances and biodegradability with respect to other existing polymer products.

The stereoconfiguration and macromolecular architecture parameters of the blending component, as well as the processing settings, were accurately selected in order to obtain *all-PLA*-based materials with improved ductility, toughness and biodegradability with respect to conventional linear PLLA.

The use of a branched atactic PLA, along with the rapid cooling rate of the compression molding process, favored practically amorphous products. Since star-shaped PLA presents extremely low likelihood of chain entanglements, a star-shaped PLA structure with relatively low MW (short branch-chain length) was exploited in order to enhance the plasticizing effect on the linear PLLA matrix and suppress its crystallinity. Such features would in principle improve conventional PLA processability, *i.e.* promote lower resistance to flow upon processing and enhanced material elongation during manufacturing and product use.

The obtained properties for the SL PLA blends are very promising compared to common low-MW or polymer plasticizers, as branching allows dramatic improvements of ductility, as well as toughness, without significant loss in structural strength and perfect miscibility of the components. Moreover, facile tailoring of final mechanical, thermal and permeability properties is possible by simply varying star PLA content. Compared to the neat linear PLLA, the water

permeability of the material was slightly increased for blends with low branching concentrations (suitable for packaging products), while addition of >20% w/w star PDLLA provides breathable films, potentially exploitable for biomedical devices and textiles.

Despite the intrinsic scarce degradation of commercially available PLAs in marine environments, biodegradability in seawater was improved for star PDLLA-containing blends (higher BOD values and weight losses over a 30-days period).This is an essential property for efficient PLA-based products in order to functionally substitute fossil-based commodities.

The screening of diverse SL PLA blends with increasing star-shaped component concentration revealed that <5% w/w star PDLLA contents are unable to provide substantial impact on mechanical and water vapour barrier properties. On the other hand, 50% w/w star PDLLA concentrations excessively affected thermal stability, despite the drastic increase in ductility and biodegradability. Therefore, the diverse and significant effects resulting from branched PLA incorporation should be taken into account for future development of SL PLA materials, depending on the intended application.

Chapter 3 .Tailoring conventional PLA performances for large-scale manufacturing through star PDLLA incorporation

3.1 Introduction

The comparison of SL PLA blends performances with commonly employed polymers, discussed in *Chapter 2*, revealed that star PLA could be of interest for the industry as green and highly compatible modifier of conventional PLA. Indeed, introduction of star-shaped branching has been found to provide efficient tailoring of linear PLLA mechanical properties with no blend miscibility issues, in addition to enhanced material biodegradability. Therefore, this approach could enable the production of flexible and tough PLA-based products (*e.g.* flexible packaging films and tapes, cutlery, cups, biomedical devices), thus filling the gap in bioplastics market offer.

Therefore, once assessed the versatility and potential applications of star-shaped PLA, it was essential to evaluate the scalability of such star/linear PLA blends by means of high-throughput processing techniques commonly used to realize the aforementioned consumer products, such as extrusion and injection molding.[39,221]

One of the main issues to take into account proceeding into this second phase was the typical degradation of bio-based polyesters upon common manufacturing conditions, which involve high shear rates and heating.[13,16,78] Indeed, it has been demonstrated that PLA undergoes increasingly significant degradation for every processing cycle it is subjected to (*i.e.* from batch compounding of the raw material to the molding of the final commercial item).[13,37] PLA thermo-mechanical and thermo-oxidative degradation generally results in drastic losses in mechanical performance of the final product, with further increase in brittleness and poor optical properties. Such complication forces to keep low processing shear rates to avoid further material deterioration, thus consequently reducing PLA production throughputs.[13,75]

Therefore, the investigation of material degradation during PLA processing is essential to evaluate the performance of the selected processing configuration, as well as final product performances.

Despite thermal stability was found to be affected by star PDLLA incorporation upon the applied manufacturing conditions, this property could be easily improved by using a branched PLA architecture with slightly higher MW. Such modification could impart sufficient thermal resistance to the final material while preserving the functional effect of the branched architecture on mechanical performances, crystallinity and biodegradability. Furthermore, the analysis of the effect of increasing star PDLLA fractions on final blend properties from *Chapter 2* revealed that 5% w/w content of the star-shaped component provide small variation from neat linear PLLA properties. On the other hand, the addition of 50% w/w star PDLLA was found to consistently decrease the thermal stability and structural strength, which could lead to a final PLA-based product with insufficient mechanical and thermal resistance (especially upon the more drastic and prolonged processing conditions of extrusion and injection molding), as well as poor material durability, due to the extremely high degradation rate in aqueous environment and high permeability to water vapour. Therefore, the blends containing 10 and 20% of star-shaped PDLLA were selected for further scale-up of the SL PLA materials production process, as they had reported considerable improvement of ductility and biodegradability without drastic loss in material resistance.

The introduction of branching could have also important effects on PLA rheological behaviour. Indeed, it is well known that branched poly(lactide) structures, such as star-shaped PLA, exhibit lower viscosity and increased shear thinning behaviour than their linear analogues. Therefore, star-shaped PLA could act as a flow modifier for conventional PLA, reducing the melt flow during processing and thus allowing to work at higher shear rates (and potentially also lower temperatures) without consistent material degradation. The additional possibility to work at lower temperatures thank to the lower melting point of star PLA, could further improve PLA processability and reduce production energy costs.

The high compatibility of the star and linear PLA components represents another important factor for improving PLA performances. Indeed, extrusion is typically used as first processing cycle to achieve optimal mixing of the various compounds (*e.g.* blending components, additives or fillers) and obtain pelletized master batches for further processes that lead to the final polymer materials production.[222] The several required processing cycles consequently determine increased polymer degradation. Noteworthy, in the case of the studied star-shaped PLA architecture an optimal compatibilization of the components could already be achieved

through a direct injection molding process, eliminating the need of pre-blending extrusion step, as demonstrated in this chapter.

3.1.1 Abstract

In this chapter, the scalability and processability of enhanced PLA products based on blends of a star-shaped PDLLA and a conventional linear PLLA were thoroughly investigated. To this aim, the star/linear PLA materials were produced through typical large-scale manufacturing techniques for thermoplastic polymers. In the first case, the two polymers were blended through melt extrusion resulting into pellets, and subsequently the pellets were compression molded for the production of star/linear PLA (SL PLA) films. Alternatively, the star PDLLA/linear PLLA materials were developed by direct blending through injection molding in the shape of dumb-bell specimens (as representative shape of detailed items obtainable through this technique). Thermo-mechanical degradation induced by the different processes was evaluated and the performances of the SL PLA products were thoroughly compared. The effect of the short-branched, amorphous, star polymeric component on rheological, thermal and mechanical properties of the conventional PLLA was comprehensively investigated for both processing configurations.

3.2 Materials and Methods

3.2.1 Materials

Linear semicrystalline PLA Ingeo 4043D (Mw= 110 kDa, dispersity index Đ= 1.5, D-isomer content ~4.25%) was purchased from Resinex Srl (IT) and used as linear PLLA matrix. A star-shaped PDLLA (Mw= 19 kDa, Đ= 1.3) was supplied by Michrotech Srl (IT) and exploited as green modifier of the conventional high-L-content PLA. Both starting materials were grinded into powder of 3 mm particle size by means of a Pilotina MC-IKA dry mill (IKA-Werke GmbH, DE) for an optimal homogenization of the components. Resulting powders were dried at 50 °C under reduced pressure for 8 hours before any processing step to remove water moisture.

3.2.2 Blends preparation and processing

PLA blends. Blends of linear PLLA containing 0 (as reference), 10 and 20 % w/w of star PDLLA were produced by melt extrusion and injection molding as follows:

Extrusion/compression molding. Extrusion was performed using a co-rotating twin-screw Rheoscam extruder (Scamex, France) equipped with five temperature zones, at a screw speed of 300 rpm and a temperature profile ranging from 175 °C to 190 °C (die). The extruded filaments were subsequently pelletized and dried. The resulting blended SL PLA pellets were then compression-molded by means of a CH Carver Press (Carver, Inc. (US)), heating at 170 °C for 5 min with no pressure, followed by an applied pressure of 4 tons for further 5 min. For each blend, a free-standing transparent PLA-based sheet (~0.5 cm thickness) was obtained.

Injection molding. The polymer mixtures of star PDLLA and linear PLLA were injection molded at 190 °C by means of a Babyblast 6/12 injection molding machine (Rambaldi group, IT) into ISO normalized dumbbell-shaped mould of specimens for tensile testing (76 mm × 4mm × 2 mm). Mold temperature was set to 0 °C to ensure fast cooling ramp and avoid crystallization.

The blends produced in this study will be denoted in the rest of the text as PLA SLx, where x is the percentage of star PDLLA, followed by the corresponding processing method: *I*, *E* and *EC*, respectively for injection molding, extrusion, and extrusion followed by compression molding (extrusion/compression). For instance, PLA SL10_EC refers to the blend produced by extrusion of a 10% w/w star-polymer and 90% w/w of linear PLLA, followed by compression molding of extruded pellets.

3.2.3 Physico-chemical characterization

Gel permeation chromatography (GPC) was performed on an integrated OMNISEC system (Malvern Panalytical Ltd., UK) equipped with a D6000M and a D4000 column (10 and 6 μm particle size respectively, 300 x 8 mm) using a triple detection method (refractive index, viscometer, and dual angle light scattering detector at 7° and 90°). THF stabilized with 250ppm BHT was used as eluent at a temperature of 35 °C and a flow rate of 1.0 mL/min. The system was calibrated with Polystyrene (PolyCal standards, Malvern Panalytical Ltd., UK) 105 kDa narrow standard and verified with a 250 kDa broad standard of known dispersity, intrinsic viscosity and dn/dc. Data analysis was performed using OMNISEC software V10. Prior to each analysis, samples were dissolved in THF at a known concentration, allowed to fully dissolve for 1.5 hours at room temperature under stirring and the solution filtered through a 0.22 μm PTFE filter.

3.2.4 Optical and morphological characterization

Transparency was determined by measuring the film transmittance at 600 nm using a UV–Vis spectrophotometer Varian Cary 6000i (Varian Inc, US), as reported in ASTM D1746-15.[223] Specimens were cut into rectangular pieces and directly placed in the spectrophotometer test cell. An empty test cell was used as the reference. Each measurement was performed in triplicate and transmittance values were normalized to the film thickness.[224,225] The micromorphology of tensile fractured surface of the PLA LS blends was characterized by scanning electron microscopy (SEM), using a JEOL JSM-6490LA (JEOL, Japan) microscope operated with an acceleration voltage of 10 kV, under high vacuum. Prior to imaging, each sample was coated with a 10 nm thick gold layer, using a Cressington 208HR high-resolution sputter coater.

3.2.5 Mechanical characterization

Mechanical properties were determined by uniaxial tensile tests on a dual-column Instron 3365 universal testing machine (Instron, UK) equipped with a 500 N load cell. The tensile measurements were conducted according to ASTM D882 procedure.[195] All the stress-strain curves were recorded after one-week conditioning period (at 25 °C) from sample fabrication and the dumbbell-shaped samples were stretched at a rate of 10 mm/min. Five measurements were conducted for each sample and the results were averaged to obtain a mean value. Analysis was repeated after 60 days, in order to ascertain that no star PDLLA migration or shrinkage phenomena occurred. Data of Young's modulus, ultimate tensile strength, elongation at break and toughness were calculated from the resulting stress-strain curves.

3.2.6 Thermal characterization

The thermal stability of the SL PLA blends were investigated by means of thermo-gravimetric analysis (TGA) using a Q500 analyzer (TA instruments, US). Measurements were performed on 3–5 mg samples in an aluminum pan at a heating rate of 10 °C/min, from 30 to 600 °C under nitrogen atmosphere. The weight loss of the specimens was recorded as a function of time and temperature simultaneously. Onset of decomposition and maximum decomposition temperature were determined from TGA and its non-zero first derivative (DTG curve), respectively.

Differential scanning calorimetry (DSC) thermograms were acquired with a Q2500 (TA Instruments, US) DSC system equipped with a RCS-90 refrigerated cooling system. Samples (~ 5 mg) were cut from the PLA SL specimens, and loaded into hermetic aluminum pans. A conventional heating-cooling-heating cycle was performed between -20° and 180 °C with a temperature ramp of 10 °C/min under nitrogen atmosphere. Equilibration isothermal periods

of 2 minutes were applied prior to each scan. Melting (T_m) and cold crystallization (T_{cc}) temperatures were measured as maximum of the corresponding phase transition peaks. Glass transition (T_g) temperature was calculated by inflection method. Reported DSC data were calculated from 2nd heating run. Cold crystallization and melting enthalpies (respectively labeled as ΔH_{cc} and ΔH_m) of each sample were determined by normalizing the measured enthalpies from DSC thermograms for the corresponding blended fraction of linear PLLA (crystallizable fraction).

3.2.7 Rheological characterization

Melt flow index (MFI) measurements were conducted using a CEAST MF30 melt flow tester apparatus (Instron, US), which determines MFI based on ASTM D1238-13 standard[226]. The weight used was 2.16 kg and the temperature 190 °C. SL PLA samples obtained from injection and extrusion process were cut in small pieces comparable to pellets size and dried (60 °C, 0.1 mbar) prior to performing the measurements. Each sample was analysed in triplicate.

Shear rheometry measurements were performed on a LCR7001 capillary rheometer (Dynisco Polymer Test, US), equipped with temperature and pressure sensors, at 190 °C, following ASTM D5422 standards. Star/linear PLA pellets obtained by extrusion (SL_E) were dried at 60 °C and reduced pressure for 8 hours before rheology testing. Shear viscosity was recorded by LabKARS software (Dynisco Polymer Test, US) at different shear rates ranging from 100 to 2000 s^{-1}. Conventional procedure for the calculation of true viscosity (η) was applied as follows: each measurement was carried out using two different capillaries of identical diameter and different active lengths (corresponding to length-to-diameter ratios (L/D) of 20 and 5). This allowed calculation of pressure drop in the inlet of the capillary and adjusted capillary lengths, thus determining Bagley correction factor as previously reported.[227] Weissenberg-Rabinowitsch correction[228] was performed automatically by the software and true viscosity (η) and corrected shear rate ($\dot{\gamma}$) of SL PLA blends were obtained. Experimental data were automatically fitted by the software into a Cross-Zero flow model.[229,230]

3.3 Results and Discussion

PLA blends containing 0 (as the reference), 10 and 20 % w/w of star PDLLA, were fabricated either by melt extrusion and compression molding (double-step manufacturing process) or by direct injection molding (single-step manufacturing process), obtaining transparent films or dumbbell-shaped specimens, respectively (Figure 3.1). Identical processing temperatures were

employed for all the blends with varying star-polymer contents, in order to better compare the final products performances. The resulting PLA-based products present diverse flexibility depending on the star PDLLA content and the processing method applied. The star PDLLA employed as plasticizer of conventional PLLA was specifically selected for its relatively high molecular weight - compared to common plasticizers (~20 kDa)-[90] and short chain-branching. Indeed, it has been demonstrated that branched structures can improve ductility and ease the melt flow of rigid linear polymeric matrices (through decrease of viscosity and enhanced mobility of the polymer coil) only if the polymer arms length is below a certain critical value. Above such length the branches begin to entangle, leading to higher viscosities than for linear polymers of similar molecular weights.[160]

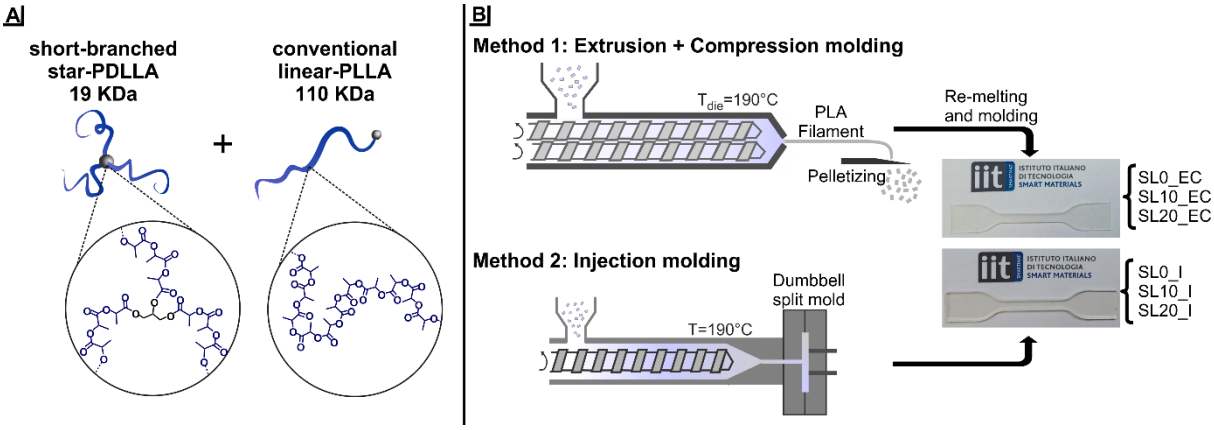

Figure 3.1. A, Graphic representation of chemical structures and macromolecular architectures employed for the star/linear PLA blends production: the left scheme shows the 3-armed star PDLLA (glycerol core is displayed in black); the right shows the linear polymeric network of conventional PLLA. **B,** Schematic representation of the two manufacturing methods applied for the star/linear PLA blends production. Method 1: The two polymers were blended in the extruder and the extruded filaments were pelletized and then remolded in films by compression molding. Such films were cut in dumbbell shapes for further analyses. Method 2: The two polymers were blended into the injection molding machine and the samples were directly injected in a dumbbell mold. Representative photographs of the star/linear PLA products obtained for each processing method are shown, with corresponding samples labels.

3.3.1 Processing-induced material degradation

The impact of thermo-mechanical degradation of the materials induced by the different manufacturing steps was assessed by gel permeation chromatography (GPC), as it is well known that PLA molecular weight generally decreases during melt processing, mainly due to random chain scission reactions.[38] The molecular weight of the blended samples decreased almost

proportionally to the star PDLLA content, as expected from its lower molecular weight contribution, albeit to different extent depending on the processing method (Table 3.1).

Table 3.1: Compositions, MW, dispersities and optical transparency data of the produced SL/PLA blended samples after each processing step, with corresponding samples' coding. Measured data for the unprocessed components were also reported, as reference.

Processing method	Sample	Star PDLLA content, % w/w	Mn, kDa[a]	Mw, kDa[a]	Đ[a]	Transparency, %
Unprocessed	Linear PLLA	0	74.1	110.7	1.5	-
	Star PDLLA	100	15.9	19.0	1.3	-
Injection molding	SL0_I	0	52.8	94.8	1.8	98
	SL10_I	10	50.1	85.2	1.7	99
	SL20_I	20	37.9	69.7	1.8	99
Extrusion	SL0_E	0	39.2	70.8	1.8	-
	SL10_E	10	36.6	66.0	1.8	-
	SL20_E	20	29.0	54.9	1.9	-
Extrusion + Compression	SL0_EC	0	22.5	51.7	2.3	87
	SL10_EC	10	21.1	41.7	2.0	89
	SL20_EC	20	17.0	30.3	1.9	90

[a] Average molecular weight and corresponding dispersities as detected by tripled detection GPC. Data correspond to bimodal distributions in the case of blended samples (Figure 3.2).

Indeed, the lower MW contribution on the bimodal molecular weight distributions is more visible in the case of the directly injected products (Figure 3.2). Comparison of the unprocessed and processed linear PLA samples also highlights a limited loss in MW detected for the injected samples (I), with respect to the extruded (E) and even more to the extruded/compression molded (EC) samples. The observation is similar for the processed blended samples with 10% w/w (SL10) and 20% w/w (SL20) of star PDLLA, where the weight average molecular weight (Mw) after the injection molding was 85.2 kDa and 69.7 kDa, respectively. After extrusion, the Mw became 66.0 kDa and 54.9 kDa, and after extrusion followed by compression molding it decreased to 41.7 kDa and 30.3 kDa, for samples with 10 and 20% w/w of star PDLLA, respectively. This suggests that extruded samples undergo higher degradation with respect to injection molded samples, even though the maximum processing temperature was in both cases 190 °C, given the longer residence time and higher shear stresses involved during extrusion.

The subsequent step of compression molding following extrusion seems to cause even further deterioration of the materials, with significantly higher dispersities and rapid decline of MW. Indeed, the MWs of SL10_EC and SL20_EC were 58% and 55% lower than the corresponding ones for SL10_I and SL20_I.

Noteworthy, SL0_I and SL0_EC samples, which contain only linear PLLA, reached a final Mw corresponding, respectively, to 86% and 47% of their starting values before processing, confirming the deteriorating effect of multiple processing steps on conventional PLA.[13]

When subjected to consistent thermal degradation, also the optical properties of the biopolymers might change, turning from clear to opaque and yellowish.[37] Although both SL_I and SL_EC products appeared transparent and colourless, their transparency factor in the visible wavelength of 600 nm, assessed by spectrophotometry, revealed subtle differences (Table 3.1). All injected samples showed transparency percentage close to 100%, with slightly higher values for blended products with respect to pure linear PLLA. The transparency of the films produced after extrusion and compression molding was lower than the injected ones, but still with satisfying values of 87.7, 89.7 and 90.0 for SL0_EC, SL10_EC and SL20_EC, respectively, greater than the translucent materials threshold of 80% transparency.[223]

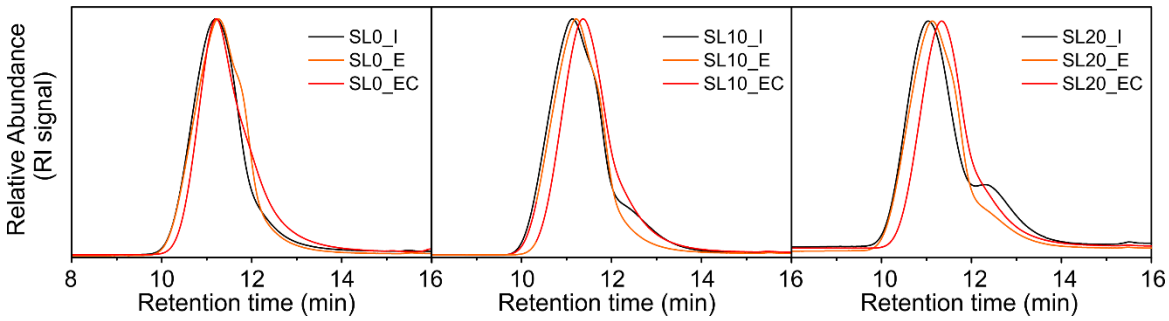

Figure 3.2: Normalized refractive index detector traces of SL PLA blends analyzed by GPC in THF. Black: injected samples, orange: extruded samples, red: extruded and compression molded samples.

3.3.2 Rheological behaviour

The variation in rheological performances of the star/linear PLA blends with increasing star PDLLA content was firstly characterized by melt flow index measurements. Melt flow index (MFI) is a measure of the resistance to flow of a polymer melt at a fixed temperature and applied force over a predetermined time. Melt flow rate is inversely proportional to viscosity of the melt at the conditions of the test[231] and for this reason, MFI is routinely used as common indicator of thermoplastic materials rheological behaviour. The MFI of the star/linear PLA products was

measured after each processing step (Figure 3.3), to better distinguish the effect of the increasing star PDLLA content on viscosity. The samples SL0_I reported a MFI value of 4.4 g/10 min, which is slightly higher than the one measured for the unprocessed linear PLLA material (4.0 g/10 min, raw material data not shown), whereas for SL0_E and SL0_EC the MFI increased even further to 4.6 g/10 min and 5.3 g/10 min, respectively. As visible from the graph, the addition of star PDLLA produced a reasonable fluidizing effect (reduction in viscosity) with respect to neat linear PLLA sample. A first consistent increase was detected with incorporation of 10% w/w of star PDLLA, reaching MFI values of 5.6 g/10 min, 6.4 g/10 min and 7.1 g/10 min for SL10_I, SL10_E and SL10_EC samples, respectively. Finally, all SL20 blends showed MFI values ~50% higher than the original linear PLLA materials, except for the extruded/compressed sample (SL20_EC), which showed very unstable MFI in the range of 8.7-9.8 g/10 min. These results denote that the incorporation of the short-branched structure prevents polymer chain entanglements, thus decreasing viscosity. However, it is clear that processing deterioration has a drastic effect on bio-based polyesters and a double step processing, as for extruded and re-molded SL PLA samples, cannot ensure the desired product performances.

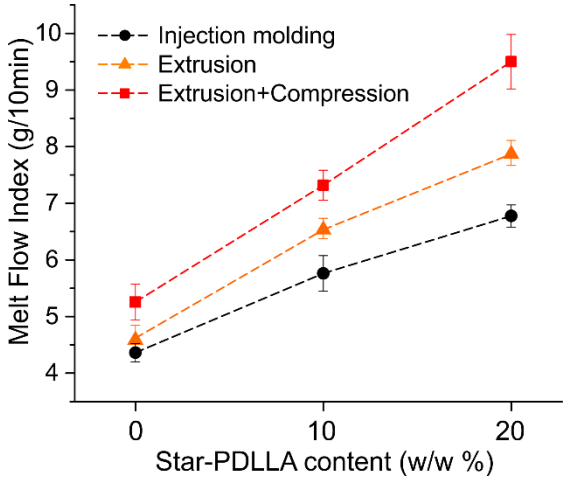

Figure 3.3: MFI trends of SL PLA blends for increasing star PDLLA contents. Test was performed at 190 °C with 2.16 Kg load after each processing step.

Despite melt flow index represents a direct and useful indication of zero shear viscosity at a given temperature, rheometry measurements allow to study the viscosity decrease resulting from incorporation of the star-shaped component as a function of shear rate. Particularly, capillary rheometry measurements can be performed at relatively high shear rates, thus allowing simulation of processing conditions (typically corresponding to 100-1000 s^{-1} for extrusion and 500-2000 s^{-1} for injection molding).[232]

Therefore, star/linear PLA blends, in the form of extruded pellets (SL_E), were characterized by means of a capillary rheometer at 190 °C (corresponding to the applied temperature for both extrusion and injection processes) and the resulting trends of melt shear viscosity vs shear rate are reported in Figure 3.4. The samples clearly exhibited non-Newtonian behaviour, as expected for shear rates >10 s^{-1}, and the shear viscosity trend was well described by the Cross-Zero flow model in this shear rate region.[233] Interestingly, star PDLLA influence on rheology at shear rates comparable to common extrusion processes was evident. First of all, the branched component displayed, as expected, a fluidizing effect (zero shear viscosity reduction), which is favoured by the combined effect of the lower molecular weight and star-shaped compact structure. Indeed, for increasing branched polymer concentration the calculated zero shear viscosity decreased, from 1165 Pa·s for SL0_E to 774 Pa·s for SL10_E and finally reaching 740 Pa·s in the case of SL20_E. Most importantly, star PDLLA accentuated the shear thinning behaviour of the material with respect to neat linear PLLA, as faster decrease of viscosity with shear rate (increased curve slope) was observed for the star-containing blends. Such enhanced pseudoplastic behaviour is typical of branched polymers, and improves processability, not only facilitating the melt flow of the material during processing, but also allowing to increase the processing shear rate without providing further degradation. This feature is also very useful for manufacturing processes requiring melt elongation (*e.g.* cast extrusion, stretch blow molding).[85,131]

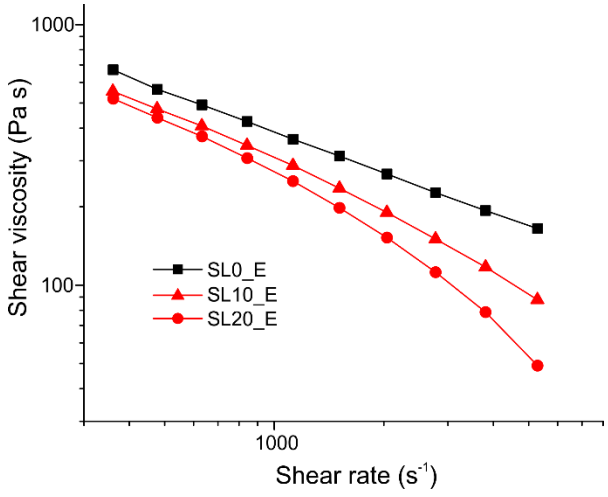

Figure 3.4: Shear viscosity vs shear rate profiles of the fabricated PLA SL_E samples in capillary shear flow field. Based on previous analyses, pelletized samples (required material form to conduct this measurement) were assumed to present intermediate properties between SL_I and SL_EC products at this processing stage.

3.3.3 Blend miscibility, glass transition and crystallizability

A pre-blending or compatibilization processing step is generally required to obtain a homogeneous polymeric formulation before manufacturing of the final plastic product.[234] Therefore, differential scanning calorimetry analysis was required to ascertain the formation of a miscible blend, especially for the injection molding method, which should favour proper mixing of the components through a single-step blending process. The thermal analysis confirmed optimal miscibility between the two PLA-based components for both processing configurations, as only one glass transition step was observed for all samples (Figure 3.5). The high compatibility of the two PLA architectures, bearing polymer backbones with identical chemical structure, ensured optimal blending. Moreover, the glass transition temperature (Tg) decreased as a function of star PDLLA concentration, independently of the applied manufacturing process. The glass transition was detected at 57 °C for SL0_I samples (in accordance with literature data)[37] and decreased to 50 °C and 47 °C for SL10_I and SL20_I, respectively. In the case of extruded and compression molded samples, Tg was reduced from 55 °C for SL0_EC to 51°C and 48 °C for SL10_EC and SL20_EC, respectively (Table 3.2). Such values denote a plasticizing effect of the star PDLLA on the linear PLLA matrix. Interestingly, SL_EC samples showed a stronger enthalpic relaxation upon glass transition. This thermal behaviour was reasonably caused by aging phenomena, as samples were subjected to more prolonged stresses and higher pressures.

Characteristic trends in the crystallization and melting area (between 90 °C and 155 °C) attributable to the different processing methods, were detected for the star/linear PLA materials. DSC curves of films produced after extrusion and compression molding were characterised by slightly lower temperatures of cold crystallization and melting but higher capability of crystallization, with respect to injected products (Table 3.2). Noteworthy, all samples underwent crystallization upon heating, both before (1st heating, data not shown) and after erasing their thermal history (2nd heating, Table 3.2), despite no crystallinity was detected in both scans.

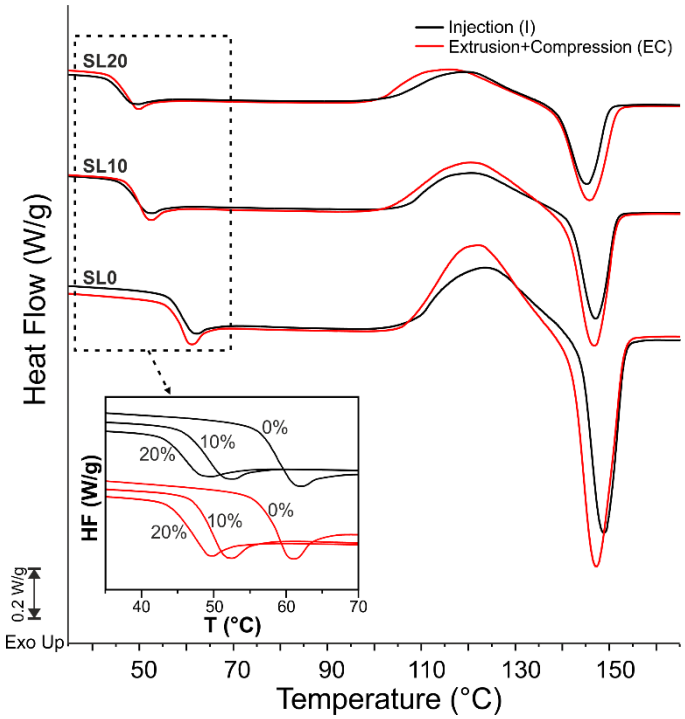

Figure 3.5: DSC thermograms of second heating run for all SL/PLA products, manufactured by extrusion followed by compression molding (red) or injection molding (black). The inset shows in detail the Tg step shifts to lower temperatures upon increasing star PDLLA contents (expressed in % w/w) and for the different processing methods.

Cold crystallization enthalpies of the linear PLLA reference samples (22.7 J/g for SL0_I and 29.6 J/g for SL0_EC) were reduced by 54% and 44%, respectively, when 20% w/w star PDLLA was added to the linear PLLA matrix (Table 2.2). In addition, crystallization temperatures gradually decreased in presence of higher amounts of star-polymer, (*i.e.* 2-5 °C and 1-7 °C difference for injected and extruded samples, respectively), with similar trends also for melting transitions (Table 3.2). Therefore, the atactic, short-branched PDLLA significantly reduced crystallizability of the linear PLLA matrix, by preventing formation of entanglements between polymer chains and impeding lamella formation. Taken together, these data confirmed that the incorporation of star PDLLA allows the formation of a more flexible polymeric system.

Table 3.2: Thermal properties of the processed SL PLA blends. Transition temperatures and normalized enthalpies of cold crystallization and melting (ΔH_{cc} and ΔH_m) were calculated from DSC second heating run. Onset decomposition temperature ($Tdeg_{onset}$) and maximum decomposition temperature ($Tdeg_{max}$) were obtained by elaboration of corresponding TGA curves.

Sample	Tg, °C	Tcc, °C	Tm, °C	ΔH_{cc}, J/g	ΔH_m, J/g	$Tdeg_{onset}$, °C	$Tdeg_{max}$, °C
SL0_I	57	125	150	22.7	23.8	321	356
SL10_I	50	123	150	13.9	14.8	314	353
SL20_I	47	120	147	12.3	12.4	311	351
SL0_EC	55	124	149	29.6	30.2	296	349
SL10_EC	51	123	148	15.8	16.2	287	346
SL20_EC	48	117	142	13.0	12.9	286	343

Measured Tg of pure star PDLLA was 29 °C. [a]Reported data of phase transition enthalpy normalized by the corresponding weight fraction of the linear PLLA component, as star PDLLA is unable to undergo crystallization.

3.3.4 Thermal decomposition behaviour

The thermal decomposition data of the SL PLA blends, measured by thermogravimetic analysis (TGA), were found in good accordance with the findings reported for GPC analysis. Indeed, the injected blends (SL_I) start degrading at higher temperatures than the extruded and compression-molded (SL_EC) ones. In particular, the respective onset degradation temperatures ($Tdeg_{onset}$) were 321 vs 296 °C, 314 vs 287 °C and 311 vs 286 °C, in order of increasing star PDLLA content (Table 3.2). Derivative TGA (DTG) revealed a more consistent weight loss at low temperatures (~300 °C) for the SL_EC blends, especially for higher star PDLLA contents (Figure 3.6). Most likely, random chain scission and intramolecular transesterification phenomena were more significant during extrusion/compression process, as seen from the consistent reduction in MW reported by GPC. However, temperatures of maximum degradation ($Tdeg_{max}$) were practically identical for both processing conditions and remained almost unchanged with the star polymer addition, with a maximal difference of 8 °C between SL20_I and SL20_EC samples. Star PDLLA addition progressively shifted the $Tdeg_{onset}$ to lower temperatures. According to previous results, (see *Chapter 2*) a certain loss in thermal stability could be observed with the addition of a low-MW branched PLA component. Nevertheless, here a maximum reduction of only 7 °C was detected, between SL0 and SL10, for both injected and extruded/compressed samples (respectively, 321 °C vs 314 °C and 296

°C vs 286 °C), confirming the increased thermal resistance of the relatively higher MW of the star PDLLA component used in this case. Moreover, for all the samples, the observed $Tdeg_{onset}$ were way higher than PLA processing temperatures.[31] Therefore, the obtained star/linear PLA blends still possess discrete thermal stability. It is important to mention that identical processing conditions were applied independently of the star PDLLA content to provide proper comparison of samples for each fabrication method. Nevertheless, the incorporation of the amorphous star PDLLA would allow lower processing temperatures, reasonably resulting in lower deterioration of the material during processing with respect to neat linear PLLA.

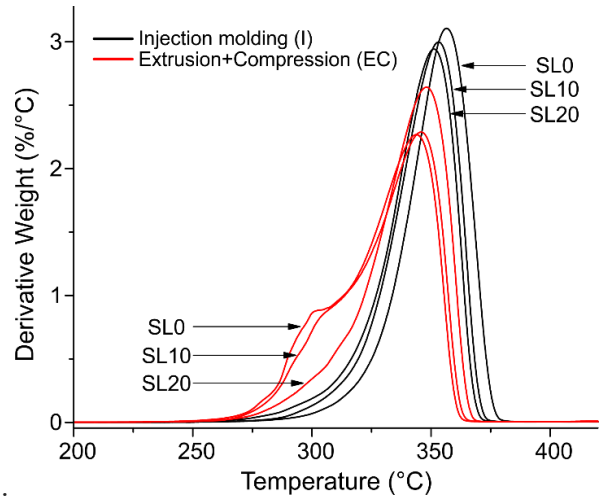

Figure 3.6: Non-zero first derivative TGA curves of the various SL PLA blends obtained by injection molding (I) or extrusion followed by compression molding (EC) with diverse star PDLLA contents.

3.3.5 Mechanical properties and fracture morphology

The incorporation of star PDLLA was found to progressively enhance the flexibility of the material, as observed from the resulting stress-strain curves of both extruded/compressed films and injected dumbbell specimens (Figure 3.7A), yet to a different extent depending on the processing method. Indeed, similar trends of mechanical behaviour with varying star PDLLA content were observed for both extruded/compressed and injected samples. Neat linear PLLA samples, SL0_EC and SL0_I, showed the typical PLA brittle fracture at low elongation values. On the contrary, the star containing blends always displayed an evident yield point followed by necking behaviour before fracture (in good accordance with findings obtained in *Chapter 2*), thus revealing a gradual transition from brittle to ductile mechanical behaviour. In agreement with the so far presented results, the extruded/compressed products displayed poorer mechanical performances and less evident effect of the star polymer on the final properties, due to the

higher degradation and MW loss reported for this type of processing. Additionally, the direct injection of the material into the dumbbell-shaped mold inevitably induced chain orientation along the flow direction,[235] with consequent improvement of the tensile properties along the longitudinal direction (anisotropy). Nevertheless, a clear plasticizing effect due to incorporation of star PDLLA was observed, especially for the injected blends. In particular, elongation at break values progressively increased from 11% for SL0_I, up to maximum elongations of 17% (+154%) and 25% (+227%) for SL10_I and SL20_I, respectively. SL10_EC and SL20_EC samples reported instead a good improvement in tensile elongation of 110% and 180%, respectively compared to SL0_EC original value (Figure 3.7B). Moreover, stress resistance drastically increased upon star PDLLA incorporation, as confirmed by the resulting enhanced toughness for both extruded/compressed and injected products (*i.e.* total increase of 222% and 265%, respectively). Interestingly, the star PDLLA structure only moderately influenced the elastic response and mechanical stability of the final materials. Indeed, the Young's modulus decreased from 1.9 GPa for SL0_I to 1.7 GPa for SL20_I (-12 %) and from 1.7 GPa for SL0_EC to 1.4 GPa for SL20_EC (-10%). Moreover, ultimate tensile strength trends reported an overall decrease of 15% for injected products and only 8% for the extruded/compressed blends after star PDLLA incorporation.

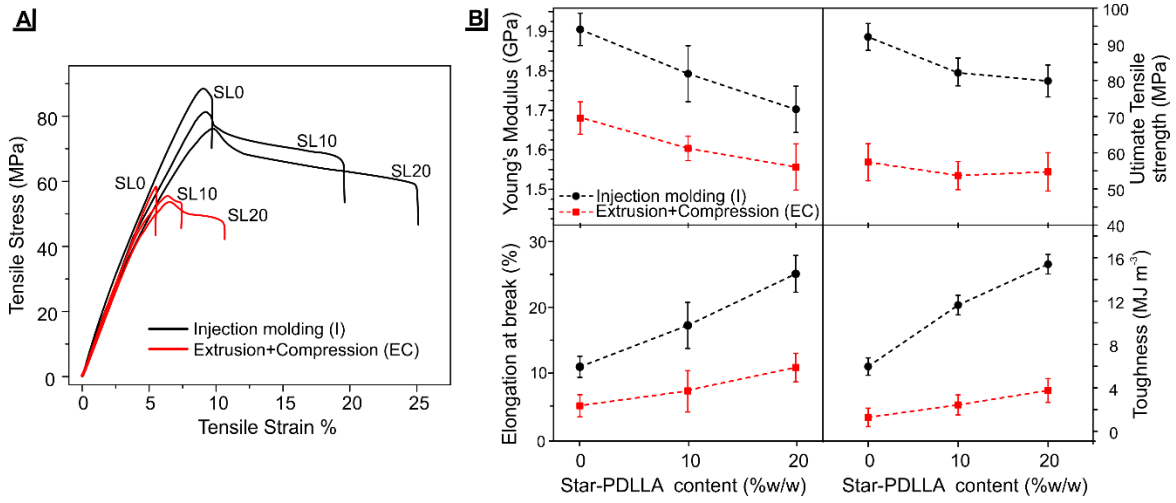

Figure 3.7: **A,** Representative stress-strain curves of the star/linear PLA manufactured products. **B,** Comparison of mechanical properties measured by tensile test on the star/linear PLA products. Variation of Young's modulus, elongation at break, ultimate tensile strength, and toughness are displayed as a function of star PDLLA content and for the two different manufacturing configurations.

The fractured surfaces of processed star/linear PLA products were studied by cross-section SEM (Figure 3.8), in order to investigate the effect of star PDLLA ductilization – as observed from tensile test- on mechanical failure behavior of conventional PLLA. SEM fractographs of pure linear PLLA samples appeared more brittle: they presented a neat and regular fractured surface (*i.e.* typical feature of shear yielding of glassy and amorphous thermoplastic polymers)[236] and almost no trace of plastic deformation or crazing was detected. As 10% w/w of star PDLLA was added (SL10_I), a more ductile failure seemed to occur, with formation of several ridges and folds on the fracture surface, denoting plastic deformation. A further increase in star PDLLA content (SL20_I) produced more consistent necking upon tensile stress application and an extremely ragged and irregular fracture surface, as a result of the prolonged plastic deformation after yielding. The typical whitening of the fractured region due to strain-induced chains orientation was also visible in both injection molded blends. However, no particle agglomeration or micro voids formation was detected by SEM, confirming the proper blending of the two PLA-based components.[237] Star-containing extruded and compression molded blends SL10_EC and SL20_EC also showed increasing formation of edges and more rippled fracture surfaces, compared to the neat linear PLLA extruded sample, yet with less evident variations than the corresponding injected blends. In agreement with the behavior observed in the stress-strain curves, the gradual transition from brittle to ductile failure mechanism upon star PDLLA addition was also visible in the photographs of the fractured samples, shown as insets in Figure 3.8.

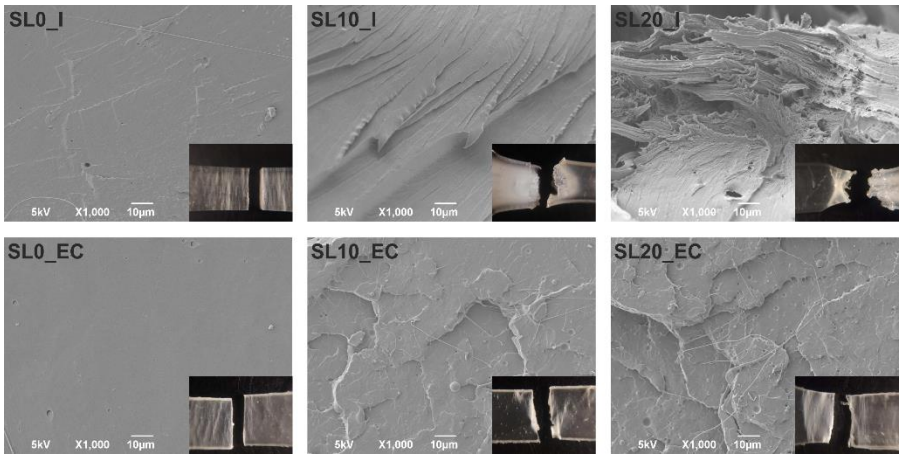

Figure 3.8: SEM cross-section images of tensile fractured surfaces of PLA SL blends. Scale bar: 10 µm. For each fractograph, the corresponding photographs of fractured samples from tensile test are reported as inset.

3.4 Conclusions

The processing performances of diverse star PDLLA/linear PLLA blends were investigated by means of commonly employed large-scale manufacturing techniques for thermoplastic polymers, *i.e.* extrusion and injection molding. The effect of star PDLLA incorporation on the rheological, mechanical and thermal properties of linear PLLA was evaluated. Material characterization revealed the ability of star-shaped architecture to improve processability and reduce typical brittleness of conventional PLA.

Compared to other PLA modification strategies, such as blending with other low-MW plasticizers or rubbery polymers, the use of a star-shaped atactic PDLLA provided excellent miscibility of the components and improvement of both rhelogical and mechanical behavior of conventional PLA without altering the chemical nature of the material nor requiring the addition of compatibilizers.

Comparison of the processing-induced degradation and resulting products performances demonstrated that the two PLA architectures can be optimally blended though a single-step injection molding process with resulting better properties, thus avoiding consistent degradation typically observed when subjecting PLA to multiple processing cycles. Despite lower performances were observed in the case of the film molding by extrusion, the presence of the amorphous star PDLLA component would allow to perform extrusion at lower processing temperatures (where common PLA is generally too viscous to be treated) or higher shear rates, due to the enhanced melt flow and lower melting points of SL PLA blends. This would reduce material degradation and overall production costs, with resulting improved product performances.

Consequently, this star PDLLA/linear PLLA systems appear as very promising materials for the production of injected, flexible and transparent items (*e.g.* single-use cutlery, cups, containers), with also enhanced biodegradability with respect to neat conventional PLA materials. Customization of final performances is also possible by simply varying star PDLLA concentration.

Chapter 4 .Production of a library of multi-armed poly(lactide)s with variable architecture and tacticity by a novel lactide ROP method: synthesis and material characterization

4.1 Introduction

In previous chapters, the flow enhancement and plasticization performance of short-branched star-shaped PLA as an additive for conventional PLA (linear semicrystalline PLLA) was investigated. These studies showed branched PLA to have great potential for the production of enhanced processability (reduced viscosity) *all-PLA*-based materials.

The simplest form of branching (3-armed) was sufficient to allow amorphous PDLLA to significantly improve the mechanical and rheological performance of linear, semicrystalline PLLA, with increasing effect according to branched PLA concentration (properties fine-tuning by variation of branching content). Therefore, these results prompted a thorough investigation on the effect of increasing branching degree and/or stereoconfiguration as modulators of these properties (fine-tuning by variation of branched topology). However, there is currently poor availability of well-defined and customizable branched polyesters architectures, due to their often troublesome design and production, despite the rising demand for both industrial polymer manufacturing and pharmaceutical purposes.[81,133,169]

To this aim, a novel and versatile lactide ROP protocol for the controlled synthesis of multi-armed poly(lactide) with tunable architectures and stereoconfigurations was developed, thus enabling a systematic evaluation of the effect of these synergic parameters on the final PLA materials properties (*i.e.* conformation, crystallizability, rheological behavior and degradability).

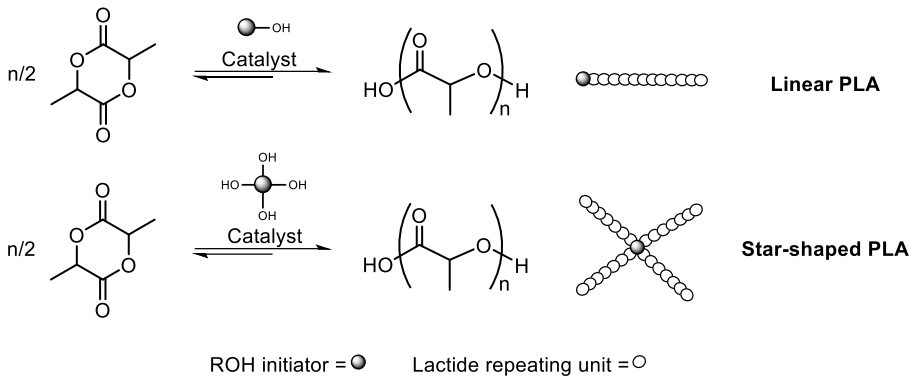

Scheme 4.1: General scheme of lactide ring-opening polymerization and resulting architecture for a linear and star-shaped PLA, respectively using a mono- or multifunctional alcohol as the initiator.

In macromolecules, possibly the most common, and surely the most controlled form of branching is the one presented by star architectures; star polyesters are typically obtained via ring-opening polymerization (ROP) of cyclic ester(s) using a multifunctional initiator, in a *core-first* synthetic approach (Scheme 4.1).[142,143]

It is worth recalling that ROPs are thermodynamically driven, equilibrium processes, where the direction of the process (growth or depolymerization) can change depending on e.g. temperature (above its ceiling temperature, a polyester converts to its cyclic monomers) or the balance of polar interactions between monomer and solvent, and growing chain and solvent. The use of multifunctional alcohols initiators (*e.g.* small polyols, polysaccharides or other hydroxylated polymeric macroinitiators) is often marred by a poor definition of the macromolecular architectures and a broad MW dispersity,[165,176,238] due to variable reactivity (*i.e.* the OH groups on the same initiator do not initiate with the same efficiency)[178] and high hygroscopicity (*i.e.* parasitic water-initiation of polymer chains or esters hydrolysis) compared to monofunctional alcohols.[176] Further, they are often not very soluble in the apolar solvents commonly used in lactide ROP (*i.e.* chloroform ($CHCl_3$), dichloromethane (DCM), toluene, tetrahydrofuran (THF)), [133,165] and the better solubility obtained at high temperatures comes at the price of parasitic reactions and broader MW distributions.[239] Solvent-free ROP has also been widely employed to overcome both solubility and environmental issues in large-scale productions; however, most polyols are hardly soluble in the lactide monomer, and the harsher conditions prevent an efficient polymerization control and typically exacerbate side reactions, such as intra- and intermolecular transesterifications, leading to racemization, formation of impurities and broadening of the MW distributions.[24,133,185] Moreover, formation of stereoregular poly(lactide)s and *in situ* post-functionalization are generally more difficult in

solvent-free ROP because of the high temperature required.[88,173,185] On the other hand, while polar solvents are advantageous in terms of the better solubilization of the hydroxylated initiators, but they may lower the ROP equilibrium constant, which means a lower ceiling temperature. Therefore, above all in the presence of such solvents, the optimization of polymerization conditions is crucial.

Traditionally, branched polyesters are prepared via metal complex-mediated living ROP, using metal complexes as catalysts, such as the well-known tin(II) 2-ethylhexanoate (tin octoate, $Sn(Oct)_2$)(MC-1, Figure 4.1). Indeed, stannous octoate presents lower toxicity than most other metal-based ROP catalysts. However, high $Sn(Oct)_2$ amounts are generally needed due to its low catalytic activity, and its often inefficient removal drastically affects final PLA performances.[240,241] Moreover, metal complex-mediated ROP proceeds through a coordination insertion mechanism, requiring elevated temperatures to achieve a fast reaction rate.[242–244] As previously mentioned, all these factors typically result in broad distributions and poor control on final architectures, despite high-MW PLA (Mw >60 kDa) can be achieved.[80,185,243,245,246] Over the years, more efficient metalorganic catalysts have been developed. An example are the Al-salen complexes such as (MC-2) shown in Figure 4.1, which is sufficiently active under milder reaction conditions (70 °C vs >100 °C for $Sn(Oct)_2$-mediated ROP) and may provide stereoselective catalysis, due to its structure symmetry and slightly lower temperatures.[128,247,248]

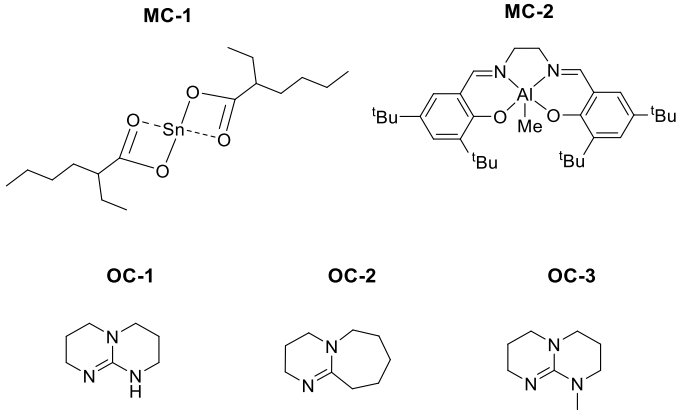

Figure 4.1: Major metalorganic (MC) and organic (OC) catalysts for star poly(lactide)s production via ROP. **MC-1**: $Sn(Oct)_2$; **MC-2**: ^{tBu}[salen]AlMe ; **OC-1**: TBD; **OC-2**: DBU; **OC-3**: MTBD.

Recent developments in organocatalysis have introduced various organic compound-based catalytic systems for linear poly(lactide)s synthesis via ROP of lactide. The pioneering work by Hedrick and Waymouth have demonstrated the great potential of organocatalysts, such as 1,5,7-

Triazabicyclo[4.4.0]dec-5-ene (TBD), 1,5-diazabiciclo[5.4.0]undec-7-ene (DBU) and 7-Methyl-1,5,7-triazabicyclo[4.4.0]dec-5-ene (MTBD) (respectively OC-1, OC-2, OC-3 in Figure 4.1) as highly reactive and inexpensive metal-free alternatives for cyclic esters ROP.[249–252] The organic base-mediate ROP of lactide generally proceeds as an anionic polymerization process and can be carried out under mild conditions (usually at room temperature), with negligible catalyst loadings and reaction rates comparable to -or even faster than- the organometallic catalytic systems operating at elevated temperatures.[133] The high selectivity of the organic catalysts and the low reaction temperatures – minimizing/suppressing transesterifications- provide poly(lactide)s with very narrow dispersities values (typically <1.1).[251,253,254]

Nevertheless, the application of organocatalysis for branched polyesters synthesis via ROP has not been demonstrated until more recently.[255,256] Very little information regarding the use of such systems for the production of controlled branched structures is available, reporting in any case low molecular weights upon use of undesirable (high toxicity) solvents, such as DCM, DMF, toluene and chloroform.[254,255,257] For example, Eldessouki *et al.* managed to synthesize 4-armed PLA by ROP in DMF at 60 °C, using the mild 4-(dimethylamine)pyridine (DMAP) base as the catalyst. Despite the good agreement between theoretical and experimental degree of polymerization per arm (DParm) values, a maximum average molecular weight of ~25 kDa was obtained.[257] In another study, β-cyclodextrin was used as macroinitiator (21 arms, 1.5 kDa) for L-LA ROP in DCM at room temperature. In this case, higher MW (Mn = 54kDa) could be achieved by using a DParm of only 20 units (corresponding to a $Mn_{branch} \approx$ 2.5 kDa).[254] However, despite the high number of arms, the presence of such short-length branches connected to a discrete core like cyclodextrin (cyclic structure), causes the loss of peculiar PLA characteristics on macroscopic properties (high modulus, strength, melting point), which would make it suitable for large scale processing, thus limiting its application to drug-delivery or similar biomedical purposes. High-MW branched PLAs could be eventually achieved (> 100 kDa) by means of a hyperbranched PEG core (*hb*PEG, 60 kDa) through DBU-mediated ROP of lactide, yet along with poorly controlled architectures and inevitably high dispersities (Đ = 1.4-1.5) due to the random branching framework.[258]

Among all the major ROP organocatalysts, DBU has been demonstrated as the currently most suitable for linear PLA synthesis, in terms of reactivity and selectivity. Indeed, other guanidine species such as the strongly basic TBD catalyst is too reactive toward lactide ring opening, leading to excessively fast and uncontrolled polymerizations and even consistent transesterification compared to DBU (higher Đ values).[249] On the contrary, when the cyclic amidine MTBD was tested for L-LA ROP in presence of a monofunctional initiator, it was

found less reactive than DBU, reporting lower final MWs and slower polymerizations.[249,259] Therefore, DBU is generally preferred for lactide ROP, while TBD is rather used for less-strained cyclic esters (*e.g.* valerolactone or caprolactone) ROP, which is less thermodynamically favored and need a highly reactive catalyst to trigger the polymerization.

It becomes evident that, despite substantial advances in ring-opening polymerization methods, versatile and controlled syntheses of industrially relevant branched polyester structures - hence bearing defined architectures, relatively high molecular weights and narrow molecular weight distributions - are still not available.[133,142] Consequently, the development of a versatile and green(er) synthesis of star-shaped poly(lactide)s provides a valuable mean to finally enable extensive industrial exploitation of such branched PLA structures.

4.1.1 Abstract

Here we developed a versatile route to branched poly(lactide)s based on the use of DBU as a catalyst, and of N-methyl pyrrolidone (NMP) as a solvent. A rational optimization of the kinetic and thermodynamic parameters of the process allowed the production of a library of low MW dispersity poly(lactide)s structures with variable multi-armed topology (linear, star, comb) and tacticity (PLLA, PLLA-*b*-PDLLA, PDLLA-*b*-PLLA, PDLLA). The direct access to a library of tailor-made branched PLA architectures and stereoconfigurations enabled a systematic characterization and evaluation of these synergistic structural parameters on final PLA properties, with respect to the corresponding linear structures. Finally, comparative investigation of the hydrolytic degradation mechanism of linear and branched PLAs, depending on the presence of branching points and/or crystalline phases, could provide further insights for the development of *all-PLA*-based materials with tunable biodegradability.

4.2 Materials and Methods

4.2.1 Materials

D,L-lactide (DL-LA), L-lactide (L-LA), 1,8-Diazabicyclo[5.4.0]undec-7-ene (DBU), acetic acid, benzyl alcohol (BnOH) pentaerythritol (PET), dipentaerythritol (diPET), Sucrose (Sucr) and Polyvinyl alcohol (PVA, 80% hydrolyzed, Mn = 13 kDa, Đ =1.3) were purchased from Sigma Aldrich (Merck Life Science, IT). *N*-methyl pyrrolidone (NMP) and 1,4-benzendimethanol (BDM) were purchased from Fluorochem. Prior to use: DL-LA and L-LA were recrystallized

twice in dry toluene, dried under vacuum and stored under inert atmosphere until needed. BnOH was distilled at 120 °C, 90 mbar. BDM was recrystallized twice from dry $CHCl_3$ and then dried in vacuum oven (around 0.1 mbar) at 40 °C for 2 days. PET was sublimated at 240 °C and 60 mbar and stored under reduced pressure. In order to remove water, DiPET and PVA dissolved in toluene were introduced in a round-bottomed flask and refluxed using a Soxhlet apparatus filled with 3Å molecular sieves for 3 hours (water removed as a minimum azeotrope is trapped by the molecular sieves); the solvent was then removed under vacuum and dry DiPET and PVA at the bottom of the flask; they were used within 12 hours by adding the appropriate polymerization solvent to the same flask and thereby producing stock solutions of the two initiators. Sucrose was freeze-dried and subsequently kept in vacuum oven (0.1 mbar, 35 °C) for 48 hours prior to use. DBU was vacuum distilled at 85 °C, 0.6 mbar and stored under reduced pressure for up to two weeks; NMP was stirred overnight with calcium hydride and subsequently vacuum distilled (75 °C, 5 mbar).

4.2.2 Synthesis of multi-armed poly(lactide)s

All experiments were performed in a 12-position Carousel parallel reactor (Radleys, UK), heated under vacuum and subsequently purged with nitrogen for 5 minutes prior use. In a typical polymerization, the final number average degree of polymerization per arm (DParm) was set to 100 and the monomer concentration was maintained constant at 1 M. Four sets of experiments were performed in the presence of different multifunctional initiators: 1) L-LA alone, 2) DL-LA alone, 3) L-LA first (50% of the monomer feed) and then DL-LA, 4) the reverse of 3). A BnOH-initiated PLA was produced for every set of experiments, as a linear polymer reference. Firstly, stock solutions of DL-LA and L-LA (1.4 M) and initiators (140, 70, 35, 23.3, 17.5 and 9.5 mM for BnOH, BDM, PET and diPET, Sucr and PVA, respectively) in dry NMP were prepared under inert atmosphere. Subsequently 2 mL of the monomer and 400 μL of each initiator stock solution were transferred into the corresponding Carousel vessels and equilibrated at 5 °C, using an ice bath. The total amount of desired monomer isomer was dosed to the reaction mixture by two equal additions of 50 eq.s at 0 and 3h. 200 μL of a 140 mM DBU solution in dry NMP were added to start each polymerization (corresponding to a 1:1 [OH]:[DBU] molar ratio), thus providing a starting concentration of 1 M in monomer and 0.02 M in OH groups (corresponding to 20, 10, 5, 3.33, 2.5, 0.14 mM concentration of BnOH, BDM, PET, diPET, Sucr and PVA, respectively). After 3 h, the remaining 50 eq.s of monomer solution (2 mL) were added, followed by 800 μL of fresh NMP, so that monomer concentration was maintained at 1 M, while the desired final [M]:[OH] molar ratio of 100 was reached. Indeed, the

initial [M]:[OH] ratio was set to a DParm of 50, thus lower than the target value, in order to not exceed a monomer concentration of 1 M during the reaction.

Polymerization was monitored over a 24h period: aliquots (~50 μL) were collected at predetermined time points and placed in glass vials each containing a NMP solution of acetic acid (3-fold excess to the estimated DBU concentration in the aliquot). If further monomer was added at intermediate time points, samples were collected prior to its addition. These samples were then dried under vacuum in a Genevac centrifugal evaporator (SP Scientifics, US) for 60 min at 30 °C, 1 mbar. The obtained pellets were dissolved in $CDCl_3$ for ^{1}H-NMR analysis and characterized by triple detection GPC using THF as eluent. After 6 hours most of the crude reaction mixture (5 mL) was collected and added to a solution of acetic acid in NMP (3:1 ratio to DBU) to stop the polymerization. Excess NMP was removed by Genevac centrifugal evaporator (1 mbar, RT) and the crude product was redissolved in 2 mL of DCM and precipitated in cold isoamyl alcohol (1:15 solvent/non-solvent volume ratio). After centrifugation, the process was repeated using cold methanol as a non-solvent. The final product was dried by means of a Genevac centrifugal evaporator (1 mbar, RT) as a fine white powder and characterized by ^{1}H-NMR and GPC in THF (or SLS analysis in THF).

4.2.3 Physico-chemical characterization

4.2.3.1 Gel permeation chromatography (GPC)

GPC was performed on an integrated OMNISEC system (Malvern PANalytical Ltd., UK) equipped with a D6000M and a D4000 column (10 and 6 μm particle size respectively, 300 x 8 mm) using a triple detection method (refractive index, viscometer, and dual angle light scattering detector at 7° and 90°). THF stabilized with 250 ppm BHT was used as eluent at a temperature of 35 °C and a flow rate of 1.0 mL/min. The system was calibrated with polystyrene (PolyCal standards, Malvern PANalytical Ltd., UK) 105 kDa narrow standard and verified with a 250 kDa broad standard of known dispersity, intrinsic viscosity and dn/dc. Data analysis was performed using OMNISEC software V11.10. Prior to each analysis, samples were dissolved in THF at a known concentration and room temperature and the resulting solutions were filtered through a 0.22 μm PTFE filter. Triple detection was used to obtain absolute molecular weight distributions, intrinsic viscosity, radius of gyration (R_H) and Mark−Houwink parameters (*logK* and *a*) of the poly(lactide)s. The radius of gyration *Rg* could not be calculated, as the synthesized poly(lactide)s have excessively low dn/dc and hydrodynamic size to produce anisotropic scattering, which is required for *Rg* calculations.

4.2.3.2 Static light scattering (SLS)

A 5.0 mg/mL stock solution of each polymer (*i.e.* PVA-*comb*-PLLA, PVA-*comb*-PDLLA, PVA-*comb*-(PLLA-*b*-PDLLA) and PVA-*comb*-(PDLLA-*b*-PLLA)) in THF was filtered through a 0.2 μm PTFE syringe-filter and then diluted with the same solvent in order to produce five concentrations ranging between 1.5 and 5.0 mg/mL. 1.5 mL of each solution were injected into a Dawn Heleos II multi-angle light scattering (MALS) detector, operating at 660 nm and 25 °C (Wyatt Technology, Santa Barbara, California) using a syringe pump (Kent Scientific Corporation, Torrington, Connecticut). The software ASTRA version 7.1.4.8 (Wyatt Technology, Santa Barbara, California) was used to collect and analyse SLS data and obtain weight average molecular weight, radius of gyration (*Rg*) and second virial coefficient (A2) using the nominal concentration of the solutions and the dn/dc previously obtained for the polymers with the same composition analysed by GPC. All samples were analysed using the Debye formalism with fit degree equal to 1 for both angle and concentration.

4.2.3.3 Nuclear magnetic resonance (NMR)

Evaluation of monomer conversion and polymer chemical structure was carried out by ^{1}H-NMR experiments, performed on a Bruker Avance III 400 MHz spectrometer (Bruker Ltd., US) equipped with a Broad Band Inverse probe and Z-gradients. The polymers were dissolved at a concentration of 10 mg/mL in deuterated $CHCl_3$. ^{1}H-NMR spectra are referenced using the residual solvent peak at δ 7.26. Measurements were performed at 27 °C. Results were analysed using Mestrenova (Mestrelab Research S.L., ES) software.

For tacticity study, ^{1}H-NMR spectra were acquired on ~10 mg/mL polymer solutions in deuterated $CHCl_3$ on a Bruker ASCEND 600 spectrometer. The methyl protons (δ ~ 1.5 ppm) were decoupled from the methine protons (homonuclear decoupling) during the acquisition time.[260,261]

The sequences of stereocentres in the macromolecular chains are interpreted on the basis of the possible combinations of *m* ("meso" or isotactic, i.e. pairwise relationship -RR- and -SS-) and *r* ("racemic" or syndiotactic, i.e. -RS- and -SR-) diads.[262] The probability P*r* to obtain an *r* diad (ranging between 0 for fully isotactic and and 0.5 atactic PLA structures, respectively) and is calculated as:

$$Pr = \sqrt{(2 \cdot [rmr])}$$

where [*rmr*] is the concentration of an *rmr* tetrad, which is calculated from the relative intensities of methine signals. After homonuclear decoupling, tetrads *mrm*, *mmm*, *mmr* and hexads *mmmrr*, *mmmrm*, and *mrmrm* can be recognized in the ^{1}H NMR spectra, respectively with resonances at = 5.18, 5.19, 5.20, 5.22, 5.23, 5.24 ppm; since only the last hexad contains the *rmr* tetrad, the corresponding area can be used to calculate [*rmr*] as follows:

$$[\text{rmr}] = \frac{\text{Area (rmr)}}{\text{Area (tot)}}$$

The percentage of racemization (%rac) was calculated by deconvolution of methine multiplet of the ^{1}H-NMR homonuclear decoupled spectrum using the Mestrelab software fitting tool.

4.2.3.4 Thermal analysis

Differential scanning calorimetry (DSC). DSC thermograms were acquired with a Q2500 (TA Instruments, US) DSC system equipped with a RCS-90 refrigerated cooling system. Powder polymer samples (~ 5 mg) were loaded into hermetic aluminium pans, and a conventional heating-cooling-heating scan was performed between -20 and 180 °C with a temperature ramp of 10 °C/min under nitrogen atmosphere. Equilibration isothermal periods of 2 minutes were applied prior to each scan. Melting (Tm) and crystallization (Tcc) temperatures were measured as the maxima of the corresponding phase transition peaks; in some instances, it was useful differentiate the location of the onset and that of the maximum of the melting process, and in these occasions Tm_{onset} and Tm_{max} were correspondingly used. The glass transition temperatures (Tg) were calculated as the inflection points of the transition in the second heating run. Melting enthalpy (ΔH_m) and, if present, cold crystallization enthalpy (ΔH_{cc}) were determined by integration of the corresponding transition peaks in the first heating DSC thermograms. Crystallinity (X_c) was subsequently calculated as follows:

$$X_c = \frac{\Delta H_m - \Delta H_c}{\Delta H_m^{\,0}} \cdot 100$$

Where $\Delta H_m^{\,0}$ is the enthalpy of fusion of 100% crystalline PLLA (poly(L-lactide), 93 J/g).[196]

Thermogravimetric analysis (TGA). TGA analysis was performed on the precipitated poly(lactide)s in powder form using a Q500 analyzer (TA instruments, US). Measurements were performed on 3–5 mg samples in an aluminum pan at a heating rate of 10 °C/min, from 30 to 600 °C under nitrogen. The weight loss of the specimens was recorded as a function of time and

temperature simultaneously. Onset of decomposition and maximum decomposition temperature were determined from TGA and its non-zero first derivative (DTG curve), respectively.

4.2.3.5 X-rays diffraction analysis (XRD)

X-ray diffraction (XRD) measurements of multi-armed poly(lactide) powder samples were performed on a PANalytical Empyrean X-ray diffractometer using a Cu Kα anode (λ = 1.5406 Å) operating at 45 kV and 40 mA. The diffraction patterns were collected in the range 2-70° 2θ with a 0.04° step size.

4.2.3.6 Shear rheometry

Measurements were performed on 6-armed poly(lactide) samples using a Haake Mars 40 Rheometer (Thermo Fisher Scientific, US) equipped with a flat probe P35/Ti (parallel plate geometry). The storage modulus (G') and loss modulus (G") were measured as a function of temperature, which was linearly decreased (ΔT = 5 °C/s) from 200 °C to 25 °C, applying a shear stress and an oscillation frequency (*f*) of 25 Pa and 1 Hz, respectively. Once defined the complex modulus as $G^* = \sqrt{(G'^2 + G''^2)}$, the complex viscosity was obtained as $\eta^* = G^*/(2\pi f)$.

4.2.3.7 Atomic-force microscopy (AFM)

Samples preparation. Homogenous polymer films were produced by drop casting of 20% w/V $CHCl_3$ solutions of the poly(lactide)s on ⌀ = 13 mm circular glass coverslips, employed as rigid support. Solvent was slowly removed by leaving samples at ambient pressure and RT for 3 days, followed by 24h under reduced pressure and RT in a vacuum oven. Subsequently, films were annealed at 80°C for 10 hours, in order to reach the maximum crystallinity depending on the polymer stereoconfiguration.

Measurements. Nanoindentation studies were performed in air using a Molecular Force Probe 3D AFM (Model MFP-3D, Asylum Research – Oxford Instruments, UK). A TESPA-V2 sharp tip (Bruker AFM Probes, Camarillo, CA) was used for all measurements. The actual spring constant (*k*) was determined by the thermal noise method, *k* = 33 N/m. On each sample analyzed, several force maps were acquired performing 36 indentation curves (maximum force applied = 1μN) within a 20 μm × 20 μm area (spatial resolution ≈ 11 μm^2) at 0.25 Hz (0.75 μm/s). Corresponding force maps were acquired. The relative elastic modulus was calculated by fitting the force-indentation data with the Hertz sphere model (Hertz sphere-on-flat model).

4.2.3.8 Hydrolytic degradability

The hydrolytic degradation profile of the multi-armed poly(lactide)s was assessed by monitoring the molecular weight distribution (degradation) and weight loss (erosion) over a 50-days period of incubation in phosphate-buffered saline (PBS) medium. In order to evaluate the effect of tacticity and topology on degradation kinetic, two different architectures were selected for the experiment, 1-armed linear and 4-armed star, with varying corresponding stereoconfigurations: PLLA, PLLA-*b*-PDLLA, PDLLA-*b*-PLLA and PDLLA for star architecture and only PLLA and PDLLA for the linear reference. For each polymer, ~ 15 mg samples (in the form of powder) were placed in 2 mL of PBS solution and left at 30 °C under gentle agitation for different periods of time:0, 4, 14, 24, 34 and 50 days. Once concluded the incubation period, samples were centrifuged (14000 g, 10 minutes) and washed with fresh milliQ water. Resulting pellets were then freeze-dried to remove any water residue for weight loss assessment. Samples were then directly redissolved in THF (2mL) for further GPC analysis. Each experiment was performed in triplicate.

4.3 Results and Discussion

4.3.1 Preliminary screenings and synthesis optimization

The main objective of the synthesis optimization was to find a polymerization system that allows solubilisation of a wide variety of multi-functional hydroxyl initiators. Such features could be hardly achieved through bulk polymerization, as polyols with high functionalities are generally found completely insoluble in the lactide monomer melt. On the other hand, these compounds are generally poorly soluble also in commonly employed solvents for solution ROP.[178,257]
After screening diverse alternative solvents systems, N-methyl pyrrolidone was found as an excellent alternative for the novel synthetic protocol, as it allows the use of multi-functional initiators of diverse nature (*e.g.* common polyols, sugars, hydroxylated polymers) with lower environmental and safety issues than commonly used solvents such as DCM, $CHCl_3$, DMF or toluene.[263–265]

A preliminary screening of DBU-mediated lactide ROP in the NMP solvent was previously carried out using a standard benzyl alcohol (BnOH) as monofunctional initiator and kinetic profiles were obtained in NMP by varying temperature (35, 25 and 5 °C), monomer

concentration (ranging 0.1 to 2 M) and, consequently, the total degree of polymerization (Figure 4.2).

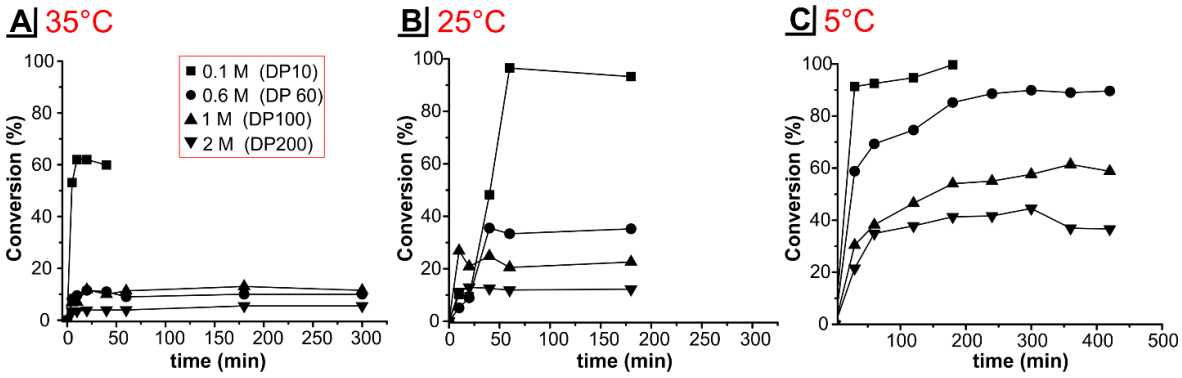

Figure 4.2: Kinetic profile of linear poly(D,L-lactide) polymerization in NMP at **A,** 35 °C **B,** 25 °C and **C,** 5 °C. The [OH]:[DBU] ratio was maintained constant at 1:1 while [LA] was varied.

Since ROP is an equilibrium polymerization, the ability of lactide to polymerize is highly influenced by reaction parameters (*i.e.* temperature, concentration of reagents) and solvent (i.e. ring strain) which drive the equilibrium towards monomer or polymer. While more thermodynamically favoured solvent systems for cyclic esters ROP (*i.e.* $CHCl_3$, DCM) knowingly provide polymerization completion within 1 hour at RT,[249,255] lactide ROP in NMP initially showed low conversions under the same conditions (25 °C, [DBU]:[OH] =1), which were further reduced at 35 °C. The findings indicate that lactide ROP in NMP exhibits a relatively low ceiling temperature (Tc). The Tc is the temperature at which the rate of polymerization and depolymerization are equal; note, the residual monomer concentration of a polymerization that reaches the Tc is termed the monomer concentration at equilibrium ($[M]_{eq}$). Indeed, when the polymerization temperature was decreased to 5 °C, considerable conversions and narrow dispersities (<1.1 for all DP values, data not shown) were obtained in less than three hours. This is consistent with the theory that depolymerization is entropically driven (higher disorder), whereas polymerization is enthalpically driven: in the Gibbs free energy equation ($\Delta G = \Delta H - T \cdot \Delta S$), higher T increases the enthalpic contribution and thus depolymerization.

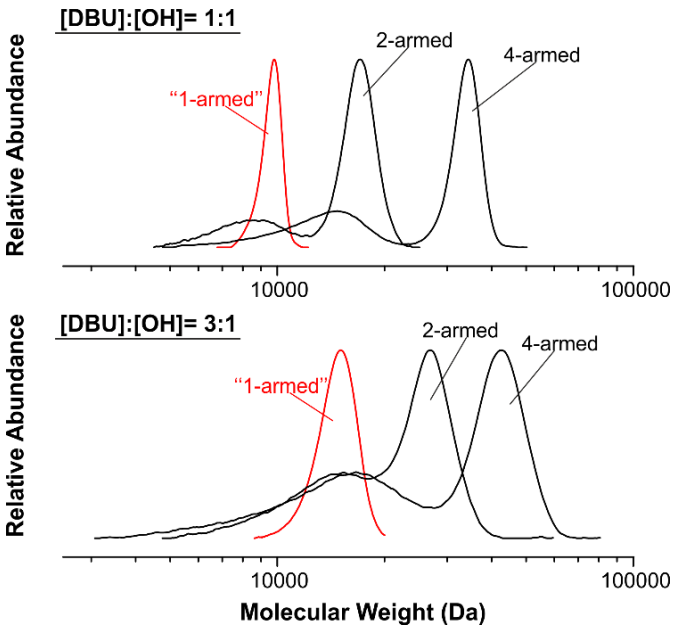

Figure 4.3: GPC molecular weight distributions of the lactide ROP in NMP performed at equimolar (top) or excess molar (bottom) content of DBU with respect OH groups, in presence of a mono-, bi- or tetra-functional initiator.

However when multi-functional initiators (2- and 4-armed) were used under the same reaction conditions ([DBU]:[I]:[M] of 1:1:100, 1 M [LA]), a secondary, lower MW product appeared; its relative presence appeared to increase when larger DBU-to-OH molar ratios were used in an attempt to increase the polymerization yield (compare Figure 4.3, top and bottom, and Table 4.1).

Table 4.1: Molecular weight and dispersities of 1-, 2- and 4-armed PDLLA after 3 hours of polymerization in NMP. DBU loading was varied from 1 to 3x molar excess to OH groups. BnOH was used as mono-hydroxyl initiator. Benzendimethanol (BDM, OH function = 2) and pentaerythritol (PET, OH function = 4) provided respectively a 2-armed linear and a 4-armed star PDLLA.

#arms	[DBU]:[OH]	Conversion (%)[a]	Mn_{GPC} (kDa)[b]	Đ[b]	$A_{sub\text{-}prod}$ (%)[c]
1	1:1	61	9.5	1.01	n.d.
2	1:1	68	15.6	1.12	18
4	1:1	64	35.2	1.23	19
1	3:1	92	14.5	1.09	n.d.
2	3:1	98	19.2	1.26	30
4	3:1	98	39.8	1.41	33

All polymerization were performed at 5 °C and 1M monomer concentration. [LA]:[OH] (DParm) was maintained constant at 100. [a] Measured by ^{1}H-NMR in $CDCl_3$ after 3 hours. [b] Measured by GPC in THF using triple detection. In the case of #arms >1, data correspond to average MW calculated from the obtained bimodal distribution. [c] Relative contribution of sub-product calculated as corresponding percentage on total GPC chromatograms integral by peak deconvolution.

Recent studies have highlighted that DBU promotes cyclic ester ROP through two possible activation mechanisms, namely alcohol deprotonation (alcohol activation pathway, AAP, Scheme 4.2A), and monomer activation (nucleophilic-attack pathway, NAP, Scheme 4.2B).[249,255]

Importantly, NAP leads to linear polymer chains irrespective of the presence of initiators, although the product would be difficult to distinguish from that of a monofunctional initiator. On the contrary, if NAP is operational when multifunctional initiators are used, the linear PLA secondary product would be easier to distinguish from its branched analogs due to its lower molecular weight (higher monomer to "initiator" ratio).

Mechanistic studies on the DBU-mediated ROP, using mono-functional initiators and DCM solvent, showed that the AA pathway is much more kinetically favored (activation kinetic constant ka= 9.88 x10^4 s^{-1}) than NAP (ka= 7.91 x10^{-4} s^{-1}) and therefore, the former is typically the most probable initiation to occur. However, the occurrence of NAP can be favored by reaction conditions, such as an excess of DBU with respect to the OH groups, which was found to promote the undesired concomitant activation of the monomer and its subsequent propagation.[255]

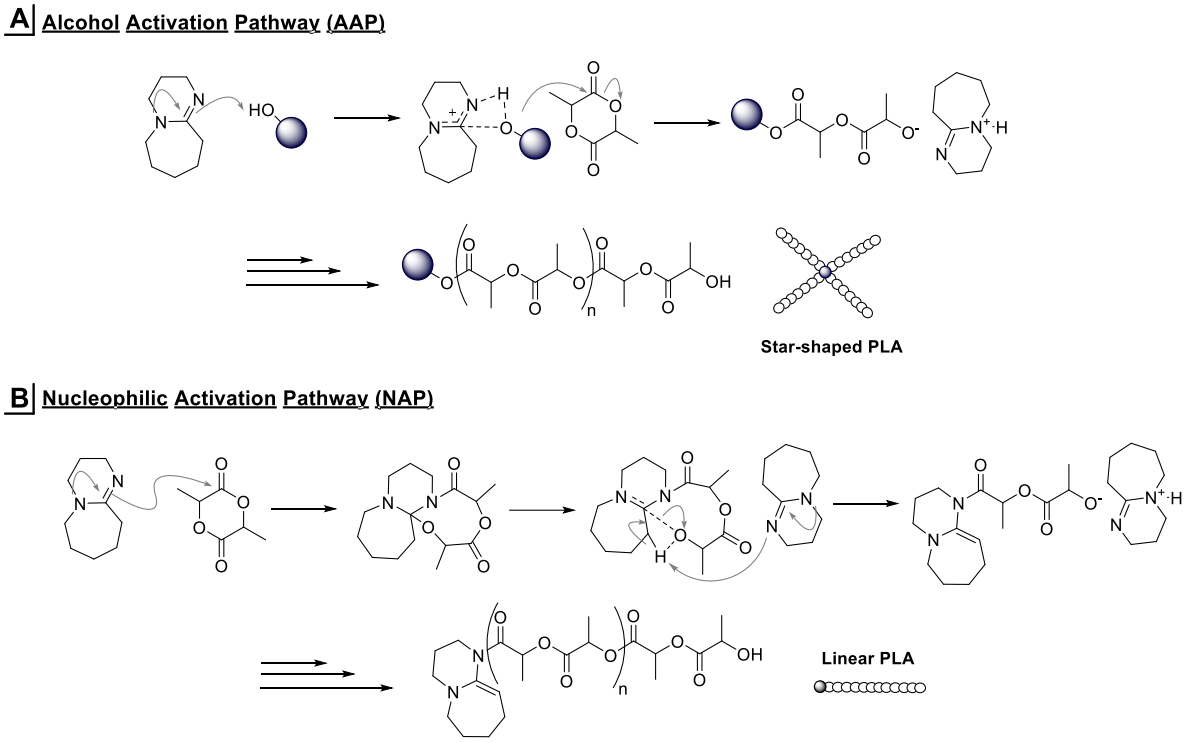

Scheme 4.2: Comparison of possible activation pathways provided by DBU for lactide ROP, adapted from Sherk *et al.*[255] A, Alcohol activation pathway (AAP), DBU act as a base and activate the multifunctional alcohol, which in turns provides the initiation, thus obtaining a branched PLA. B, Nucleophilic activation pathway of DBU, where DBU directly initiates the ring-opening by nucleophilic attack of the monomer, yielding a linear (1-armed) PLA chain.

These findings are in agreement with the obtained results for lactide polymerization in NMP, though in this latter case a certain contribution of the low-MW sub-product was observed also with equimolar [DBU]:[OH] ratio when multi-functional polyols were used.

However, it should be noted that the aforementioned mechanistic studies were conducted in solvents in which ROP is more thermodynamically favored ($[M]_{eq} \approx 0$) and employing mono-hydroxyl initiators. It was speculated that the contribution of NAP pathway could be more favored in presence of highly polar solvents, such as NMP, in which the stronger monomer-solvent interactions could partially compensate the ring-strain, thus providing lower polymerization rates and increasing $[M]_{eq}$ (higher amount of monomer available for DBU activation), compared to polymerizations performed in DCM or $CHCl_3$.

In this instance, control of the reagents molar ratios, specifically [OH]:[DBU] and [LA]:[DBU], is a key factor to minimize the occurrence of NAP and to ensure a controlled character of the polymerization.[255] However, increasing the [OH]:[DBU] ratio might not be advised in solvents that have less favorable thermodynamics, such as NMP, since lower DBU content would lead to an overall reduced polymerization efficiency, with slower alcohol-initiation and propagation

rate ($k_{i,OH}$ and k_p Scheme 4.3). Conversely, provided a sufficiently fast alcohol-initiation rate, the equilibrium of propagation reaction can be shifted toward the products by controlling the [LA]:[DBU] molar ratio, to ensure high propagation rate and minimum amount of monomer available for alternative initiations.

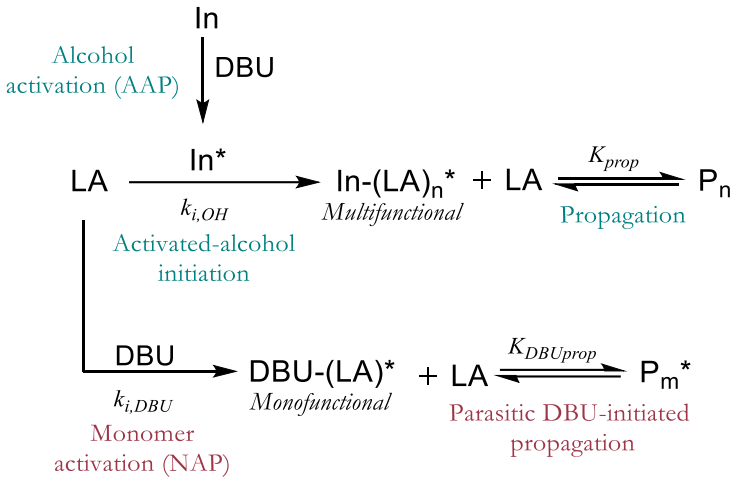

Scheme 4.3: Description of alcohol-activated initiation and propagation and competing parasite monomer activation by DBU, which leads to a linear polymer. In* = activated alcohol initiator, $k_{i,OH}$ = kinetic constant of alcohol chain initiation, K_{prop} = constant of alcohol initiated propagation, $K_{DBUprop}$ = reaction constant of undesired DBU-activated propagation. Higher $k_{i,OH}$ can be favored by higher OH-to-monomer contents (lower DParm), reducing contribution of parasitic initiation.

Therefore, we have adopted a starve-fed (monomer-starved) approach, in which [LA]:[DBU] was reduced while keeping the other parameters constant (*i.e.* [OH]:[DBU] and LA concentration) to ensure the equilibrium of propagation reaction would be shifted toward the desired multi-armed products.

In this new set of polymerizations, the [LA]:[OH] molar ratio was varied by dosing the monomer in two equal stacked additions (50 eq at 0 h and 50 eq at 3 h), while maintaining equimolar ratio of [OH]:[DBU] throughout the polymerization.

The initial theoretical DParm was set at 50 in order to maintain LA concentration constant (1 M) along polymerization. After the second LA addition, the theoretical DParm thus corresponded to 100 units per arm, providing sufficiently high MW. Since DBU was fully added at 0 h, both catalyst and initiator were diluted as a consequence of the second monomer addition (solution in NMP).

Polymerization kinetics were utilized to determine the appropriate time for both the addition of the second monomer aliquot (reaction completion in 3 h) and the final quenching of the reaction (reaction completion in 6 h), thus to prevent broadening of the dispersities due to the occurrence of transesterification and NAP parasitic reactions (Table S. 1).

Under these new conditions, highly monodispersed and multi-armed poly(lactide)s were obtained, with no detectable side-product formation and good correspondence with specifics (Figure 4.4 and Table 4.2). Indeed, the lower DParm (per polymerization step), together with the use of equimolar content of DBU and OH, promoted higher alcohol-initiation (hence propagation) rates with resulting increased conversions and better control over polymerization kinetics. The faster polymerization also allowed lower residual monomer (~10% within 3 hours, Table S. 1) at the time of the second addition, thus ensuring high selectivity and sufficiently high MW.

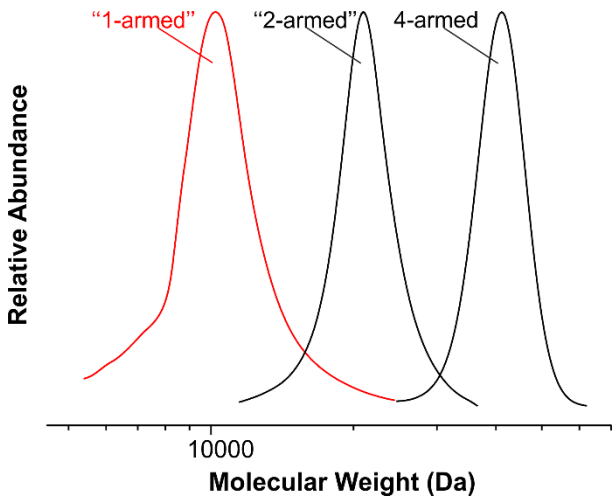

Figure 4.4: GPC traces of the 1-, 2- and 4-armed poly(lactide)s synthesized under the optimized ROP conditions (monomer-starved) after 6-hours polymerization.

4.3.2 Synthesis of a library of multi-armed poly(lactide)s with varying topology and tacticity

With the optimized conditions in hand, the versatility and robustness of the novel lactide ROP protocol in NMP was evaluated by employing diverse polyol initiators and lactide isomers, in order to obtain a library of controlled multi-armed poly(lactide)s with diverse topology and tacticity (Figure 4.5). Multi-functional initiator of diverse nature and functionality were tested, such as common polyols (benezendimethanol, pentaerythritol and dipentaerythritol), sugars (sucrose) and hydroxylated polymers (poly(vinyl alcohol), PVA 80% hydrolyzed) and compared to their 1-armed analogue. This provided different multi-armed PLA architectures, ranging from linear (1-, 2-armed) to star-shaped (4-, 6-, 8-armed). Also a previously unaccessible high-MW comb PLA structure could be obtained by means of the PVA macroinitiator (number of arms ≈ 140, 80% hydrolyzed). Indeed, the high hydrophilic character of such hydroxylated polymers prevents its use as initiator with commonly used solvents or bulk ROPs.

For each of the selected architectures, the versatility of the devised protocol enabled the synthesis of PLLA and PDLLA homopolymers, as well as of block-copolymers of diverse stereoconfigurations by simply varying the feed monomer isomer at the different stage of polymerization. Indeed, the alternate addition of L- and DL-lactide yielded PLA block (stereo-)copolymers: similarly to soft-hard block copolymers, each PLA arm was formed by a rigid L-lactide-based block, due to its capability of crystallization, and a mobile DL-lactide-based block. Therefore, for each architecture, multi-armed PLLA-*b*-PDLLA and PDLLA-*b*-PLLA structures were synthesised, respectively bearing the crystallisable segment close to the branching point or as terminal block.

The different and varying tacticity would interestingly influence final thermal and mechanical properties of the material, as the crystalline L-lactide chain segments act as additional physical constraints in the complex branched framework. Therefore, the synergistic effect of topology and tacticity could then provide materials with different chain mobility and crystallizability.

A degree of polymerization of 100 units per arm (DParm) was set as target for all polymers, in order to obtain equal arm lengths for all architectures and thus comparable chain propagation kinetics, along with increasing molecular weights as a function of the branching degree. It was speculated that the average resulting branch size (approximately 14 kDa for DParm =100) could provide relatively flexible and highly biodegradable poly(lactide)s as reduced likelihood of

entanglements are favored by relatively short branch lengths,[143] yet ensuring sufficient thermal stability for melt processing (initial thermal degradation temperature above 200-250 °C).

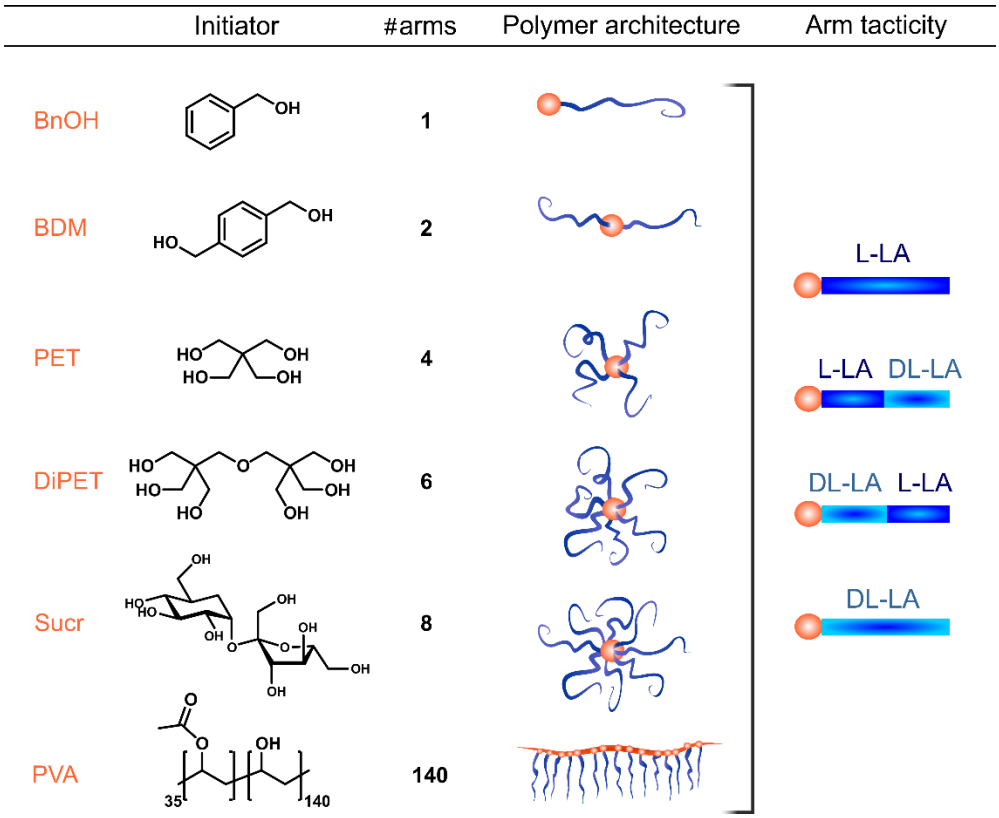

Figure 4.5: Linear and branched poly(lactide)s architectures produced via ring-opening polymerization of L-LA and DL-LA in NMP by DBU catalysis. PLA with linear (1-armed, 2-armed), star (2-8 armed) and comb (~140 arms, 80% hydrolyzed PVA macroinitiator of Mn = 13kDa) structures were produced. For each architecture four poly(lactide)s with different tacticity were obtained. From top right: PLLA, PLLA-*b*-PDLLA, PDLLA-*b*-PLLA, PDLLA.

Monomer conversion and molecular weight were monitored over the entire polymerization period through ^{1}H-NMR and GPC analysis. As visible from the summarized results in Table 4.2, the novel lactide ROP protocol provided highly-monodispersed poly(lactide) structures (Figure 4.6) with excellent correlation between NMR and GPC data. The synthesized multi-armed PLAs possess Mw ranging between 10 kDa and 2000 kDa, with dispersities values far below typical values reported for multi-armed polyesters of comparable molecular weights, especially in the case of bulk polymerizations.[173,176,185]

Table 4.2: Summary of the main molecular weight results for the library of multi-armed poly(lactide)s with diverse tacticity and degree of branching after precipitation.

Sample label[a]	#arms[b]	Conversion (%) [c]	Mn_{NMR} (kDa) [d]	Mn (kDa) [e]	Mw (kDa) [e]	Đ [e]
***L*_(PLLA)**	1	88	12.7	12.7	14.4	1.13
***L*_(PLLA)$_2$**	2	88	14.1	24.0	25.5	1.05
***S*_(PLLA)$_4$**	4	86	49.5	44.1	47.8	1.08
***S*_(PLLA)$_6$**	6	89	76.9	74.6	76.1	1.02
***S*_(PLLA)$_8$**	8	75	92.4	86.8	88.9	1.02
***C*_(PLLA)$_{140}$**	140	78	1572	-	1913[f]	-
***L*_(PLLA-*b*-PDLLA)**	1	81	11.5	11.9	12.3	1.05
***L*_(PLLA-*b*-PDLLA)$_2$**	2	82	23.5	22.9	24.0	1.05
***S*_(PLLA-*b*-PDLLA)$_4$**	4	79	45.4	43.2	47.2	1.09
***S*_(PLLA-*b*-PDLLA)$_6$**	6	76	65.7	69.4	74.0	1.07
***S*_(PLLA-*b*-PDLLA)$_8$**	8	77	81.8	82.3	82.8	1.01
***C*_(PLLA-*b*-PDLLA)$_{140}$**	140	69	1391	-	2033[f]	-
***L*_(PDLLA-*b*-PLLA)**	1	79	11.4	11.8	11.4	1.03
***L*_(PDLLA-*b*-PLLA)$_2$**	2	80	22.9	21.5	23.7	1.10
***S*_(PDLLA-*b*-PLLA)$_4$**	4	78	45.1	42.1	46.5	1.07
***S*_(PDLLA-*b*-PLLA)$_6$**	6	77	66.9	69.7	77.3	1.11
***S*_(PDLLA-*b*-PLLA)$_8$**	8	73	91.2	79.3	89.0	1.12
***C*_(PDLLA-*b*-PLLA)$_{140}$**	140	73	1472	-	1673[f]	-
***L*_(PDLLA)**	1	84	12.1	10.8	11.7	1.10
***L*_(PDLLA)$_2$**	2	83	23.9	22.9	24.5	1.07
***S*_(PDLLA)$_4$**	4	82	47.2	38.3	42.5	1.11
***S*_(PDLLA)$_6$**	6	79	68.3	64.4	70.6	1.10
***S*_(PDLLA)$_8$**	8	76	87.4	76.5	81.1	1.06
***C*_(PDLLA)$_{140}$**	140	67	1351	-	1229[f]	-

[a] *L* stands for linear, *S* for star, *C* for comb. [monomer] = 1 M, polymerizations were performed in a parallel fashion, in NMP at 5 °C for 6 hours, with a theoretical DParm=100 and using DBU in equimolar ratio to the OH groups: (i.e. [M]:[OH]:[DBU]=100:1:1).
[b] Theoretical number of arms = functionality of the initiator. Since in no polymer we observed the ^{1}H-NMR resonances of unreacted alcohols (at e.g. d = 3.8 ppm for PET), the actual and theoretical arm number were assumed to be identical.
[c] DL-LA and L-LA were added to the reaction mixture by staggered additions in a starved-fed (monomer-starved) polymerization with a DL:L molar ratio of 1:1 (0.5 eq at 0 h and 0.5 eq at 3 h). The conversion is expressed as the consumed monomer at a given time point, as detected by ^{1}H-NMR in $CHCl_3$.
[d] Measured by ^{1}H-NMR in $CHCl_3$ by calculating the corresponding monomer conversion.
[e] Molecular weight and dispersities measured by GPC in THF using triple detection.
[f] Mw calculated by static light scattering (SLS) measurements in THF (see Table S. 2)

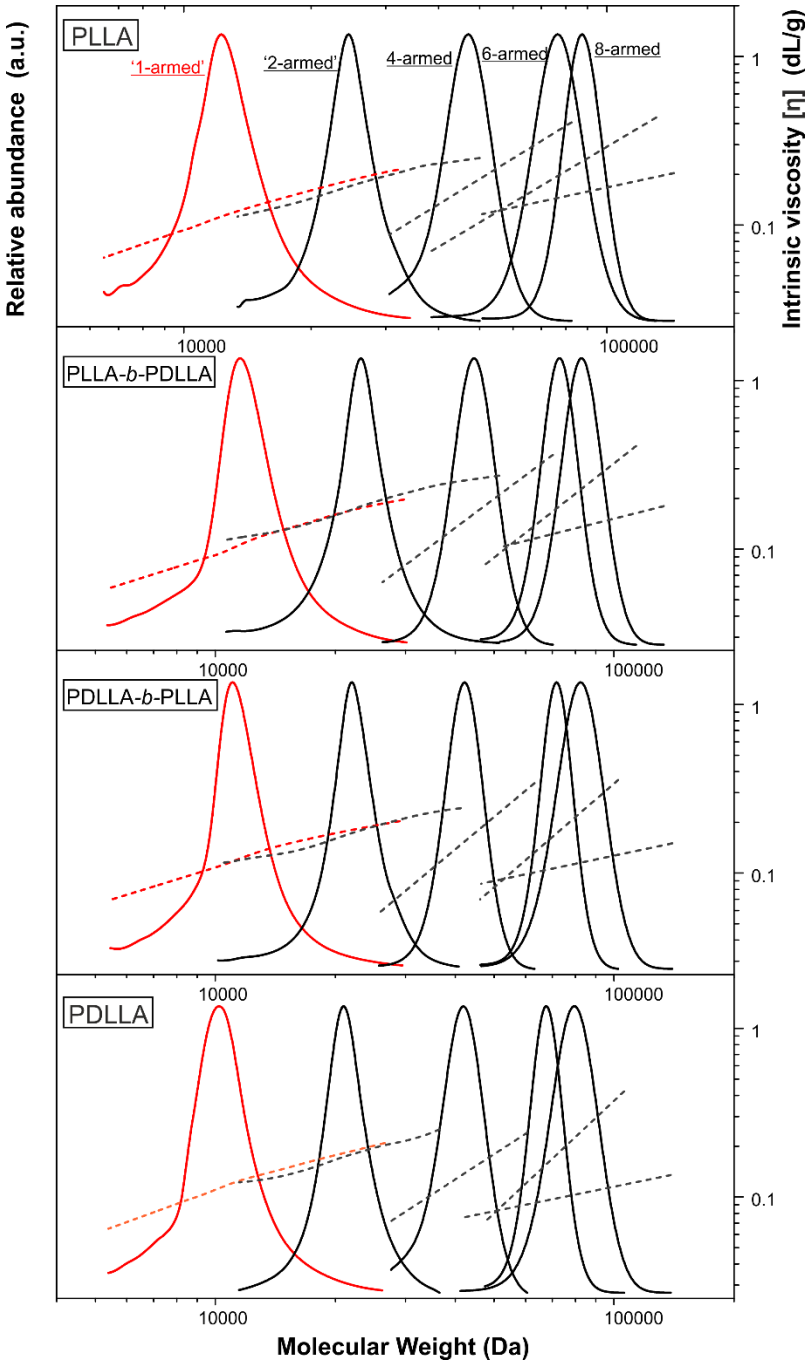

Figure 4.6: Distribution plots and intrinsic viscosity ([η]) trends of the linear and star poly(lactide)s according to their diverse stereoconfigurations (PLLA, PLLA-*b*-PDLLA, PDLLA-*b*-PLLA and PDLLA) as measured by triple detection GPC in THF. For the same MW, progressively lower viscosities are observed along with increasing branching degree.

In the case of the PVA-*comb*-PLA structures, the absolute average molecular weight was calculated through SLS measurements, as the MW was exceeding GPC columns separation limit (Figure S. 1). The resulting Mw confirmed that also in this case the final Mw values were found in good accordance with NMR data. Moreover, GPC analysis of the PVA-*comb*-PLAs was

anyway exploited to acquire additional information regarding conformation, compactness and hydrodynamic size of such architecture with respect to the other produced multi-armed poly(lactide).

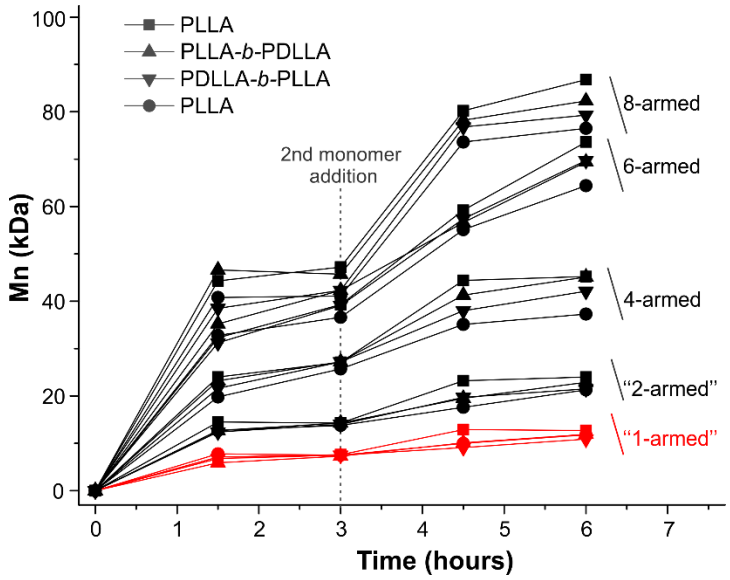

Figure 4.7: Number average molecular weight growth over a 6-hours polymerization period for the linear (1, 2 arms) and star (4, 6 and 8 arms) PLAs with varying tacticities as monitored by GPC analysis.

Good conversions (average value of 79%) were obtained for all multi-armed poly(lactide)s after 6-hours polymerization, although slightly lower values were detected for increasing branching degree (*e.g.* 88% vs 76% for the 1-armed linear and comb PLLAs, respectively). A controlled increase of the number average molecular weight during the polymerization period was observed, according to the number of branch points (Figure 4.7); note, a sudden increase in Mn was detected after the second monomer addition at 3 hours, due to the higher initial polymerization rate. Additionally, despite the different reactivity of the OH groups (three secondary and four primary alcohols), optimal accordance with theoretical molecular weights were observed also when the disaccharide sucrose was used as initiator, along with comparable conversions with respect to the other polyols. This suggested that all PLA arms were efficiently formed and with reasonably similar kinetics (for additional information regarding kinetics and MW growth over polymerization time, see Table S. 1.

It should be mentioned that the external/second block is probably shorter than the one closer to the core, as first likely reaches near 100% conversion, whereas the second block may range from 34-78% conversion, as the polymerization reaches equilibrium.

Noteworthy, higher conversions and molecular weights were obtained when higher L-lactide isomer contents were used. Indeed, independently of the architecture, an increasing trend of Mn from PDLLA to PLLA structures (lower retention volume in the GPC chromatograms, Figure 4.8) was observed. This behavior was ascribed to the higher rigidity of PLLA polymer chains with respect to PDLLA, due to the capability of assuming helical conformation in solution.[266,267] Therefore, the structurally stiff terminal L-lactide segments are more available for new monomer addition during the polymer chain propagation with respect to the flexible DL-LA-based chains, which are more coiled and thus hidden into the polymer core.

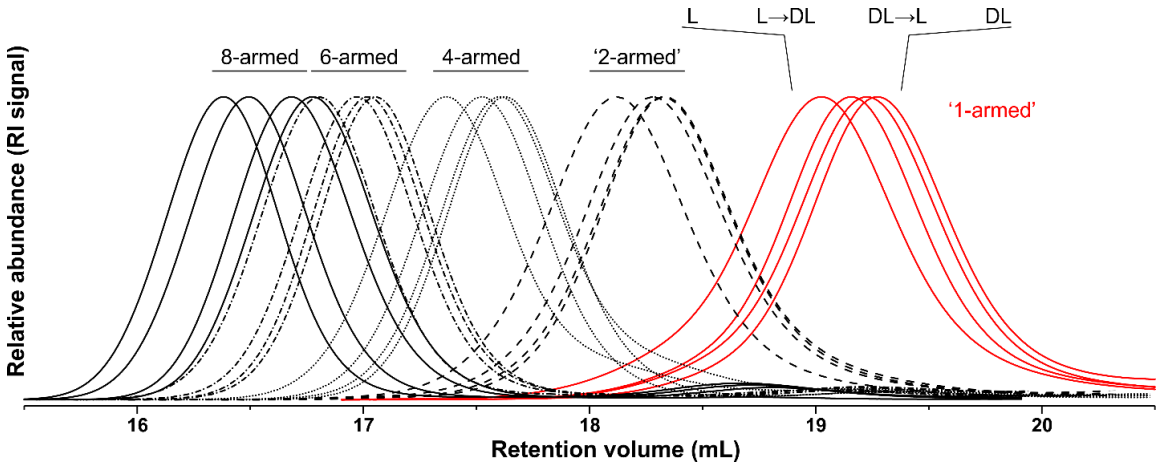

Figure 4.8: GPC chromatograms (as normalized RI detector traces vs retention volume) of the 1-, 2-, 4-, 6- and 8-armed poly(lactide) obtained by the optimized monomer-starved conditions over a 6-hours polymerization time and varying the monomer stereoisomer in the feed (L-LA, DL-LA or alternated addition of the two isomers).

By comparing MW distributions and intrinsic viscosity trends of the linear and star-poly(lactide)s (Figure 4.6), it is apparent that, for equal molecular weights, the solution viscosity decreased with increasing branching degree, as a result of the inherently lower hydrodynamic volume of branched architectures. The two linear structures (1- and 2-armed) showed instead comparable intrinsic viscosity values at the same molecular weight.

The introduction of branching dramatically changed the macromolecular structure. Indeed, a decreasing trend of the Mark Houwink *a* parameter as a function of the number of arms was observed (Figure 4.9A), demonstrating that the polymer coils progressively became more compact with increasing number of arms. Linear poly(lactide)s showed, as expected, a contraction behavior typical of swollen coils ($1 > a > 0.5$), denoting a diffuse macromolecular conformation. On the other hand, star and comb poly(lactide)s gradually approached globular structures ($a < 0.5$) as function of the branching degree, reaching *a* values of approximately 0.25

in the case of the 8-armed poly(lactide)s. Slightly higher values of the *a* parameter (~0.4) were found for the PVA-*comb*-PLA structures, as previously reported in literature for comb polymers bearing number of arms higher than 20 (and extremely high MWs).[158,268] Interestingly, higher *a* values were always obtained by PLLA structures (for the same architecture), which are indeed more rigid and thus reasonably less susceptible to contraction. Conversely, D-LA-containing poly(lactide)s were found more compact (independently of the location or length of the D-segments), probably due to the higher mobility of the polymer chains. These results suggested that shorter crystallizable (L-LA units) blocks of PLA stereo-copolymers negligibly affect the macromolecular conformation, as results of the high macromolecular crowding around the branching point.

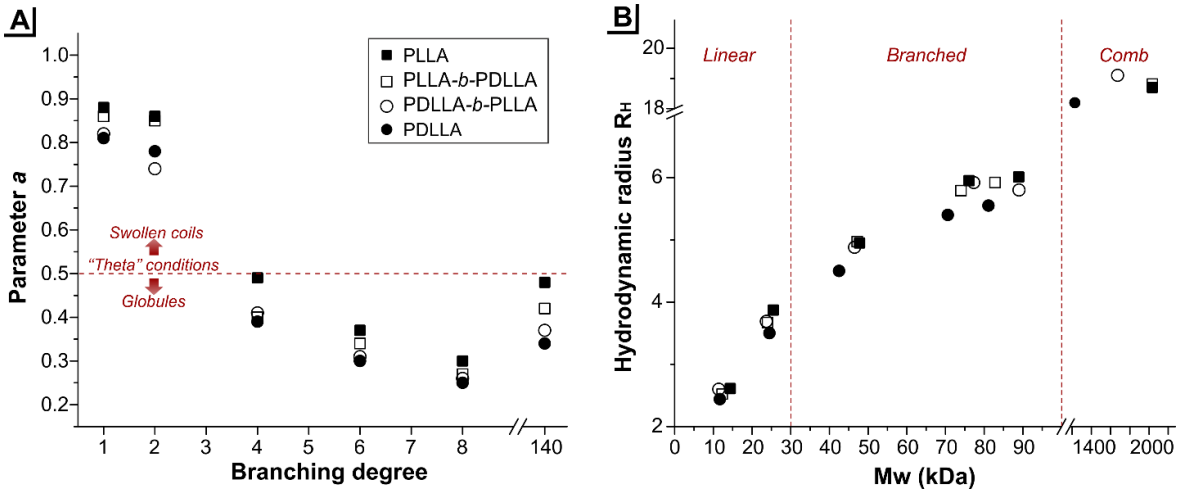

Figure 4.9: A, Mark−Houwink conformational parameter *a* vs number of arms; it is apparent that all branched PLAs (number of arms >2) are rather compact structures (0.2 ≥ a ≥ 0.5). **B,** Plots of hydrodynamic radius (R_H) vs weight average molecular weight (Mw) for all polymers. Measurements were obtained by triple detection GPC at a sample concentration of ~3 mg/mL in THF and a temperature of 35 °C.

Moreover, a slow increase of the hydrodynamic radius as a function of molecular weight was observed (*e.g.* an increase of >20 kDa from 2-armed to 4-armed structure corresponded to approximately 1 nm variation of the R_H, Figure 4.9B),[158] as a result of the contraction induced by branching introduction. Noteworthy, the calculated R_H values of the PVA-comb-PLA structures are comparable to the Rg values obtained through static light scattering measurements (Figure S. 1), ranging between 18 and 21 for the diverse PLA stereoconfigurations. Even though these Rg and R_H data were obtained by different techniques (hence with different sensitivity), these values indicatively correspond to a shape factor ρ

(=R_g/R_H) between 1 and 0.9 for the comb PLA structure. Such result indicates a globular conformation (hard sphere), in spite of the extremely high MW (>1500 kDa).[157]

Comparison of the different PLA stereoconfigurations by ^{1}H-NMR analysis clearly showed the disappearance of methine coupling related to racemic adjacent repeating units (atactic sequences) for increasing L-lactide contents, independently of the architecture (Figure 4.10A), thus confirming that higher polymer stereoregularity (isotacticity) is obtained in presence of PLLA segments.

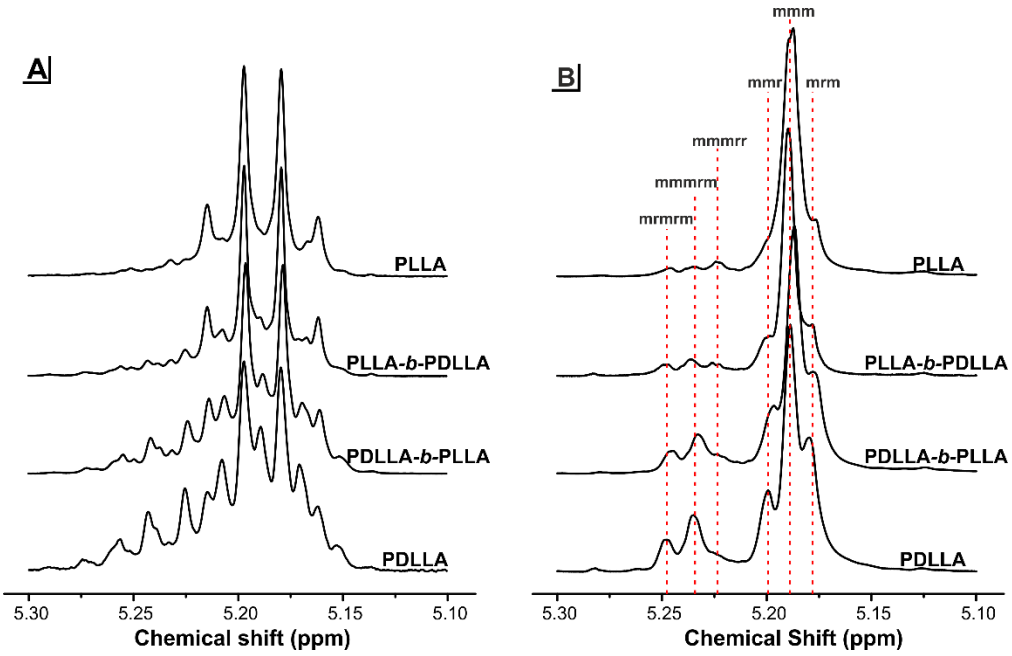

Figure 4.10: Methine region (5.1-5.3 ppm) of representative multi-armed PLAs in (**A**) ^{1}H-NMR spectra and (**B**) homonuclear decoupled ^{1}H-NMR spectra (coupling with methyl group is suppressed) with relative tetrads and hexads assignments.

In order to assess the exact tacticity of the diverse multi-armed PLAs, homonuclear decoupled ^{1}H-NMR experiments were then performed, allowing the assignment of poly(lactide) tetrads signals due to the improved resolution of the methine resonance. The subsequent integration of resulting methine multiplets provided quantification of the racemic diads (*r*), which can be used to determine the P*r* parameter, defined as the probability of finding a *r* diad, as well as the overall degree of racemization (%rac), as a measure of transesterification (Table 4.3).
PLLA homopolymers are very isotactic (P*r* values from 0.13 to 0.16), albeit with slightly higher, and increasing with degree of branching, P*r* than expected. This result could be partially ascribed to the occurrence of transesterification (the remaining contribution is yet not been identified).

Indeed, the detected *mmmrr* hexad (5.22 ppm) is generally absent in poly(lactide) resulting from L- and/or D-lactide, expect in the case of transesterification reactions, which knowingly determine racemization (loss of chiral information upon esters interchange).[262,269] The percentage of racemization (%rac, Table 4.3), obtained by deconvolution of the corresponding peak, confirmed that transesterification contribution is extremely low for all polymers (< 6%), especially compared to bulk polymerizations,[185] as expected given the highly monodispersed MW distributions.

Predictably, higher contribution of racemic diads was detected for increasing DL-LA units: increasingly atactic poly(lactide)s were obtained from PLLA to PDLLA structure, with predominantly atactic character in the case of the PDLLA-*b*-PLLA and PDLLA structures ($0.25 \geq P_r \geq 0.5$, Figure 4.10B). Furthermore, stereoregularity was found to be disturbed by introduction of branching, as a result of the lower likelihood of entanglements, thus reporting an increasing trend of P_r as a function of branching degree, for equal L/DL ratios in the feed. However, a statistically fully atactic poly(lactide) ($P_r = 0.5$) was not obtained. Therefore, L-rich polymer arms were preferentially formed, as also suggested by the faster L-lactide polymerization kinetics (Figure 4.8). A certain preference to form isotactic poly(lactide) arrays was also previously reported in DBU- and TBD-catalyzed ROPs.[249,270] Interestingly, such feature would suggest the formation of a L-lactide units gradient along the DL-blocks in the synthesized stereo-copolymers.

Table 4.3: Summary of tacticity analyses results for the synthesized multi-armed poly(lactide)s. The probability of finding a racemic P*r* (ranging between 0 for fully isotactic and 0.5 for atactic PLA) was assessed by means of homonuclear decupled ^{1}H-NMR experiments. Percentage of racemization (%rac) was successively calculated for all the multi-armed poly(lactide)s, as corresponding to the contribution of *mmmrr* sequence signal to the total polymer stereoconfiguration.

Sample	Pr [a]	%rac [b]
*L*_(PLLA)	0.13	6.3
*L*_(PLLA)$_2$	0.13	4.8
*S*_(PLLA)$_4$	0.12	4.4
*S*_(PLLA)$_6$	0.14	3.6
*S*_(PLLA)$_8$	0.18	3.4
*C*_(PLLA)$_{140}$	0.22	2.2
*L*_(PLLA-*b*-PDLLA)	0.16	4.7
*L*_(PLLA-*b*-PDLLA)$_2$	0.23	2.9
*S*_(PLLA-*b*-PDLLA)$_4$	0.23	2.5
*S*_(PLLA-*b*-PDLLA)$_6$	0.22	3.0
*S*_(PLLA-*b*-PDLLA)$_8$	0.27	1.8
*C*_(PLLA-*b*-PDLLA)$_{140}$	0.28	2.6
*L*_(PDLLA-*b*-PLLA)	0.30	2.3
*L*_(PDLLA-*b*-PLLA)$_2$	0.33	1.8
*S*_(PDLLA-*b*-PLLA)$_4$	0.29	1.4
*S*_(PDLLA-*b*-PLLA)$_6$	0.32	1.6
*S*_(PDLLA-*b*-PLLA)$_8$	0.32	0.9
*C*_(PDLLA-*b*-PLLA)$_{140}$	0.33	0.7
*L*_(PDLLA)	0.37	2.1
*L*_(PDLLA)$_2$	0.36	1.3
*S*_(PDLLA)$_4$	0.36	1.5
*S*_(PDLLA)$_6$	0.35	0.7
*S*_(PDLLA)$_8$	0.36	0.8
*C*_(PDLLA)$_{140}$	0.37	0.9

[a]Calculated following the equation $Pr = \sqrt{(2 \cdot [rmr])}$, where [*rmr*]= Area (*rmr*)/Area (tot). [b] %rac corresponds to Area (*mmmrr*)/Area(tot)·100

4.3.3 Material characterization

The *convergent* crowding of star-shaped poly(lactide)s dramatically limited the capability of chain folding into lamella, despite the presence of crystallizable segments (Figure 4.11A). Indeed, the synthesized PLLA structures reported reduced crystallinity as a function of the degree of branching, independently of the MW, as characterized by DSC and XRD (Table 4.4 and Figure 4.11C). Crystallinity rapidly decreased from approximately 33% for the linear poly(L-lactide)s to a minimum value of 6% in the case of the 8-armed PLLA, as visible from the progressively lower melting enthalpies with branching (Figure 4.11B).

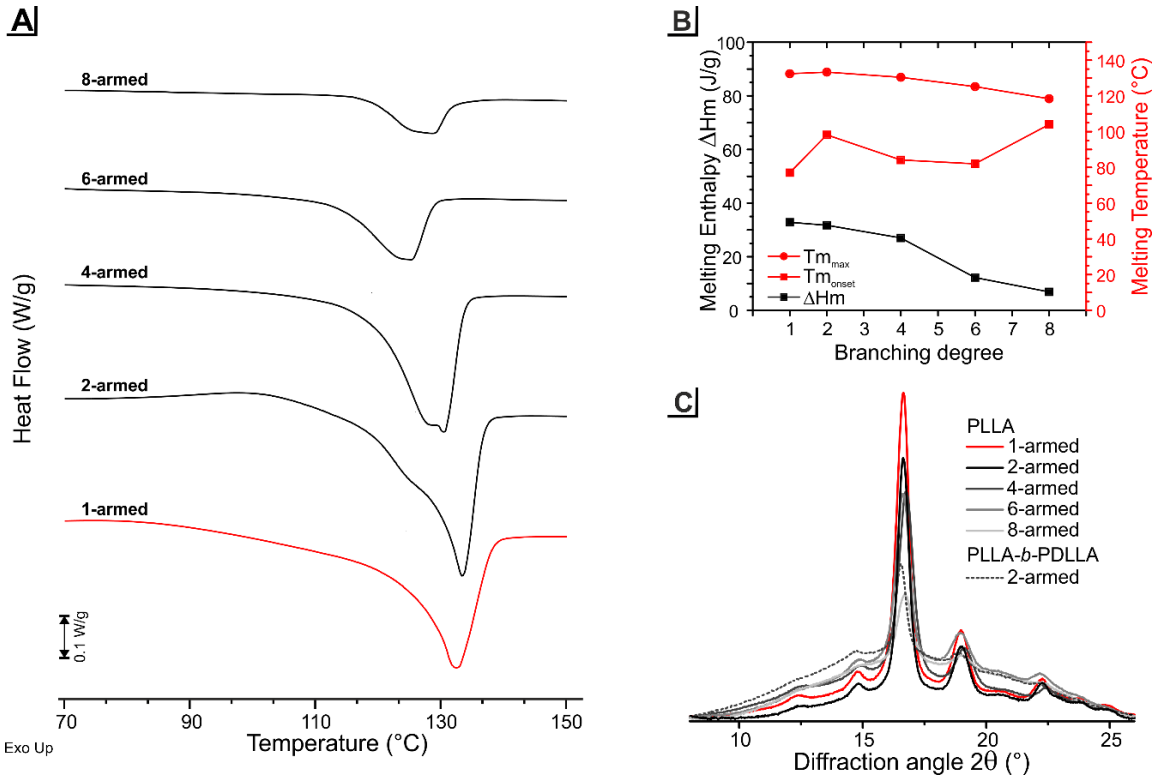

Figure 4.11: Thermal characterization of the multi-armed PLLA poly(lactide)s **A,** DSC first heating thermograms. PVA-*comb*-PLLA sample did not report any phase transition phenomena in this region, as a result of the high macromolecular crowding. No crystallization and melting transitions during cooling and second heating scans were observed. **B,** Trends of crystallinity (Xc), maximum melting temperature (Tm_{max}) and onset melting temperature (Tm_{onset}) of the reported PLLAs in function of the branching degree. **C,** Powder-XRD diffraction patterns of the synthesized semicrystalline PLA samples reporting a crystalline phase.

Linear polymers showed instead comparable melting enthalpies, despite in the case of the longer 2-armed PLLA chains also an additional, yet minimal cold crystallization phenomena was detected (ΔH_{cc} of 2 J/g), with resulting slightly lower crystallinity (Table 4.4).

Furthermore, it should be mentioned that the *parallel* crowding provided by the comb structure would typically facilitate intramolecular crystallization, due to the high packing density of the arms for this particular architecture.[158,271] Nevertheless, no crystallization or melting were observed for the synthesized PVA-*comb*-PLA structure. Most probably, the intercalated poly(vinyl acetate) (PVAc) units present in the PVA-rich backbone (80% hydrolysed PVAc) completely hampered interaction and packing of the PLA arms, given the excessive distance and macromolecular disorder. As a result, the poly(lactide) chains of the comb structure were unable to crystallize, independently of the stereoconfiguration.

Noteworthy, the PLA stereo-block systems were found amorphous (no crystallization or melting transitions detected during first or second heating run), with the exception of *L*_(PLLA-*b*-PDLLA)$_2$, as also confirmed from XRD analysis (Figure 4.11C). This suggested that, in PLLA-*b*-PDLLA branched structures the isotactic blocks are too close to the branching point to undergo crystallization, due to the excessive crowding around the branch point. Nevertheless, in this case of the corresponding linear structure with higher MW (2-armed), the crystallizable segments of each arm act as a single and sufficiently long L-LA-based linear chain with no effective branching points, thus presenting certain capability of crystallization (6% Xc). Alternatively, the significant entropy loss required for the ordering and entangling of the external mobile L-blocks in the PDLLA-*b*-PLLA copolymers did not allow crystallization.

Glass transition temperature (Tg) was found to be more significantly dependent on the molecular weight, rather than the branching degree of the poly(lactide)s, yet with subtle variations, as previously reported in literature.[129] Indeed, Tg ranged between 47 °C and 55 °C, with slightly increasing trends according to the MW and the L-lactide content, hence the isotacticity character of the structure, which reasonably promoted a more rigid framework.

Moreover, TGA analysis showed only small changes in onset degradation temperature ($Tdeg_{onset}$), whereas maximum degradation temperatures ($Tdeg_{max}$) ranged approximately between 300 and 360 °C, independently of the MW and branching degree, albeit a few degrees improvement for increasing isotacticity. For all polymers broad decomposition profiles were observed (independently of tacticity and branching degree, Figure S. 2), which could be ascribed to a poorly efficient work up and consequent minimal residual monomer or solvent, as even few ppm of such impurities are knowingly able to accelerate thermo-oxidative degradation process.[272–274]

Table 4.4: Thermal properties of the multi-armed poly(lactide)s measured by DSC and TGA analyses.

Structure	# arms	Tg (°C)[a]	Tm_{onset} (°C)[b]	Tm_{max} (°C)[b]	Xc (%)[c]	$Tdeg_{onset}$ (°C)[d]	$Tdeg_{max}$ (°C)[e]
PLLA	1	50	77	132	35	261	361
	2	52	98	133	32[f]	260	298
	4	53	84	130	27	262	315
	6	53	82	125	12	262	308
	8	53	104	118	6	268	361
	140	55	-	-	-	257	357
PLLA-*b*-PDLLA	1	48	-	-	-	249	359
	2	50	106	-	7	259	301
	4	52	-	-	-	258	300
	6	52	-	-	-	261	309
	8	53	-	-	-	266	362
	140	53	-	-	-	255	358
PDLLA-*b*-PLLA	1	47	-	-	-	251	358
	2	49	-	-	-	251	295
	4	51	-	-	-	254	305
	6	51	-	-	-	255	307
	8	50	-	-	-	267	362
	140	52	-	-	-	250	357
PDLLA	1	47	-	-	-	242	360[g]
	2	50	-	-	-	245	310
	4	51	-	-	-	246	308
	6	52	-	-	-	257	309
	8	52	-	-	-	252	361
	140	52	-	-	-	252	359

[a]Glass transition temperature (Tg) was calculated by half-height method from DSC 2nd heating scan. [b] Melting temperatures as measured from DSC 1st heating scan. [c] Calculated as $X_C=(|\Delta H_{cc}-\Delta H_m|/\Delta H_m^0)\cdot 100$, where $\Delta H_m^0= 93$ J/g (100% crystalline PLLA)[203] and $\Delta H_{cc}\neq 0$ only for 2-armed PLLA. [d]Onset degradation temperature ($Tdeg_{onset}$) was extrapolated from TGA curves. [e]Maximum degradation temperature ($Tdeg_{max}$) was detected by d-TGA. [f] Corresponding to a $\Delta H_{cc}=2$ J/g and $\Delta H_m=32$ J/g.

The effect of tacticity on final polymer properties, independently of the polymer architecture, was assessed in the melt state through shear rheometry measurements. The measurements were performed by directly melting the polymer at 200 °C in the instrument and monitoring the shear modulus and viscosity variations from 200 °C (hence above the melting point) until glass transition. Interestingly, both block PLA systems showed rheological behavior more similar to semicrystalline PLLA, with considerably higher viscosity values than the more mobile PDLLA structure at any temperature. Therefore, despite the lack of a crystalline phase (as for atactic PDLLA), the PLA stereo-block systems present capability of short-range interactions between

polymer chains and thus more rigid and viscous networks than PDLLA in the melt, with rather comparable profiles to the corresponding PLLA structure.

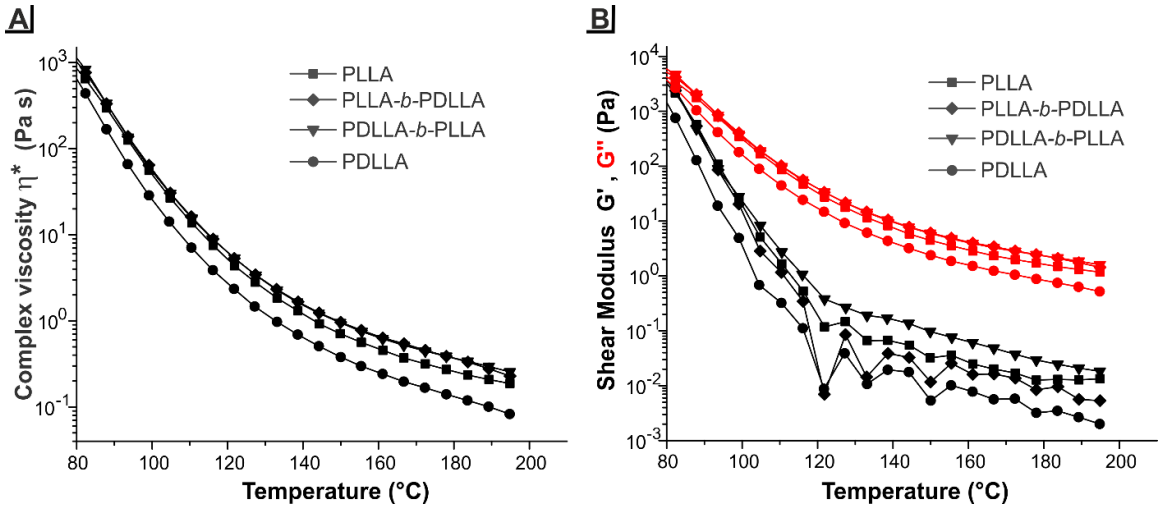

Figure 4.12: Complex shear viscosity (η*) (**A**) and storage (G') and loss (G") modulus (**B**) dependency on temperature for 6-armed poly(lactide)s in stress-controlled oscillatory experiments (parallel-plate geometry, frequency: 1Hz). Temperature was lowered from 200 to 25 °C with a 5 °C/min ramp.

This behavior was further investigated by measurement of material stiffness through AFM nanoindentation of branched poly(lactide) annealed films (Figure 4.13). It is apparent that the stereo-block copolymers presents intermediate elastic modulus compared to the corresponding homopolymers, notwithstanding the reduced crystallizability of the star poly(lactide). PLLA-*b*-PDLLA copolymer reported considerably enhanced elastic response compared to PDLLA. Therefore, the L-block is able of intermolecular interactions, thus providing a relatively rigid PLA material, with more similar mechanical stiffness to the isotactic PLLA structure. PDLLA-*b*-PLLA showed instead minimal increase in elastic modulus with respect to the highly atactic PDLLA structure, thus denoting that the shorter and external (higher chain mobility) L-block has negligible effect on final material properties, despite the presence of L-lactide repeating units. This resulted in a more ductile PLA structure.

Noteworthy, the higher distribution of elastic modulus values for PLLA and PLLA-*b*-PDLLA samples indicated the presence of heterogeneously distributed crystalline domains, as clearly visible from the nanoindentation force maps (Figure S. 3).

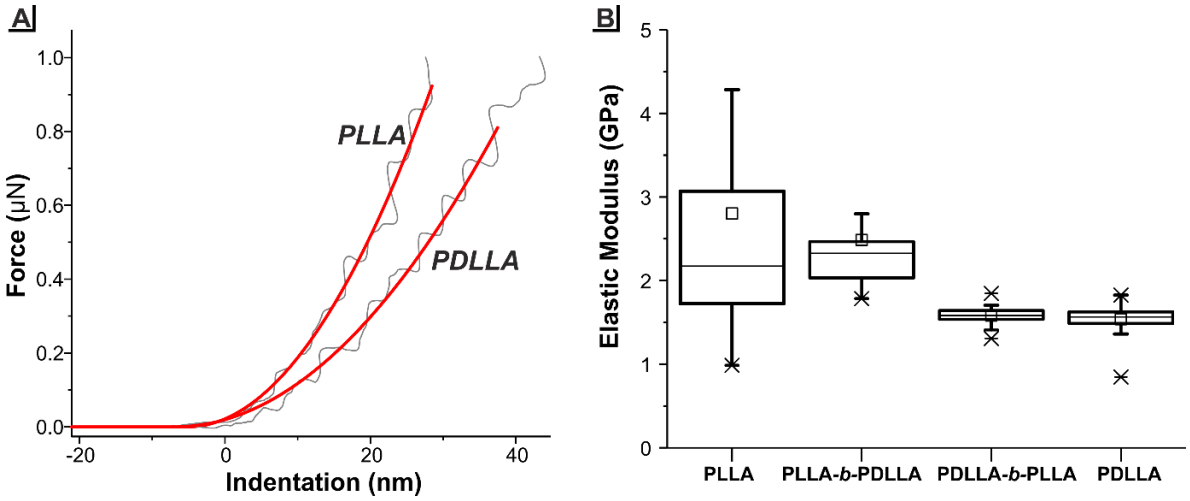

Figure 4.13: **A,** Examples of indentation curves obtained on PLLA and PDLLA samples. **B,** Elastic modulus trend of the annealed 6-armed star poly(lactide) films depending on stereoconfiguration (PLLA, PLLA-*b*-PDLLA, PDLLA-*b*-PLLA and PDLLA), as obtained from AFM nanoindentation measurements. 6-armed PLA, as representative branched PLA, was prepared in the form of polymeric film and subsequently annealed prior analysis, in order to achieve maximum crystallinity of samples, depending on the corresponding stereoconfiguration.

Similarly to the observed modulation of rheological- and mechanical- properties, degradation profiles demonstrated a dependency on the polymer stereochemistry and branching.

The combined effect of this two parameters, was assessed by monitoring the erosion (weight loss) and degradation (associated reduction in MW) profiles of the synthesized linear (1-arm) and branched PLAs (4-arm) with diverse tacticity over time at 37 °C in phosphate buffer (pH 7.4). The 4-armed PLAs were selected for critical comparison of the hydrolytic degradation behavior with respect to the simple 1-armed semicrystalline (PLLA) and fully amorphous (PDLLA) structures, as they possess the closest molecular weight to the 1-armed linear PLA samples, in addition to an equal branch length. The aqueous buffer was preferred to unbuffered medium, as the pH decrease induced by lactic acid and oligomers formation during degradation has been reported to accelerate the hydrolysis process (acid-catalyzed hydrolysis) with faster chain scission kinetics on terminal end groups, present in higher number for branched structures.[180,275,276]

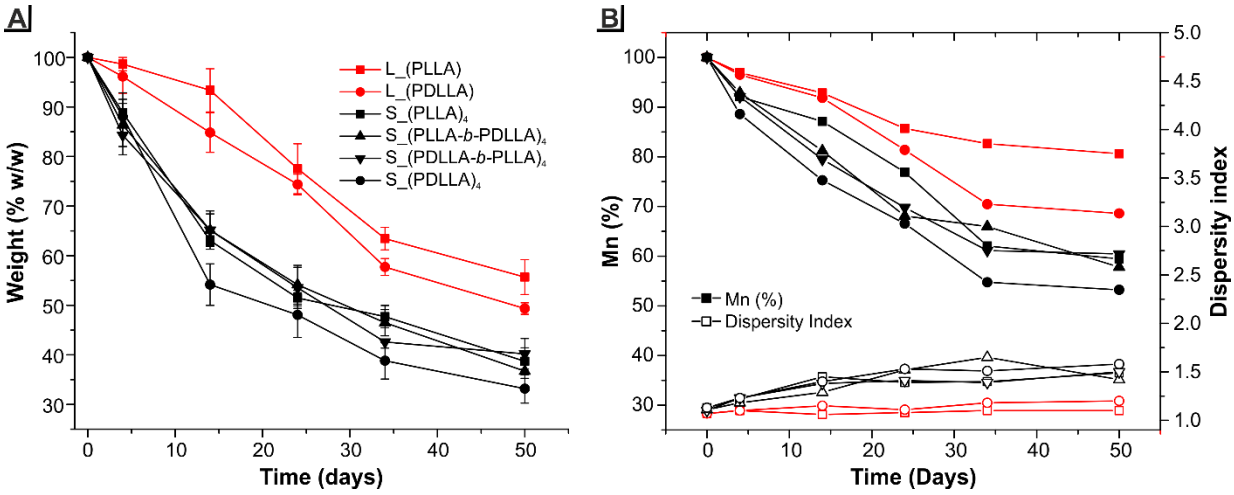

Figure 4.14: **A,** Erosion profile of linear (red) vs 4-armed star-poly(lactide)s (black) with varying tacticity during hydrolysis at 37 °C. **B,** Hydrolytic degradation profiles of linear and 4-armed poly(lactide)s with varying tacticity at 37 °C. The left axis reports number average molecular weight data as a percentage of Mn at day 0, the right one those of dispersity index (both from triple detection GPC measurements in THF).

The introduction of branching can promote faster degradation rates, owing to an increased coil mobility and hydrophilic terminal groups of the globular branched architecture, as well as higher diffusion coefficient of water due to the lower polymer viscosity. This was demonstrated by the considerably faster erosion (Figure 4.14A) and the degradation (Figure 4.14A) of the branched PLAs with respect to their linear counterparts (with almost twice larger reduction in sample weight and Mn) at any time point. Erosion profiles reported gradual weight decrease for all polymers over the entire incubation period, with approximately 65% and 50% weight loss for star and linear poly(lactide)s, respectively. A variation of molecular weight was observed since early time points, with more consistent effect for branched polymers. The average Mn of the star-shaped PLAs linearly decreased up to 50% of the original value after 34 days, with respect to approximately 35% loss observed for the linear poly(lactide)s. Thereafter, degradation kinetic apparently reached a plateau, as Mn values were found practically unchanged after 50-days incubation, independently of the architecture. This suggested that the hydrolytic degradation of both branched and linear PLA structures substantially proceeded through a bulk erosion, although with an accelerated kinetics in the latter case, as previously reported in literature.[179,183,277]

These hydrolytic degradation kinetics are in accordance with the findings from biodegradation experiments reported in *Chapter 2* on 3-armed PDLLA, which revealed fast fragmentation.

Within the same architecture, reduced rates of degradation were observed with increasing presence of crystalline/dense amorphous regions (more resistant to hydrolysis due to lower water diffusion rate)[180] : PLLA > PLLA-*b*-PDLLA ≈ PDLLA-*b*-PLLA > PDLLA. While variation in the sequence of the (stereo)blocks did not significantly affect degradation rates, a more significant contribution of stereoconfiguration was observed in the case of PLLA and PDLLA poly(lactide)s, especially at late hydrolysis times (15% vs 7% maximal variation for linear and branched PLAs, respectively, Figure 4.14B). Taken together, these data confirmed that structure stiffness and compactness of the amorphous regions, which are promoted by higher chain isotacticity, further influences the hydrolysis rate. However, the suppression of crystallinity and the substantially higher coil mobility provided by branching introduction, most probably, reduced the effect of stereoregularity on final degradation rates.

These findings suggested that, despite the high macromolecular contraction of branched structures with respect to linear analogues, the reduced likelihood of entanglements and lower crystallizability provided by branching significantly enhanced the permeation of water molecules, as well as the overall hydrolytic degradation rate.[179,183] Moreover, the fine-tuning of degradation kinetics could be achieved by gradually increasing racemic lactide units.

4.4 Conclusions

In this work, a novel and versatile lactide ROP protocol for the controlled synthesis of branched PLA architectures was successfully developed, by employing the alternative solvent NMP upon DBU catalysis. NMP enables the use of wide variety of multi-functional alcohol initiators (*i.e.* small polyols, sugars, polymeric macroinitiators), providing well-defined and highly monodispersed branched PLA structures and less safety issues compared to commonly used solvents ($CHCl_3$, DCM). Diverse multi-armed controlled architecture could be efficiently produced, ranging from linear, to star and comb structures, demonstrating the high versatility of this novel synthetic route. Interestingly, the novel ROP protocol in NMP allowed also the use of a highly hydrolyzed PVA macroinitiator, which is highly hydrophilic and typically insoluble in common organic solvents, thus yielding PVA-*comb*-PLA structures with extremely high MW. Very low transesterification contribution was observed for all the synthesized poly(lactide)s, thanks to the low polymerization temperatures and improved catalyst selectivity, reporting also decreasing contribution as a function of the branching degree. The versatility and high end-group fidelity of the optimized protocol enabled the production of a library of PLA-based block copolymers by simply varying the monomer feed during the second addition

(PLLA-*b*-PDLLA and PDLLA-*b*-PLLA), in addition to isotactic (PLLA) or atactic (PDLLA) homopolymeric structures.

The effect of the variation in topology and stereoconfiguration on the poly(lactide) properties was systematically investigated, in terms of macromolecular conformation, crystallizability, rheological behavior, mechanical stiffness and (hydrolytic) degradation behavior.

The negligible likelihood of entanglements induced by branching introduction was found to efficiently suppress crystallinity and promote macromolecular contraction as well as viscosity reduction. By gradually varying stereoconfiguration through the use of the PDLLA/PLLA block systems in addition to PLLA and PDLLA homopolymers, further modulation of PLA tacticity could be achieved. This resulted in gradual increase in polymer viscosity and mechanical stiffness for increasing L-lactide contents, despite the lack of a crystalline phase in the PLA stereo-copolymer systems and independently of polymer architecture. Importantly, the introduction of star-shaped branching significantly improved hydrolytic degradation and erosion kinetics with respect to the simple linear PLLA structure, thanks to the increased coil mobility of the branched structures, with additional possibility of fine-tuning the degradation rate by simply varying the stereoconfiguration (*i.e.* faster hydrolytic degradation as a function of increasing stereoerrors from homo PLLA, to block copolymers, up to the highly flexible, atactic PDLLA).

4.4.1 Final considerations and future perspectives

This work provided additional insights concerning the effect of macromolecular architecture and stereochemistry on final poly(lactide) thermal, rheological, mechanical and degradation properties. The results confirmed the findings of previous chapters regarding the efficient modulation of flexibility (few entanglements) and rheology (reduces viscosity), compared to the conventionally used linear semicrystalline PLA, without altering the chemical nature of the material.

Indeed, the observed physico-chemical and mechanical properties, coupled with a sufficient thermal stability to stand melt-processing conditions (200-250 °C) and enhanced biodegradability, make the synthesized branched poly(lactide)s extremely interesting for future industrial development of flexible and highly biodegradable PLA-based materials.

In the perspective of industrial utilization, the 6-armed poly(lactide) structure presents the most promising features, among the synthesized well-defined branched PLA architectures, for further

exploitation as green and compatible flow modifier of conventional PLA. The relatively high degree of branching provided discrete thermal stability, due to the high overall MW, combined with significant suppression of crystallinity, viscosity reduction and improvement in polymer coil mobility. Considering the great improvement in hydrolytic degradation rate displayed by star poly(lactide) with equal branch length, excellent (bio)degradability is also expected, with respect to high-MW conventional PLA. However, also slightly lower degree of polymerization per arm might be tested, in the attempt of further decrease the Tg and enhance final plasticizing and toughening effect.
Moreover, the inexpensive DL-lactide feedstock would be preferred to provide *all-PLA*-based materials with extremely high biodegradation rates and flexibility (*e.g.* flexible single-use items), whereas increasing L-LA contents could be employed if higher barrier properties and thermal resistance are required (*e.g.* food packaging).

However, the novel ROP protocol provides facile design and customization of branched poly(lactide) structures for different purposes, from large scale melt-processing to drug delivery. For example, it could be exploited to produce branched PLA stereo-complexes by alternating D- and L-based blocks, with resulting improved crystallinity and modulus, as well as higher melting points, to provide materials suitable for long-shelf life packaging or extremely rigid durable items (*e.g.* automotive products).

References

[1] S. Lambert, M. Wagner, *Chem. Soc. Rev.* **2017**, *46*, 6855–6871.

[2] M. Nofar, D. Sacligil, P. J. Carreau, M. R. Kamal, M.-C. Heuzey, *Int. J. Biol. Macromol.* **2019**, *125*, 307–360.

[3] I. S. Fahim, H. Chbib, H. M. Mahmoud, *Sustain. Chem. Pharm.* **2019**, *12*, 100142.

[4] Eropean Commission, *On the Reduction of the Impact of Certain Plastic Products on the Environment*, **2018**.

[5] European Commission, *Communication from the Commission to the European Parliament, the Council, the European Economic and Social Committee and the Committee of the Regions. A European Strategy for Plastics in a Circular Economy*, **2018**.

[6] C. Bastioli, *Handbook of Biodegradable Polymers*, Rapra Technology, **2016**.

[7] F. M. Lamberti, L. A. Román-Ramírez, J. Wood, *J. Polym. Environ.* **2020**, *28*, 2551–2571.

[8] K. J. Jem, B. Tan, *Adv. Ind. Eng. Polym. Res.* **2020**, *3*, 60–70.

[9] European Bioplastics, *Bioplastics Market Data 2019*, **2020**.

[10] V. H. H. Sangeetha, H. Deka, T. O. O. Varghese, S. K. K. Nayak, *Polym. Compos.* **2018**, *39*, 81–101.

[11] M. Niaounakis, *Eur. Polym. J.* **2019**, *114*, 464–475.

[12] M. S. Singhvi, S. S. Zinjarde, D. V. Gokhale, *J. Appl. Microbiol.* **2019**, *127*, 1612–1626.

[13] S. Farah, D. G. Anderson, R. Langer, *Adv. Drug Deliv. Rev.* **2016**, *107*, 367–392.

[14] K. Hamad, M. Kaseem, M. Ayyoob, J. Joo, F. Deri, *Prog. Polym. Sci.* **2018**, *85*, 83–127.

[15] D. Garlotta, *J. Polym. Environ.* **2001**, *9*, 63–84.

[16] E. Castro-Aguirre, F. Iñiguez-Franco, H. Samsudin, X. Fang, R. Auras, *Adv. Drug Deliv. Rev.* **2016**, *107*, 333–366.

[17] S. Domenek, S. Fernandes-Nassar, V. Ducruet, *Adv. Polym. Sci.* **2018**, *279*, 303–341.

[18] Q. Yan, H. Dong, J. Su, J. Han, B. Song, Q. Wei, Y. Shi, *Engineering* **2018**, *4*, 729–742.

[19] M. Murariu, P. Dubois, *Adv. Drug Deliv. Rev.* **2016**, *107*, 17–46.

[20] K. Hamad, M. Kaseem, H. W. Yang, F. Deri, Y. G. Ko, *Express Polym. Lett.* **2015**, *9*, 435–455.

[21] K. Madhavan Nampoothiri, N. R. Nair, R. P. John, *Bioresour. Technol.* **2010**, *101*, 8493–8501.

[22] M. Singhvi, D. Gokhale, *RSC Adv.* **2013**, *3*, 13558–13568.

[23] M. Jamshidian, E. A. Tehrany, M. Imran, M. Jacquot, S. Desobry, *Compr. Rev. Food Sci. Food Saf.* **2010**, *9*, 552–571.

[24] L. T. Sin, B. S. Tueen, in *Polylactic Acid*, Elsevier, **2019**, pp. 53–95.

[25] "NatureWorks | NatureWorks Announces 100 Percent Third-Party Certified Sustainable Feedstock by 2020," can be found under https://www.natureworksllc.com/News-and-Events/Press-Releases/2019/2019-02-14-100-Percent-Sustainable-Feedstock-by-2020, **2019**.

[26] K. P. Rajan1, S. P. Thomas12, A. Gopanna2, A. Al-Ghamdi1, M. Chavali3, *J. Polym. Sci. Eng.* **2018**, *1*, 1–15.

[27] J. J. Koh, X. Zhang, C. He, *Int. J. Biol. Macromol.* **2018**, *109*, 99–113.

[28] G. L. Gregory, E. M. López-Vidal, A. Buchard, *Chem. Commun.* **2017**, *53*, 2198–2217.

[29] Y. Cheng, S. Deng, P. Chen, R. Ruan, *Front. Chem. China* **2009**, *4*, 259–264.

[30] R. Auras, L. T. Lim, S. E. M. Selke, H. Tsuji, *Poly(Lactic Acid): Synthesis, Structures, Properties, Processing, and Applications*, John Wiley & Sons, Inc., Hoboken, NJ, USA, **2010**.

[31] L.-T. Lim, R. Auras, M. Rubino, *Prog. Polym. Sci.* **2008**, *33*, 820–852.

[32] S. G. Hatzikiriakos, K. B. Migler, in *Appl. Polym. Rheol.*, John Wiley & Sons, Inc., Hoboken, NJ, USA, **2011**, pp. 29–58.

[33] J. Lunt, *Polym. Degrad. Stab.* **1998**, *59*, 145–152.

[34] Z. Berk, in *Food Process Eng. Technol.*, Elsevier, **2009**, pp. 333–350.

[35] M. P. Groover, *Fundamentals of Modern Manufacturing: Materials, Processes, and Systems, 6th Edition*, John Wiley & Sons, Inc., **2015**.

[36] E. M. Mount, in *Appl. Plast. Eng. Handb.*, Elsevier, **2017**, pp. 217–264.

[37] F. Carrasco, P. Pagès, J. Gámez-Pérez, O. O. O. Santana, M. L. L. Maspoch, *Polym. Degrad. Stab.* **2010**, *95*, 116–125.

[38] I. Pillin, N. Montrelay, A. Bourmaud, Y. Grohens, *Polym. Degrad. Stab.* **2008**, *93*, 321–328.

[39] J. Ren, in *Biodegrad. Poly(Lactic Acid) Synth. Modif. Process. Appl.*, Springer Berlin Heidelberg, Berlin, Heidelberg, **2010**, pp. 142–207.

[40] M. Jamshidian, E. A. Tehrany, M. Imran, M. J. Akhtar, F. Cleymand, S. Desobry, *J. Food Eng.* **2012**, *110*, 380–389.

[41] "mechanical thermoforming proccess," can be found under https://www.custompartnet.com/wu/thermoforming, **2020**.

[42] O. Faruk, A. K. Bledzki, H. P. Fink, M. Sain, *Prog. Polym. Sci.* **2012**, *37*, 1552–1596.

[43] S. W. Hwang, J. K. Shim, S. E. Selke, H. Soto-Valdez, L. Matuana, M. Rubino, R. Auras, *Polym. Int.* **2012**, *61*, 418–425.

[44] S. M. Castellón, T. Standau, V. Altstädt, C. Bonten, **2020**, p. 020068.

[45] T. A. Osswald, G. Menges, *Materials Science of Polymers for Engineers*, Munich : Hanser, **2003**.

[46] D. Witzke, *Introduction to Properties, Engineering, and Prospects of Polylactide Polymers*, Michigan

State University, Ann Arbor, MI, **1999**.

[47] A. Clarinval, J. Halleux, in *Biodegrad. Polym. Ind. Appl.* (Ed.: R. Smith), Woodhead Publishing, **2005**, pp. 3–31.

[48] G. L. Baker, E. B. Vogel, M. R. Smith, *Polym. Rev.* **2008**, *48*, 64–84.

[49] R. Auras, S. Singh, J. Singh, *J. Test. Eval.* **2006**, *34*, 100041.

[50] H. Liu, J. Zhang, *Polym. Phys.* **2011**, 1051–1083.

[51] R. Shogren, *J. Environ. Polym. Degrad.* **1997**, *5*, 91–95.

[52] "NatureWorks | Ingeo Technical Data Sheets," can be found under https://www.natureworksllc.com/Resources, **2020**.

[53] S. Fehri, P. Cinelli, M.-B. Coltelli, I. Anguillesi, A. Lazzeri, *Int. J. Chem. Eng. Appl.* **2016**, *7*, 85–88.

[54] R. Auras, B. Harte, S. Selke, *Macromol. Biosci.* **2004**, *4*, 835–864.

[55] S. S. Karkhanis, N. M. Stark, R. C. Sabo, L. M. Matuana, *J. Appl. Polym. Sci.* **2017**, *134*, 45212.

[56] J. R. Dorgan, J. Janzen, M. P. Clayton, S. B. Hait, D. M. Knauss, *J. Rheol. (N. Y. N. Y).* **2005**, *49*, 607–619.

[57] G. Gorrasi, R. Pantani, in *Adv. Polym. Sci.*, **2017**, pp. 119–151.

[58] M. K. Mitchell, D. E. Hirt, *Polym. Eng. Sci.* **2015**, *55*, 1652–1660.

[59] G. Kale, R. Auras, S. P. Singh, *Packag. Technol. Sci.* **2007**, *20*, 49–70.

[60] M. Karamanlioglu, R. Preziosi, G. D. Robson, *Polym. Degrad. Stab.* **2017**, *137*, 122–130.

[61] Y. Tokiwa, B. P. Calabia, *J. Polym. Environ.* **2007**, *15*, 259–267.

[62] California Department of Resources Recycling and Recovery, *PLA and PHA Biodegradation in the Marine Environment (DRRR-2012-1435)*, **2012**.

[63] T. P. Haider, C. Völker, J. Kramm, K. Landfester, F. R. Wurm, *Angew. Chemie - Int. Ed.* **2019**, *58*, 50–62.

[64] H. Urayama, T. Kanamori, Y. Kimura, *Macromol. Mater. Eng.* **2002**, *287*, 116–121.

[65] L. Fambri, C. Migliaresi, in *Poly(Lactic Acid)*, John Wiley & Sons, Inc., Hoboken, NJ, USA, **2010**, pp. 113–124.

[66] A. J. Müller, M. Ávila, G. Saenz, J. Salazar, in *Poly(Lactic Acid) Sci. Technol. Process. Prop. Addit. Appl.*, **2015**, pp. 66–98.

[67] Y. Li, C. Han, X. Zhang, Q. Dong, L. Dong, *Thermochim. Acta* **2013**, *573*, 193–199.

[68] H. Tsuji, *Macromol. Biosci.* **2005**, *5*, 569–597.

[69] G. Perego, G. D. Cella, C. Bastioli, *J. Appl. Polym. Sci.* **1996**, *59*, 37–43.

[70] E. Almenar, R. Auras, in *Poly(Lactic Acid)*, John Wiley & Sons, Inc., Hoboken, NJ, USA, **2010**, pp. 155–179.

[71] H. Tsuji, S. Miyauchi, *Polym. Degrad. Stab.* **2001**, *71*, 415–424.

[72] S. Li, S. McCarthy, *Macromolecules* **1999**, *32*, 4454–4456.

[73] C. Liu, Y. Jia, A. He, *Int. J. Polym. Sci.* **2013**, *2013*, 1–6.

[74] S. Slomkowski, S. Penczek, A. Duda, *Polym. Adv. Technol.* **2014**, *25*, 436–447.

[75] A. A. Cuadri, J. E. Martín-Alfonso, *Polym. Degrad. Stab.* **2018**, *150*, 37–45.

[76] D. Kanev, E. Takacs, J. Vlachopoulos, *Int. Polym. Process.* **2007**, *22*, 395–401.

[77] I. Zembouai, M. Kaci, S. Bruzaud, A. Benhamida, Y. M. Corre, Y. Grohens, *Rev. Roum. Chim.* **2015**, *60*, 609–613.

[78] K. A. Afrifah, L. M. Matuana, *Macromol. Mater. Eng.* **2010**, *295*, 802–811.

[79] I. Zembouai, S. Bruzaud, M. Kaci, A. Benhamida, Y. M. Corre, Y. Grohens, *J. Polym. Environ.* **2014**, *22*, 449–459.

[80] D. J. A. Cameron, M. P. Shaver, *Chem. Soc. Rev.* **2011**, *40*, 1761–1776.

[81] S. Corneillie, M. Smet, *Polym. Chem.* **2015**, *6*, 850–867.

[82] A. D. Gotsis, in *Appl. Polym. Rheol.*, John Wiley & Sons, Inc., Hoboken, NJ, USA, **2011**, pp. 59–112.

[83] W. Kaminsky, *Macromol. Chem. Phys.* **2008**, *209*, 459–466.

[84] L. Gu, Y. Xu, G. W. Fahnhorst, C. W. Macosko, *J. Rheol. (N. Y. N. Y).* **2017**, *61*, 785–796.

[85] S. Nouri, C. Dubois, P. G. Lafleur, *J. Rheol. (N. Y. N. Y).* **2015**, *59*, 1045–1063.

[86] R. Avolio, R. Castaldo, G. Gentile, V. Ambrogi, S. Fiori, M. Avella, M. Cocca, M. E. Errico, *Eur. Polym. J.* **2015**, *66*, 533–542.

[87] S. R. Andersson, M. Hakkarainen, A. C. Albertsson, *Polymer (Guildf).* **2013**, *54*, 4105–4111.

[88] Y. Bian, X. Leng, Z. Wei, Z. Wang, Z. Tu, Y. Wang, Y. Li, *Biomacromolecules* **2019**, *20*, 3952–3968.

[89] W. Li, Q. Sun, B. Mu, G. Luo, H. Xu, Y. Yang, *Int. J. Biol. Macromol.* **2019**, *131*, 495–504.

[90] R. N. Darie-Niţă, C. Vasile, A. Irimia, R. Lipşa, M. Râpă, *J. Appl. Polym. Sci.* **2016**, *133*, 43223.

[91] T. W. D. F. Rising, T. D. W. Claridge, N. Davies, D. P. Gamblin, J. W. B. Moir, A. J. Fairbanks, *Carbohydr. Res.* **2006**, *341*, 1574–1596.

[92] D. Li, Y. Jiang, S. Lv, X. Liu, J. Gu, Q. Chen, Y. Zhang, *PLoS One* **2018**, *13*, e0193520.

[93] M. Maiza, M. T. Benaniba, G. Quintard, V. Massardier-Nageotte, *Polímeros* **2015**, *25*, 581–590.

[94] O. Martin, L. Avérous, *Polymer (Guildf).* **2001**, *42*, 6209–6219.

[95] J. N. Hahladakis, C. A. Velis, R. Weber, E. Iacovidou, P. Purnell, *J. Hazard. Mater.* **2018**, *344*, 179–199.

[96] M. A. Huneault, H. Li, *Polymer (Guildf).* **2007**, *48*, 270–280.

[97] I. Fortelny, A. Ujcic, L. Fambri, M. Slouf, *Front. Mater.* **2019**, *6*, 206.

[98] S. Su, R. Kopitzky, S. Tolga, S. Kabasci, *Polymers (Basel).* **2019**, *11*, 1193.

[99] R. Al-Itry, K. Lamnawar, A. Maazouz, *Rheol. Acta* **2014**, *53*, 501–517.

[100] Y. Ding, W. Feng, D. Huang, B. Lu, P. Wang, G. Wang, J. Ji, *Eur. Polym. J.* **2019**, *118*, 45–52.

[101] P. F. M. Finotti, L. C. Costa, M. A. Chinelatto, *Macromol. Symp.* **2016**, *368*, 24–29.

[102] R. Supthanyakul, N. Kaabbuathong, S. Chirachanchai, *Polymer (Guildf).* **2016**, *105*, 1–9.

[103] M. Akrami, I. Ghasemi, H. Azizi, M. Karrabi, M. Seyedabadi, *Carbohydr. Polym.* **2016**, *144*, 254–262.

[104] S. M. Lai, Y. C. Lan, *J. Polym. Res.* **2013**, *20*, 1–8.

[105] E. Oliaei, B. Kaffashi, S. Davoodi, *J. Appl. Polym. Sci.* **2016**, *133*, n/a-n/a.

[106] N. Bitinis, R. Verdejo, P. Cassagnau, M. A. Lopez-Manchado, *Mater. Chem. Phys.* **2011**, *129*, 823–831.

[107] W. Chumeka, P. Pasetto, J. F. Pilard, V. Tanrattanakul, *Polymer (Guildf).* **2014**, *55*, 4478–4487.

[108] Y. Xu, J. Loi, P. Delgado, V. Topolkaraev, R. J. McEneany, C. W. Macosko, M. A. Hillmyer, *Ind. Eng. Chem. Res.* **2015**, *54*, 6108–6114.

[109] S. Pivsa-Art, J. Kord-Sa-Ard, W. Pivsa-Art, R. Wongpajan, N. O-Charoen, S. Pavasupree, H. Hamada, in *Energy Procedia*, Elsevier Ltd, **2016**, pp. 353–360.

[110] Y. Wang, M. A. Hillmyer, *J. Polym. Sci. Part A Polym. Chem.* **2001**, *39*, 2755–2766.

[111] Y. F. Kim, C. N. Choi, Y. D. Kim, K. Y. Lee, M. S. Lee, *Fibers Polym.* **2004**, *5*, 270–274.

[112] G. Biresaw, C. J. Carriere, *Compos. Part A Appl. Sci. Manuf.* **2004**, *35*, 313–320.

[113] E. Castro-Aguirre, R. Auras, S. Selke, M. Rubino, T. Marsh, *Polymers (Basel).* **2018**, *10*, DOI 10.3390/polym10020202.

[114] J. Bai, R. D. Goodridge, R. J. M. Hague, M. Okamoto, *Polym. Compos.* **2017**, *38*, 2570–2576.

[115] Y. Feng, P. Ma, P. Xu, R. Wang, W. Dong, M. Chen, C. Joziasse, *Int. J. Biol. Macromol.* **2018**, *106*, 955–962.

[116] T. F. Cipriano, A. L. N. Da Silva, A. H. M. Da Fonseca Thomé Da Silva, A. M. F. De Sousa, G. M. Da Silva, M. G. Rocha, *Polimeros* **2014**, *24*, 276–282.

[117] N. A. S. Abdullah, Z. Mohamad, S. H. C. Man, B. Norfhairna, R. A. Majid, J. Mazura, N. Norzita, *Chem. Eng. Trans.* **2019**, *72*, 427–432.

[118] J. Wang, X. Jin, C. Li, W. Wang, H. Wu, S. Guo, *Chem. Eng. J.* **2019**, *370*, 831–854.

[119] G. Faludi, G. Dora, B. Imre, K. Renner, J. Móczó, B. Pukánszky, *J. Appl. Polym. Sci.* **2014**, *131*, DOI 10.1002/app.39902.

[120] M. M. Reddy, S. Vivekanandhan, M. Misra, S. K. Bhatia, A. K. Mohanty, *Prog. Polym. Sci.*

2013, *38*, 1653–1689.

[121] M. Żenkiewicz, J. Richert, A. Różański, *Polym. Test.* **2010**, *29*, 251–257.

[122] V. Nagarajan, A. K. Mohanty, M. Misra, *ACS Sustain. Chem. Eng.* **2016**, *4*, 2899–2916.

[123] M. Puthumana, P. Santhana Gopala Krishnan, S. K. Nayak, *Int. J. Polym. Anal. Charact.* **2020**, *25*, 634–648.

[124] J. Fernández, A. Etxeberria, J. R. Sarasua, *J. Mech. Behav. Biomed. Mater.* **2012**, *9*, 100–112.

[125] Z. Ning, J. Liu, N. Jiang, Z. Gan, *Polym. Int.* **2017**, *66*, 968–976.

[126] P. Tiwary, M. Kontopoulou, *ACS Sustain. Chem. Eng.* **2018**, *6*, 2197–2206.

[127] A. M. Mannion, F. S. Bates, C. W. MacOsko, *Macromolecules* **2016**, *49*, 4587–4598.

[128] M. P. Shaver, D. J. A. Cameron, *Biomacromolecules* **2010**, *11*, 3673–3679.

[129] Y. Sakamoto, H. Tsuji, *Polymer (Guildf).* **2013**, *54*, 2422–2434.

[130] M. Nerkar, J. A. Ramsay, B. A. Ramsay, M. Kontopoulou, *Macromol. Mater. Eng.* **2014**, *299*, 1419–1424.

[131] Z. G. Zhao, Q. Yang, P. Coates, B. Whiteside, A. Kelly, Y. J. Huang, P. P. Wu, *Ind. Eng. Chem. Res.* **2018**, *57*, 11312–11322.

[132] A. Michalski, M. Brzezinski, G. Lapienis, T. Biela, *Prog. Polym. Sci.* **2019**, *89*, 159–212.

[133] J. M. Ren, T. G. McKenzie, Q. Fu, E. H. H. Wong, J. Xu, Z. An, S. Shanmugam, T. P. Davis, C. Boyer, G. G. Qiao, *Chem. Rev.* **2016**, *116*, 6743–6836.

[134] L. T. E. Salaam, D. Dean, T. L. Bray, *Polymer (Guildf).* **2006**, *47*, 310–318.

[135] M. A. Ghalia, Y. Dahman, *J. Polym. Res.* **2017**, *24*, 74.

[136] F. Iñiguez-Franco, R. Auras, J. Ahmed, S. Selke, M. Rubino, K. Dolan, H. Soto-Valdez, *Polym. Test.* **2018**, *67*, 190–196.

[137] W. Radke, A. H. E. Müller, *Macromolecules* **2005**, *38*, 3949–3960.

[138] D. W. Sauter, M. Taoufik, C. Boisson, *Polymers (Basel).* **2017**, *9*, 1–13.

[139] R. Ramachandran, G. Beaucage, A. S. Kulkarni, D. McFaddin, J. Merrick-Mack, V. Galiatsatos, *Macromolecules* **2008**, *41*, 9802–9806.

[140] T. Sun, P. Brant, R. R. Chance, W. W. Graessley, *Macromolecules* **2001**, *34*, 6812–6820.

[141] M. Barón, K. H. Hellwich, M. Hess, K. Horie, A. D. Jenkins, R. G. Jones, J. Kahovec, P. Kratochvíl, W. V. Metanomski, W. Mormann, et al., *Pure Appl. Chem.* **2009**, *81*, 1131–1186.

[142] R. d'Arcy, J. Burke, N. Tirelli, *Adv. Drug Deliv. Rev.* **2016**, *107*, 60–81.

[143] M. G. McKee, S. Unal, G. L. Wilkes, T. E. Long, *Prog. Polym. Sci.* **2005**, *30*, 507–539.

[144] S. B. Kharchenko, R. M. Kannan, *Macromolecules* **2003**, *36*, 407–415.

[145] H. Abe, N. Takahashi, K. J. Kim, M. Mochizuki, Y. Doi, *Biomacromolecules* **2004**, *5*, 1606–1614.

[146] G. M. Pavlov, K. Knop, O. V. Okatova, U. S. Schubert, *Macromolecules* **2013**, *46*, 8671–

8679.

[147] P. G. Kadam, S. Mhaske, *Des. Monomers Polym.* **2011**, *14*, 515–540.

[148] K. Fukuda, Y. Doi, *Biodegradable Plastics and Polymers*, Elsevier, **1994**.

[149] A. Ortín, E. López, P. del Hierro, J. Sancho-Tello, W. W. Yau, *Macromol. Symp.* **2018**, *377*, 1–14.

[150] H. H. Chuah, D. Lin-Vien, U. Soni, *Polymer (Guildf).* **2001**, *42*, 7137–7139.

[151] N. A. Cortez-Lemus, A. Castro-Hernández, *J. Polym. Res.* **2020**, *27*, DOI 10.1007/s10965-020-02220-3.

[152] I. Teraoka, *Polymer Solutions: An Introduction to Physical Properties*, John Wiley & Sons, Inc., New York, USA, **2002**.

[153] M. Al Samman, W. Radke, *Polymer (Guildf).* **2016**, *99*, 734–740.

[154] S. B. Kharchenko, R. M. Kannan, J. J. Cernohous, S. Venkataramani, *Macromolecules* **2003**, *36*, 399–406.

[155] C. P. Lusignan, T. H. Mourey, J. C. Wilson, R. H. Colby, *Phys. Rev. E* **1999**, *60*, 5657–5669.

[156] G. Gelardi, N. Sanson, G. Nagy, R. Flatt, *Polymers (Basel).* **2017**, *9*, 61.

[157] B. M. Tande, N. J. Wagner, M. E. Mackay, C. J. Hawker, M. Jeong, *Macromolecules* **2001**, *34*, 8580–8585.

[158] R. A. Pérez-Camargo, R. D'Arcy, A. Iturrospe, A. Arbe, N. Tirelli, A. J. Müller, *Macromolecules* **2019**, *52*, 2093–2104.

[159] E. De Luca, R. W. Richards, *J. Polym. Sci. Part B Polym. Phys.* **2003**, *41*, 1339–1351.

[160] J. R. Dorgan, J. S. Williams, D. N. Lewis, *J. Rheol. (N. Y. N. Y).* **1999**, *43*, 1141–1155.

[161] J. R. Dorgan, H. Lehermeier, M. Mang, *J. Polym. Environ.* **2000**, *8*, 1–9.

[162] N. Hachana, T. Wongwanchai, K. Chaochanchaikul, W. Harnnarongchai, *J. Polym. Environ.* **2017**, *25*, 323–333.

[163] K. Dawidziuk, H. Simmons, M. Kontopoulou, J. S. Parent, *Polymer (Guildf).* **2018**, *158*, 254–261.

[164] H. Simmons, M. Kontopoulou, *Polym. Degrad. Stab.* **2018**, *158*, 228–237.

[165] P. Pladis, K. Karidi, D. Meimaroglou, C. Kiparissides, *Comput. Aided Chem. Eng.* **2016**, *38*, 1153–1158.

[166] W. Zhao, Y. Wang, X. Liu, X. Chen, D. Cui, *Chem. - An Asian J.* **2012**, *7*, 2403–2410.

[167] L. Bouapao, H. Tsuji, K. Tashiro, J. Zhang, M. Hanesaka, *Polymer (Guildf).* **2009**, *50*, 4007–4017.

[168] T. Ouchi, S. Ichimura, Y. Ohya, *Polymer (Guildf).* **2006**, *47*, 429–434.

[169] M. Bednarek, *Prog. Polym. Sci.* **2016**, *58*, 27–58.

[170] Q. Cai, Y. Zhao, J. Bei, F. Xi, S. Wang, *Biomacromolecules* **2003**, *4*, 828–834.

[171] W. Zhang, S. Zheng, *Polym. Bull.* **2007**, *58*, 767–775.

[172] Y. L. Zhao, Q. Cai, J. Jiang, X. T. Shuai, J. Z. Bei, C. F. Chen, F. Xi, *Polymer (Guildf).* **2002**, *43*, 5819–5825.

[173] L. Han, G. Shan, Y. Bao, P. Pan, *J. Phys. Chem. B* **2015**, *119*, 14270–14279.

[174] L. Wang, X. Jing, H. Cheng, X. Hu, L. Yang, Y. Huang, *Ind. Eng. Chem. Res.* **2012**, *51*, 10731–10741.

[175] A. Kundys, A. Plichta, Z. Florjańczyk, A. Zychewicz, P. Lisowska, P. Parzuchowski, E. Wawrzyńska, *Polym. Int.* **2016**, *65*, 927–937.

[176] K. Karidi, T. Mantourlias, A. Seretis, P. Pladis, C. Kiparissides, *Eur. Polym. J.* **2015**, *72*, 114–128.

[177] H. Uyama, T. Terada, T. Yanagimoto, *US Pat., Polylactic Acid Resin Composition and Additive for Polylactic Acid Resin*, **2016**, US 9290613 B2.

[178] J. Burke, R. Donno, R. D'Arcy, S. Cartmell, N. Tirelli, *Biomacromolecules* **2017**, *18*, 728–739.

[179] K. Numata, R. K. Srivastava, A. Finne-Wistrand, A. C. Albertsson, Y. Doi, H. Abe, *Biomacromolecules* **2007**, *8*, 3115–3125.

[180] H. Tsuji, in *Poly(Lactic Acid)*, John Wiley & Sons, Inc., Hoboken, NJ, USA, **2010**, pp. 343–381.

[181] P. Kucharczyk, J. Zednik, V. Sedlarik, *Macromol. Res.* **2017**, *25*, 180–189.

[182] W. Yuan, L. Zhu, X. Huang, S. Zheng, X. Tang, *Polym. Degrad. Stab.* **2005**, *87*, 503–509.

[183] L. Teng, X. Xu, W. Nie, Y. Zhou, L. Song, P. Chen, *J. Polym. Res.* **2015**, *22*, 1–7.

[184] R. Al-Itry, K. Lamnawar, A. Maazouz, *Polym. Degrad. Stab.* **2012**, *97*, 1898–1914.

[185] L. Mezzasalma, A. P. Dove, O. Coulembier, *Eur. Polym. J.* **2017**, *95*, 628–634.

[186] A. A. Septevani, S. Bhakri, in *AIP Conf. Proc.*, **2017**, p. 020038.

[187] S. Krishnan, P. Pandey, S. Mohanty, S. K. Nayak, *Polym. Plast. Technol. Eng.* **2016**, *55*, 1623–1652.

[188] M. Zuideveld, C. Gottschalk, H. Kropfinger, R. Thomann, M. Rusu, H. Frey, *Polymer (Guildf).* **2006**, *47*, 3740–3746.

[189] M. F. Cosate de Andrade, P. M. S. Souza, O. Cavalett, A. R. Morales, *J. Polym. Environ.* **2016**, *24*, 372–384.

[190] S. R. Andersson, M. Hakkarainen, A.-C. Albertsson, *Biomacromolecules* **2010**, *11*, 3617–3623.

[191] M. B. Khajeheian, A. Rosling, *J. Appl. Polym. Sci.* **2016**, DOI 10.1002/app.42231.

[192] L. Wang, X. Jing, H. Cheng, X. Hu, L. Yang, Y. Huang, *Ind. Eng. Chem. Res.* **2012**, *51*, 10088–10099.

[193] H. J. Lehermeier, J. R. Dorgan, *Polym. Eng. Sci.* **2001**, *41*, 2172–2184.

[194] A. S. Karikari, W. F. Edwards, J. B. Mecham, T. E. Long, *Biomacromolecules* **2005**, *6*, 2866–

2874.

[195] *ASTM D882-18, Standard Test Method for Tensile Properties of Thin Plastic Sheeting, ASTM International, West Conshohocken, PA, **2018**, Www.Astm.Org*.

[196] J. Mohammadi-Rovshandeh, P. Pouresmaeel-Selakjani, S. M. Davachi, B. Kaffashi, A. Hassani, A. Bahmeyi, *J. Appl. Polym. Sci.* **2014**, *131*, 1–8.

[197] *ASTM E96 / E96M-16, Standard Test Methods for Water Vapor Transmission of Materials, ASTM International, West Conshohocken, PA, **2016**, Www.Astm.Org*.

[198] T. N. Tran, U. Paul, J. A. Heredia-Guerrero, I. Liakos, S. Marras, A. Scarpellini, F. Ayadi, A. Athanassiou, I. S. Bayer, *Chem. Eng. J.* **2016**, *287*, 196–204.

[199] T. T. T. Ho, T. Zimmermann, S. Ohr, W. R. Caseri, *ACS Appl. Mater. Interfaces* **2012**, *4*, 4832–4840.

[200] M. H. Hartmann, in *Biopolym. from Renew. Resour.*, Springer Berlin Heidelberg, Berlin, Heidelberg, **1998**, pp. 367–411.

[201] M. Puchalski, S. Kwolek, G. Szparaga, M. Chrzanowski, I. Krucińska, *Polymers (Basel).* **2017**, *9*, 18.

[202] T. Blanton, *Database HighScore* **2013**.

[203] L. Avérous, in *Monomers, Polym. Compos. from Renew. Resour.*, Elsevier, **2008**, pp. 433–450.

[204] V. Arias, A. H??glund, K. Odelius, A. C. Albertsson, *J. Appl. Polym. Sci.* **2013**, *130*, 2962–2970.

[205] J. E. Mark, *Physical Properties of Polymers Handbook*, Springer, **2007**.

[206] S. Guzman-Puyol, L. Ceseracciu, J. A. Heredia-Guerrero, G. C. Anyfantis, R. Cingolani, A. Athanassiou, I. S. Bayer, *Chem. Eng. J.* **2015**, DOI 10.1016/j.cej.2015.04.092.

[207] C. Bastioli, *Macromol. Symp.* **1998**, DOI 10.1002/masy.19981350122.

[208] C. Nicolae, M. Grigorescu, R. Gabor, *Eng. Lett.* **2008**, DOI 10.1.1.148.7599.

[209] F. D. Kopinke, M. Remmler, K. Mackenzie, M. Möder, O. Wachsen, *Polym. Degrad. Stab.* **1996**, DOI 10.1016/0141-3910(96)00102-4.

[210] F. Signori, M.-B. Coltelli, S. Bronco, *Polym. Degrad. Stab.* **2009**, *94*, 74–82.

[211] M. P. Arrieta, J. López, E. Rayón, A. Jiménez, *Polym. Degrad. Stab.* **2014**, *108*, 307–318.

[212] J. Zhang, S. Wang, D. Zhao, Y. Zhang, W. Pang, B. Zhang, Q. Li, *J. Appl. Polym. Sci.* **2017**, *134*, 45194.

[213] G. Tedeschi, S. Guzman-Puyol, U. C. Paul, M. J. Barthel, L. Goldoni, G. Caputo, L. Ceseracciu, A. Athanassiou, J. A. Heredia-Guerrero, *Chem. Eng. J.* **2018**, *348*, 840–849.

[214] V. K. Thakur, M. K. Thakur, *Handbook of Sustainable Polymers: Structure and Chemistry*, Jenny Stanford Publishing, **2016**.

[215] J. A. Heredia-Guerrero, G. Caputo, S. Guzman-Puyol, G. Tedeschi, A. Heredia, L.

Ceseracciu, J. J. Benitez, A. Athanassiou, *Mater. Today Sustain.* **2019**, DOI 10.1016/j.mtsust.2018.12.001.

[216] M. Deroiné, A. Le Duigou, Y. M. Corre, P. Y. Le Gac, P. Davies, G. César, S. Bruzaud, *Polym. Degrad. Stab.* **2014**, *108*, DOI 10.1016/j.polymdegradstab.2014.01.020.

[217] H. Cai, V. Dave, R. A. Gross, S. P. McCarthy, *J. Polym. Sci. Part B Polym. Phys.* **1996**, DOI 10.1002/(SICI)1099-0488(19961130)34:16<2701::AID-POLB2>3.0.CO;2-S.

[218] Y. Doi, Y. Kanesawa, N. Tanahashi, Y. Kumagai, *Polym. Degrad. Stab.* **1992**, *36*, 173–177.

[219] T. G. Volova, A. N. Boyandin, A. D. Vasiliev, V. A. Karpov, S. V. Prudnikova, O. V. Mishukova, U. A. Boyarskikh, M. L. Filipenko, V. P. Rudnev, B. Bá Xuân, et al., *Polym. Degrad. Stab.* **2010**, *95*, 2350–2359.

[220] A. Heimowska, M. Morawska, A. Bocho-Janiszewska, *Polish J. Chem. Technol.* **2017**, *19*, 120–126.

[221] L.-T. Lim, K. Cink, T. Vanyo, in *Poly(Lactic Acid)*, John Wiley & Sons, Inc., Hoboken, NJ, USA, **2010**, pp. 189–215.

[222] P. A. Fowler, J. M. Hughes, R. M. Elias, *J. Sci. Food Agric.* **2006**, *86*, 1781–1789.

[223] *ASTM D1746-15, Standard Test Method for Transparency of Plastic Sheeting, ASTM International, West Conshohocken, PA, **2015**, Www.Astm.Org.*

[224] H. Wang, L. Wang, *J. Clean. Prod.* **2017**, *143*, 624–633.

[225] G. Scoponi, S. Guzman-Puyol, G. Caputo, L. Ceseracciu, A. Athanassiou, J. A. Heredia-Guerrero, *Polymer (Guildf).* **2020**, *193*, 122371.

[226] *ASTM D1238-13, Standard Test Method for Melt Flow Rates of Thermoplastics by Extrusion Plastometer, ASTM International, West Conshohocken, PA, **2013**, Www.Astm.Org.*

[227] G. Schramm, *A Practical Approach to Rheology and Rheometry*, Karlsruhe: Haake, **1994**.

[228] S. E. Kadijk, B. H. A. A. Van Den Brule, *Polym. Eng. Sci.* **1994**, *34*, 1535–1546.

[229] M. M. Cross, *J. Colloid Sci.* **1965**, *20*, 417–437.

[230] C. A. Hieber, H. H. Chiang, *Polym. Eng. Sci.* **1992**, *32*, 931–938.

[231] K. C. Seavey, Y. A. Liu, N. P. Khare, T. Bremner, C.-C. Chen, *Ind. Eng. Chem. Res.* **2003**, *42*, 5354–5362.

[232] M. Gahleitner, *Prog. Polym. Sci.* **2001**, *26*, 895–944.

[233] K. Sungsanit, N. Kao, S. N. Bhattacharya, S. Pivsaart, *Korea Aust. Rheol. J.* **2010**, *22*, 187–195.

[234] S. Thomas, W. Yang, *Advances in Polymer Processing: From Macro- to Nano-Scales*, Woodhead Publishing, **2009**.

[235] E. L. Cabarcos, R. K. Bayer, H. G. Zachmann, F. J. B. Calleja, W. Meins, *Polym. Eng. Sci.* **1989**, *29*, 193–201.

[236] K. T. Varughese, G. B. Nando, S. K. De, S. K. Sanyal, *J. Mater. Sci.* **1989**, *24*, 3491–3496.

[237] Y. Yang, Z. Xiong, L. Zhang, Z. Tang, R. Zhang, J. Zhu, *Mater. Des.* **2016**, *91*, 262–268.

[238] H. Korhonen, A. Helminen, J. V. Seppälä, *Polymer (Guildf).* **2001**, *42*, 7541–7549.

[239] A. Duda, A. Kowalski, in *Handb. Ring-Opening Polym.*, Wiley-VCH Verlag GmbH & Co. KGaA, Weinheim, Germany, **2009**, pp. 1–51.

[240] E. A. Appel, V. Y. Lee, T. T. Nguyen, M. McNeil, F. Nederberg, J. L. Hedrick, W. C. Swope, J. E. Rice, R. D. Miller, J. Sly, *Chem. Commun.* **2012**, *48*, 6163.

[241] C. Thomas, B. Bibal, *Green Chem.* **2014**, *16*, 1687–1699.

[242] R. F. Storey, J. W. Sherman, *Macromolecules* **2002**, *35*, 1504–1512.

[243] X. Zhang, D. A. MacDonald, M. F. A. Goosen, K. B. McAuley, *J. Polym. Sci. Part A Polym. Chem.* **1994**, *32*, 2965–2970.

[244] H. R. Kricheldorf, I. Kreiser-Saunders, C. Boettcher, *Polymer (Guildf).* **1995**, *36*, 1253–1259.

[245] D. Pholharn, Y. Srithep, J. Morris, *IOP Conf. Ser. Mater. Sci. Eng.* **2017**, *213*, DOI 10.1088/1757-899X/213/1/012022.

[246] S. H. Kim, Y.-K. Han, Y. H. Kim, S. I. Hong, *Die Makromol. Chemie* **1992**, *193*, 1623–1631.

[247] O. Santoro, X. Zhang, C. Redshaw, *Catalysts* **2020**, *10*, 800.

[248] E. D. Cross, L. E. N. Allan, A. Decken, M. P. Shaver, *J. Polym. Sci. Part A Polym. Chem.* **2013**, *51*, 1137–1146.

[249] B. G. G. G. Lohmeijer, R. C. Pratt, F. Leibfarth, J. W. Logan, D. A. Long, A. P. Dove, F. Nederberg, J. Choi, C. Wade, R. M. Waymouth, et al., *Macromolecules* **2006**, *39*, 8574–8583.

[250] A. Chuma, H. W. Horn, W. C. Swope, R. C. Pratt, L. Zhang, B. G. G. G. Lohmeijer, C. G. Wade, R. M. Waymouth, J. L. Hedrick, J. E. Rice, *J. Am. Chem. Soc.* **2008**, *130*, 6749–6754.

[251] M. K. Kiesewetter, E. J. Shin, J. L. Hedrick, R. M. Waymouth, *Macromolecules* **2010**, *43*, 2093–2107.

[252] X. Zhang, G. O. Jones, J. L. Hedrick, R. M. Waymouth, *Nat. Chem.* **2016**, *8*, 1047–1053.

[253] A. P. Dove, *ACS Macro Lett.* **2012**, *1*, 1409–1412.

[254] D. J. Coady, A. C. Engler, Y. Y. Yang, J. L. Hedrick, *Polym. Chem.* **2011**, *2*, 2619–2626.

[255] N. J. Sherck, H. C. Kim, Y.-Y. Won, *Macromolecules* **2016**, *49*, 4699–4713.

[256] D. J. Coady, K. Fukushima, H. W. Horn, J. E. Rice, J. L. Hedrick, *Chem. Commun.* **2011**, *47*, 3105–3107.

[257] M. Eldessouki, G. Buschle-Diller, Y. Gowayed, *Des. Monomers Polym.* **2016**, *19*, 180–192.

[258] M. Schömer, H. Frey, *Macromol. Chem. Phys.* **2011**, *212*, 2478–2486.

[259] X. Q. Li, B. Wang, H. Y. Ji, Y. S. Li, *Catal. Sci. Technol.* **2016**, *6*, 7763–7772.

[260] K. A. M. Thakur, R. T. Kean, E. S. Hall, M. A. Doscotch, E. J. Munson, *Anal. Chem.* **1997**,

69, 4303–4309.

[261] K. A. M. Thakur, R. T. Kean, K. A. M. Thakur, M. T. Zell, B. E. Padden, E. J. Munson, *Chem. Commun.* **1998**, 1913–1914.

[262] K. A. M. Thakur, R. T. Kean, E. S. Hall, J. J. Kolstad, T. A. Lindgren, M. A. Doscotch, J. I. Siepmann, E. J. Munson, *Macromolecules* **1997**, *30*, 2422–2428.

[263] A. Jouyban, M. A. A. Fakhree, A. Shayanfar, *J. Pharm. Pharm. Sci.* **2010**, *13*, 524–535.

[264] M. Roche-Molina, B. Hardwick, C. Sanchez-Ramos, D. Sanz-Rosa, D. Gewert, F. M. Cruz, A. Gonzalez-Guerra, V. Andres, J. A. Palma, B. Ibanez, et al., *Sci. Rep.* **2020**, *10*, DOI 10.1038/s41598-020-68350-2.

[265] K. Křížek, J. Růžička, M. Julinová, L. Husárová, J. Houser, M. Dvořáčková, P. Jančová, *Water Sci. Technol.* **2015**, *71*, 776–782.

[266] T. Hongen, T. Taniguchi, S. Nomura, J. I. Kadokawa, K. Monde, *Macromolecules* **2014**, *47*, 5313–5319.

[267] B. Cheng, L. Qian, H. J. Qian, Z. Y. Lu, S. Cui, *Nanoscale* **2017**, *9*, 14312–14316.

[268] R. d'Arcy, A. Gennari, R. Donno, N. Tirelli, *Macromol. Rapid Commun.* **2016**, *37*, 1918–1925.

[269] J. Meimoun, A. Favrelle-Huret, M. Bria, N. Merle, G. Stoclet, J. De Winter, R. Mincheva, J.-M. Raquez, P. Zinck, *Polym. Degrad. Stab.* **2020**, 109188.

[270] H. Qian, A. R. Wohl, J. T. Crow, C. W. MacOsko, T. R. Hoye, *Macromolecules* **2011**, *44*, 7132–7140.

[271] X. Leng, Z. Wei, Y. Ren, Y. Li, Y. Wang, Q. Wang, *RSC Adv.* **2015**, *5*, 81482–81491.

[272] D. Cam, M. Marucci, *Polymer (Guildf).* **1997**, *38*, 1879–1884.

[273] H. C. Yau, M. K. Bayazit, J. H. G. Steinke, M. S. P. Shaffer, *Chem. Commun.* **2015**, *51*, 16621–16624.

[274] S.-H. Hyon, K. Jamshidi, Y. Ikada, *Polym. Int.* **1998**, *46*, 196–202.

[275] R. P. Batycky, J. Hanes, R. Langer, D. A. Edwards, *J. Pharm. Sci.* **1997**, *86*, 1464–1477.

[276] C. Shih, *J. Control. Release* **1995**, *34*, 9–15.

[277] S. H. Kim, Y. H. Kim, in *Stud. Polym. Sci.*, Elsevier, **1994**, pp. 464–469.

Appendix

Supporting information for Chapter 4

1. ^{1}H-NMR characterization of the poly(lactide)s architectures ($CDCl_3$)

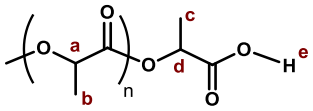

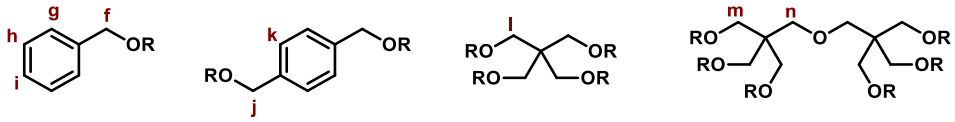

linear (1-armed). δ = 1.45−1.55 (c, terminal CH(C**H**$_3$)), 1.55−1.70 (b, main chain CH(C**H**$_3$)), 2.75−2.80 (e, CO**H**(terminal)), 4.30−4.45 (d, C**H**(CH_3)terminal), 5.10−5.30 ppm (a, C**H**(CH_3) main chain), 7.31-7.42 ppm (g,h,i, C**Har** BnOH ring).

linear (2-armed). δ = 1.45−1.55 (c, terminal CH(C**H**$_3$)), 1.55−1.70 (b, main chain CH(C**H**$_3$)), 2.75−2.80 (e, CO**H**(terminal)), 4.30−4.45 (d, C**H**(CH_3)terminal), 5.10−5.30 ppm (a, C**H**(CH_3) main chain), 7.34 ppm (k, C**Har** BDM ring).

4-armed star. δ = 1.45−1.55 (c, terminal C(H)C**H**$_3$), 1.55−1.70 (b, main chain CH(C**H**$_3$), 2.75−2.80 (e, CO**H** (terminal)), 4.05-4.25 (l, CC**H**$_2$O methylene), 4.30−4.45 (d, C**H**(CH_3) terminal), 5.10−5.30 ppm (a, C**H**(CH_3) main chain).

6-armed star. δ = 1.45−1.55 (c, terminal C(H)C**H**$_3$), 1.55−1.70 (b, main chain CH(C**H**$_3$), 2.75−2.80 (e, CO**H** (terminal)), 4.00-4.25 (m, CC**H**$_2$O methylene, non-integrable), 4.30−4.45 (d, C**H**(CH_3) terminal), 5.10−5.30 ppm (a, C**H**(CH_3) main chain).

8-armed star δ = 1.45−1.55 (c, terminal C(H)C**H**$_3$), 1.55−1.70 (b, main chain CH(C**H**$_3$), 2.75−2.80 (e, CO**H** (terminal)), 4.30−4.45 (d, C**H**(CH_3) terminal), 5.10−5.30 ppm (a, C**H**(CH_3) main chain).

Comb. δ = 1.45−1.55 (c, terminal C(H)C**H**$_3$), 1.55−1.70 (b, main chain CH(C**H**$_3$), 2.75−2.80 (e, CO**H** (terminal)), 4.30−4.45 (d, C**H**(CH_3) terminal), 5.10−5.30 ppm (a, C**H**(CH_3) main chain).

2. Conversions and molecular weight distribution variation over 24-hours polymerization period for all the multi-armed poly(lactide)s synthesised by the novel ROP protocol in NMP

Table S. 1: Conversions, molecular weight and dispersity trends of the multi-armed poly(lactide)s monitored over a 24h polymerization period through the described monomer-starved method. Monomer concentration was kept constant at 1M and a [DBU]:[OH] molar ratio of 1 was used. All polymerization were then precipitated after 6-hours (red), to avoid undesired increase in dispersity due to the enhanced occurrence of termination reactions at higher polymerization periods.

Monomer	Initiator	Reaction extent (h)	# arms	[M]:[I] (DP_{tot})	Conversion (%)[a]	Mn_{NMR} (kDa)[c]	Mn_{GPC} (kDa)[c]	Mw_{GPC} (kDa)[c]	Đ[c]
L-LA	BnOH	1.5	1	50	49 (98)	7.1	7.1	7.4	1.04
		3		50	50 (99)	7.2	7.6	8.8	1.16
L-LA		4.5		100	87	12.5	12.9	13.9	1.08
		6		100	88	12.7	12.7	14.4	1.13
		24		100	91	13.1	11.8	14.8	1.25
L-LA	BDM	1.5	2	100	47 (93)	13.5	14.5	15.4	1.06
		3		100	49 (97)	14.1	14.3	15.0	1.05
L-LA		4.5		200	81	23.3	23.2	24.1	1.04
		6		200	88	25.3	24.0	25.5	1.06
		24		200	93	26.8	26.7	27.7	1.04
L-LA	PET	1.5	4	200	38 (76)	21.9	24.0	24.3	1.01
		3		200	48 (96)	27.6	27.1	28.6	1.06
L-LA		4.5		400	82	47.2	44.4	45.3	1.02
		6		400	86	49.5	45.2	49.7	1.10
		24		400	80	46.1	43.6	50.7	1.16
L-LA	diPET	1.5	6	300	39 (78)	33.7	32.3	33.6	1.04
		3		300	48 (95)	41.5	39.3	45.9	1.17
L-LA		4.5		600	79	68.3	59.2	73.7	1.24
		6		600	89	76.9	73.6	76.5	1.04
		24		600	88	76.0	74.0	78.6	1.06
L-LA	Sucr	1.5	8	400	38 (76)	43.2	44.3	44.8	1.01
		3		400	41 (82)	47.3	47.2	51.5	1.09
L-LA		4.5		800	75	86.4	80.2	82.8	1.03
		6		800	80	92.4	86.8	88.9	1.02
		24		800	81	93.3	85.0	90.7	1.07
L-LA	BnOH	1.5	1	50	41 (82)	5.9	5.9	6.2	1.05
		3		50	49 (98)	7.1	7.3	7.9	1.08
DL-LA		4.5		100	65	9.3	10.1	10.8	1.07
		6		100	81	11.5	11.9	12.3	1.03
		24		100	75	10.8	10.8	11.3	1.05

L-LA	BDM	1.5	2	100	46 (87)	13.1	12.7	13.5	1.06
		3		100	49 (98)	14.2	14.3	15.6	1.09
DL-LA		4.5		200	65.2	18.8	19.5	21.5	1.10
		6		200	81.6	23.5	22.9	24	1.05
		24		200	79.1	22.8	22.3	22.9	1.03
L-LA	PET	1.5	4	200	42 (85)	24.4	23.2	24.9	1.07
		3		200	49 (97)	28.1	27.2	29.3	1.08
DL-LA		4.5		400	67	38.7	41.3	45.1	1.09
		6		400	79	45.4	44.9	47.5	1.06
		24		400	77	44.5	43.7	47.8	1.09
L-LA	diPET	1.5	6	300	41 (82)	35.3	35.2	37.9	1.08
		3		300	49 (97)	42.0	42.3	52.4	1.24
DL-LA		4.5		600	62	54.0	56.6	59.4	1.05
		6		600	76	65.7	69.4	74.0	1.07
		24		600	76	65.8	64.8	77.1	1.19
L-LA	Sucr	1.5	8	400	38 (76)	44.2	46.6	47.2	1.01
		3		400	41 (82)	47.6	45.7	47.0	1.03
DL-LA		4.5		800	71	81.8	78.2	81.2	1.04
		6		800	77	89.0	82.3	82.8	1.01
		24		800	75	86.4	80.6	85.6	1.06
DL-LA	BnOH	1.5	1	50	40 (80)	5.8	6.8	7.9	1.16
		3		50	48 (96)	6.9	7.5	7.9	1.05
L-LA		4.5		100	70	10.1	9.1	9.8	1.08
		6		100	79	11.4	10.0	11.4	1.14
		24		100	77	11.1	11.6	12.5	1.08
DL-LA	BDM	1.5	2	100	42 (83)	12.0	12.4	13.1	1.06
		3		100	47 (95)	13.7	14.0	15.6	1.11
L-LA		4.5		200	68	19.6	19.7	20.9	1.06
		6		200	80	22.9	21.5	24.7	1.15
		24		200	78	22.6	21.2	23.3	1.10
DL-LA	PET	1.5	4	200	40 (80)	23.0	21.6	23.5	1.09
		3		200	48 (95)	27.3	27.2	27.8	1.02
L-LA		4.5		400	68	38.9	38.0	39.5	1.04
		6		400	78	45.1	42.1	46.5	1.10
		24		400	77	44.5	44.2	45.4	1.03
DL-LA	diPET	1.5	6	300	36 (72)	31.2	31.2	31.6	1.01
		3		300	46 (92)	39.7	39.1	47.4	1.21
L-LA		4.5		600	68	59.1	57.4	60.2	1.05
		6		600	77	66.9	69.7	77.3	1.11
		24		600	75	64.8	63.5	74.8	1.18
DL-LA	Sucr	1.5	8	400	32 (64)	37.0	38.5	38.8	1.01
		3		400	40 (80)	46.3	42.3	46.5	1.10
L-LA		4.5		800	73	84.1	76.8	80.9	1.05
		6		800	79	91.2	79.3	89.0	1.12
		24		800	78	90.0	77.2	88.5	1.15
DL-LA	BnOH	1.5	1	50	43 (85)	6.2	7.8	8.2	1.05
		3		50	48 (96)	6.9	7.5	8.5	1.13
DL-LA		4.5		100	75	10.8	10.0	11.9	1.19
		6		100	84	12.1	11.8	13.4	1.14

		24		100	80	11.5	11.9	14.8	1.24
DL-LA	BDM	1.5	2	100	43 (86)	12.4	14.5	15.0	1.03
		3		100	49 (97)	14.1	14.3	15.0	1.05
DL-LA		4.5		200	75	21.6	17.6	18.1	1.03
		6		200	83	23.9	21.3	23.4	1.10
		24		200	79	22.8	24.6	26.1	1.06
DL-LA	PET	1.5	4	200	34 (68)	19.6	19.8	20.2	1.02
		3		200	48 (96)	27.6	25.7	27.0	1.05
DL-LA		4.5		400	71	40.9	35.1	38.3	1.09
		6		400	82	47.2	37.3	42.5	1.14
		24		400	76	43.8	41.1	43	1.05
DL-LA	diPET	1.5	6	300	37 (74)	32.0	32.8	37.1	1.13
		3		300	45 (90)	38.9	36.6	45.3	1.24
DL-LA		4.5		600	71	61.3	55.1	59.6	1.08
		6		600	79	68.3	64.4	70.6	1.10
		24		600	74	63.9	65.9	70.0	1.06
DL-LA	Sucr	1.5	8	400	36 (72)	41.4	40.8	41.7	1.02
		3		400	39 (79)	45.3	41.1	44.4	1.08
DL-LA		4.5		800	70	80.6	73.6	75.8	1.03
		6		800	76	87.4	76.5	81.1	1.06
		24		800	68	78.0	75.3	80.2	1.07

Sampling for analysis was performed always prior new monomer addition. [a]Percentage relative to monomer measured by ^{1}H NMR in $CHCl_3$. Conversion values with respect to current amount of monomer (DP_{arm} of 50) reported in parenthesis. [b]Measured by ^{1}H NMR in $CHCl_3$ by calculating the corresponding monomer conversion for each time point. [c]MW data for the obtained monomodal distributions measured by GPC in THF using triple detection.

3. Characterization of the comb-poly(lactide) architectures

Table S. 2: Mw and physico-chemical data of the PVA-*comb*-PLA structures measured by static light scattering (SLS) through a multi-angle light scattering (MALS) detector.

Sample	Mw (kDa)	Rg (nm)	A2 (mol·mL/g^2)
***C*_(PLLA)$_{140}$**	1913 ± 38	21 ± 3	(1.49 ± 0.12)·10^{-5}
***C*_(PLLA-*b*-PDLLA)$_{140}$**	2033 ± 69	18 ± 5	(1.45 ± 0.20)·10-^{5}
***C*_(PDLLA-*b*-PLLA)$_{140}$**	1673 ± 82	21 ± 6	(1.80 ± 0.36)·10^{-5}
***C*_(PDLLA)$_{140}$**	1229 ± 34	22 ± 4	(2.74 ± 0.28)·10^{-5}

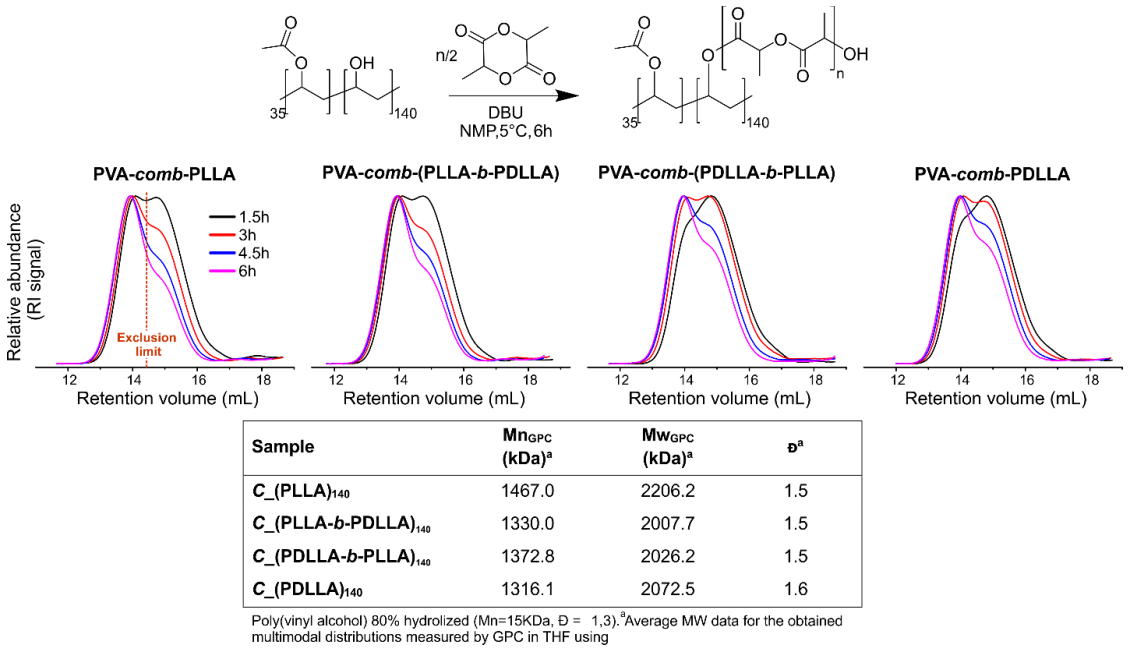

Sample	Mn_{GPC} (kDa)[a]	Mw_{GPC} (kDa)[a]	Đ[a]
***C*_(PLLA)$_{140}$**	1467.0	2206.2	1.5
***C*_(PLLA-*b*-PDLLA)$_{140}$**	1330.0	2007.7	1.5
***C*_(PDLLA-*b*-PLLA)$_{140}$**	1372.8	2026.2	1.5
***C*_(PDLLA)$_{140}$**	1316.1	2072.5	1.6

Poly(vinyl alcohol) 80% hydrolized (Mn=15KDa, Đ = 1,3).[a]Average MW data for the obtained multimodal distributions measured by GPC in THF using

Figure S. 1: GPC chromatograms (as normalized RI detector traces) and final calculated MW data of the synthesized PVA-comb-PLAs with different tacticity, as obtained by monitoring the 6-hours polymerization through GPC.

The overall MW seemed to gradually increase with polymerization time, albeit no efficient separation was achieved: all chromatograms showed a steady high-MW peak at ~14 mL retention volume followed by a drop in intensity over the entire reaction period, which remain unvaried for the entire polymerization. Such bimodal distribution is indeed typically caused by exceeding of column maximum separation limit due to the high polymer MW (weight average molecular weight ≈ 2MDa).

4. Thermogravimetric analysis (TGA)

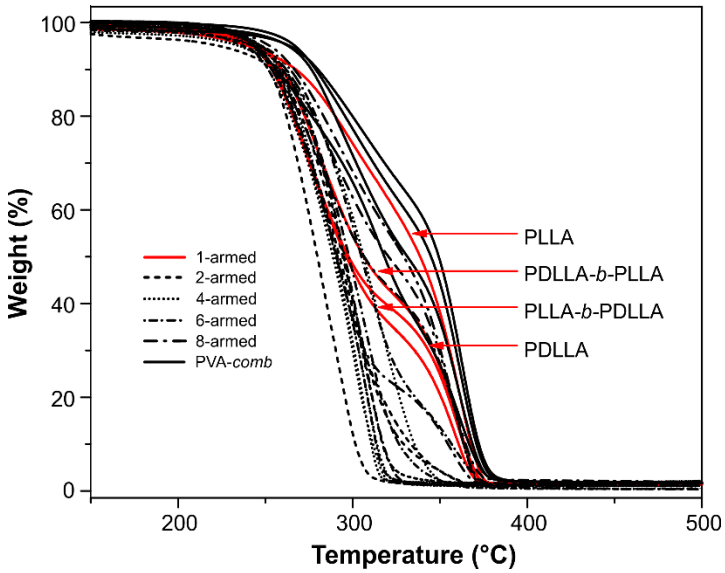

Figure S. 2: TGA traces of the synthesised multi-armed poly(lactide)s with varying architecture and tacticity.

5. Atomic force microscopy nanoindentation

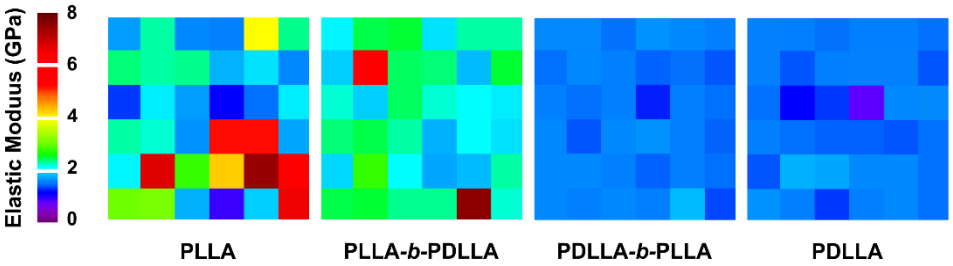

Figure S. 3: Representative force maps (indentation rate equal to 0.25 Hz) of the different 6-armed poly(lactide) stereocongifurations.